

# Unmanned Air Vehicles-to-Everything (U2X) Communications

Lead Guest Editor: Zeeshan Kaleem

Guest Editors: Majid Butt, Fadi Al-Turjman, and Sajjad Hussain



---



# **Unmanned Air Vehicles-to-Everything (U2X) Communications**

Wireless Communications and Mobile Computing

---

## **Unmanned Air Vehicles-to-Everything (U2X) Communications**

Lead Guest Editor: Zeeshan Kaleem

Guest Editors: Majid Butt, Fadi Al-Turjman, and  
Sajjad Hussain




---

Copyright © 2020 Hindawi Limited. All rights reserved.

This is a special issue published in “Wireless Communications and Mobile Computing.” All articles are open access articles distributed under the Creative Commons Attribution License, which permits unrestricted use, distribution, and reproduction in any medium, provided the original work is properly cited.

# Chief Editor






















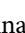

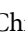


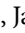





Zhipeng Cai , USA

## Associate Editors

Ke Guan , China  
Jaime Lloret , Spain  
Maode Ma , Singapore

## Academic Editors

Muhammad Inam Abbasi, Malaysia  
Ghufran Ahmed , Pakistan  
Hamza Mohammed Ridha Al-Khafaji ,  
Iraq  
Abdullah Alamoodi , Malaysia  
Marica Amadeo, Italy  
Sandhya Aneja, USA  
Mohd Dilshad Ansari, India  
Eva Antonino-Daviu , Spain  
Mehmet Emin Aydin, United Kingdom  
Parameshchhari B. D. , India  
Kalapaveen Bagadi , India  
Ashish Bagwari , India  
Dr. Abdul Basit , Pakistan  
Alessandro Bazzi , Italy  
Zdenek Becvar , Czech Republic  
Nabil Benamar , Morocco  
Olivier Berder, France  
Petros S. Bithas, Greece  
Dario Bruneo , Italy  
Jun Cai, Canada  
Xuesong Cai, Denmark  
Gerardo Canfora , Italy  
Rolando Carrasco, United Kingdom  
Vicente Casares-Giner , Spain  
Brijesh Chaurasia, India  
Lin Chen , France  
Xianfu Chen , Finland  
Hui Cheng , United Kingdom  
Hsin-Hung Cho, Taiwan  
Ernestina Cianca , Italy  
Marta Cimitile , Italy  
Riccardo Colella , Italy  
Mario Collotta , Italy  
Massimo Condoluci , Sweden  
Antonino Crivello , Italy  
Antonio De Domenico , France  
Floriano De Rango , Italy

Antonio De la Oliva , Spain  
Margot Deruyck, Belgium  
Liang Dong , USA  
Praveen Kumar Donta, Austria  
Zhuojun Duan, USA  
Mohammed El-Hajjar , United Kingdom  
Oscar Esparza , Spain  
Maria Fazio , Italy  
Mauro Femminella , Italy  
Manuel Fernandez-Veiga , Spain  
Gianluigi Ferrari , Italy  
Luca Foschini , Italy  
Alexandros G. Fragkiadakis , Greece  
Ivan Ganchev , Bulgaria  
Óscar García, Spain  
Manuel García Sánchez , Spain  
L. J. García Villalba , Spain  
Miguel Garcia-Pineda , Spain  
Piedad Garrido , Spain  
Michele Girolami, Italy  
Mariusz Glabowski , Poland  
Carles Gomez , Spain  
Antonio Guerrieri , Italy  
Barbara Guidi , Italy  
Rami Hamdi, Qatar  
Tao Han, USA  
Sherief Hashima , Egypt  
Mahmoud Hassaballah , Egypt  
Yejun He , China  
Yixin He, China  
Andrej Hrovat , Slovenia  
Chunqiang Hu , China  
Xuexian Hu , China  
Zhenghua Huang , China  
Xiaohong Jiang , Japan  
Vicente Julian , Spain  
Rajesh Kaluri , India  
Dimitrios Katsaros, Greece  
Muhammad Asghar Khan, Pakistan  
Rahim Khan , Pakistan  
Ahmed Khattab, Egypt  
Hasan Ali Khattak, Pakistan  
Mario Kolberg , United Kingdom  
Meet Kumari, India  
Wen-Cheng Lai , Taiwan


Jose M. Lanza-Gutierrez, Spain  
Pavlos I. Lazaridis , United Kingdom  
Kim-Hung Le , Vietnam  
Tuan Anh Le , United Kingdom  
Xianfu Lei, China  
Jianfeng Li , China  
Xiangxue Li , China  
Yaguang Lin , China  
Zhi Lin , China  
Liu Liu , China  
Mingqian Liu , China  
Zhi Liu, Japan  
Miguel López-Benítez , United Kingdom  
Chuanwen Luo , China  
Lu Lv, China  
Basem M. ElHalawany , Egypt  
Imadeldin Mahgoub , USA  
Rajesh Manoharan , India  
Davide Mattera , Italy  
Michael McGuire , Canada  
Weizhi Meng , Denmark  
Klaus Moessner , United Kingdom  
Simone Morosi , Italy  
Amrit Mukherjee, Czech Republic  
Shahid Mumtaz , Portugal  
Giovanni Nardini , Italy  
Tuan M. Nguyen , Vietnam  
Petros Nicolaitidis , Greece  
Rajendran Parthiban , Malaysia  
Giovanni Pau , Italy  
Matteo Petracca , Italy  
Marco Picone , Italy  
Daniele Pinchera , Italy  
Giuseppe Piro , Italy  
Javier Prieto , Spain  
Umair Rafique, Finland  
Maheswar Rajagopal , India  
Sujan Rajbhandari , United Kingdom  
Rajib Rana, Australia  
Luca Reggiani , Italy  
Daniel G. Reina , Spain  
Bo Rong , Canada  
Mangal Sain , Republic of Korea  
Praneet Saurabh , India

Hans Schotten, Germany  
Patrick Seeling , USA  
Muhammad Shafiq , China  
Zaffar Ahmed Shaikh , Pakistan  
Vishal Sharma , United Kingdom  
Kaize Shi , Australia  
Chakchai So-In, Thailand  
Enrique Stevens-Navarro , Mexico  
Sangeetha Subbaraj , India  
Tien-Wen Sung, Taiwan  
Suhua Tang , Japan  
Pan Tang , China  
Pierre-Martin Tardif , Canada  
Sreenath Reddy Thummaluru, India  
Tran Trung Duy , Vietnam  
Fan-Hsun Tseng, Taiwan  
S Velliangiri , India  
Quoc-Tuan Vien , United Kingdom  
Enrico M. Vitucci , Italy  
Shaohua Wan , China  
Dawei Wang, China  
Huaqun Wang , China  
Pengfei Wang , China  
Dapeng Wu , China  
Huaming Wu , China  
Ding Xu , China  
YAN YAO , China  
Jie Yang, USA  
Long Yang , China  
Qiang Ye , Canada  
Changyan Yi , China  
Ya-Ju Yu , Taiwan  
Marat V. Yuldashev , Finland  
Sherali Zeadally, USA  
Hong-Hai Zhang, USA  
Jiliang Zhang, China  
Lei Zhang, Spain  
Wence Zhang , China  
Yushu Zhang, China  
Kechen Zheng, China  
Fuhui Zhou , USA  
Meiling Zhu, United Kingdom  
Zhengyu Zhu , China

## Contents





---

### **Service Group Based FOFDM-IDMA Platform to Support Massive Connectivity and Low Latency Simultaneously in the Uplink IoT Environment**

Lin Shi, Ishtiaq Ahmad, YuJing He, and KyungHi Chang 




Research Article (6 pages), Article ID 8517372, Volume 2020 (2020)

### **Formal Verification of Hardware Components in Critical Systems**

Wilayat Khan , Muhammad Kamran , Syed Rameez Naqvi , Farrukh Aslam Khan , Ahmed S. Alghamdi, and Eesa Alsolami

Research Article (15 pages), Article ID 7346763, Volume 2020 (2020)

### **A Proposal for Routing Protocol for FANET: A Fuzzy System Approach with QoE/QoS Guarantee**

Jorge Souza , José Jailton , Tássio Carvalho, Jasmine Araújo , and Renato Francês


Research Article (10 pages), Article ID 8709249, Volume 2019 (2019)

### **IoT System Integrating Unmanned Aerial Vehicles and LoRa Technology: A Performance Evaluation Study**

J.-M. Martinez-Caro  and M.-D. Cano 





Research Article (12 pages), Article ID 4307925, Volume 2019 (2019)

### **Experiments with a LoRaWAN-Based Remote ID System for Locating Unmanned Aerial Vehicles (UAVs)**

Ali Ghubaish , Tara Salman, and Raj Jain

Research Article (11 pages), Article ID 9060121, Volume 2019 (2019)

### **UAV-Enabled Data Collection: Multiple Access, Trajectory Optimization, and Energy Trade-Off**

Lin Xiao , Yipeng Liang , Chenfan Weng, Dingcheng Yang , and Qingmin Zhao 

Research Article (14 pages), Article ID 9647539, Volume 2019 (2019)

### **An Efficient Contention-Window Based Reporting for Internet of Things Features in Cognitive Radio Networks**

Muhammad Sajjad Khan , Junsu Kim , Eung Hyuk Lee, and Su Min Kim 

Research Article (9 pages), Article ID 8475020, Volume 2019 (2019)

## Research Article

# Service Group Based FOFDM-IDMA Platform to Support Massive Connectivity and Low Latency Simultaneously in the Uplink IoT Environment

Lin Shi, Ishtiaq Ahmad, YuJing He, and KyungHi Chang 

*Electronic Engineering Department, Inha University, Incheon, Republic of Korea*

Correspondence should be addressed to KyungHi Chang; [khchang@inha.ac.kr](mailto:khchang@inha.ac.kr)

Received 23 July 2019; Revised 22 November 2019; Accepted 7 January 2020; Published 29 February 2020

Guest Editor: Sajjad Hussain

Copyright © 2020 Lin Shi et al. This is an open access article distributed under the Creative Commons Attribution License, which permits unrestricted use, distribution, and reproduction in any medium, provided the original work is properly cited.

Fifth generation (5G) mobile communications have many aspects of services, including the one by the technology of Internet of things (IoT). To support the diverse service types of IoT applications, heterogeneous requirements for massive connectivity and low latency are mandatory. In this paper, service group based filtered orthogonal frequency division multiplexing (FOFDM) combined with interleaved division multiple access (IDMA), i.e., FOFDM-IDMA, is proposed in order to simultaneously support massive connectivity and fulfill the low-latency requirements in the uplink (UL) IoT environment. The proposed FOFDM-IDMA platform has two focal points: first, it enables the coexistence of various time-frequency granularities suitable to diverse service groups, and second, it supports massive connectivity with low latency to provide reliable communications. Thus, the proposed FOFDM-IDMA framework can simultaneously support the requirements of uRLLC (ultrareliable low-latency communications) and mMTC (massive machine-type communications) for the next-generation communication systems. However, the 5G new radio (NR) can solely support the requirements of uRLLC and mMTC independently. Simulation results show that the proposed FOFDM-IDMA platform performs remarkably well, compared to the conventional scheme in the IoT environment.

## 1. Introduction

IoT connectivity is growing significantly faster than mobile broadband connectivity and is estimated to reach 30 billion connected devices by 2025 [1]. Therefore, a large fraction of IoT applications requires massive connectivity, wide coverage, and low device costs. However, there are still some applications that require low latency, such as tactile Internet [2] and connected cars [3].

To meet the heterogeneous requirements of various service types [4], Huawei proposed FOFDM scheme [5], which is a flexible waveform to coexist with various parameter configurations. Moreover, it utilizes a filter for each sub-band to suppress high side lobes in conventional OFDM techniques. It is a multicarrier modulation scheme and introduces the filtering process in the time domain. The filter bandwidth is designed for a certain sub-band.

IDMA is a multiple access technique [6] in which the main principle is to distinguish the users (UEs) through user-specific interleavers at the receiver (Rx) side. The advantages of IDMA are power efficiency by using low-cost multiuser detection (MUD), suitability for wide- or narrow-band transmission, and support for high numbers of users with high spectral efficiency, which can definitely benefit IoT connectivity. Also, OFDM combined with IDMA (OFDM-IDMA) [7] is proposed to adopt most of the benefits from both techniques. Unlike the contributions on resource allocation [8–13] and power control schemes [14–16] for cellular networks and the work on drone sound recognition [17, 18], this paper addresses the service group based FOFDM-IDMA platform to support massive connectivity in the uplink IoT environment.

In this paper, service group based FOFDM combined with IDMA (FOFDM-IDMA) is proposed, which enables



the coexistence of various time-frequency granularities suitable to diverse service groups, and it supports massive connectivity with low latency to provide reliable communications in the IoT environment. In addition, the proposed FOFDM-IDMA framework can simultaneously support the requirements of uRLLC and mMTC for the next generation communication systems. However, the 5G NR can only support the requirements of uRLLC and mMTC independently.

The remainder of this paper is organized as follows: Section 2 introduces the conventional OFDM-IDMA scheme. In Section 3, the details of the proposed service group based FOFDM-IDMA platform are provided, and the frame structure of the IoT environment is designed. The simulation results are discussed in Section 4, and we conclude the paper in Section 5.

## 2. Conventional OFDM-IDMA Scheme

Figure 1 shows the block diagram of the OFDM-IDMA transceiver structure in the uplink for user  $k$ . At the transmitter, information bits  $d_k$  for user  $k$  are first encoded by the encoder (ENC) module and are then spread by a length  $S$  spreading sequence. Afterwards, the chips within the spread data sequence  $\tilde{c}_k$  are interleaved by a user-specific interleaver,  $\{\pi_k\}$ . Then, the resultant signal  $x_k$  is modulated and mapped onto subcarriers by inverse fast Fourier transform (IFFT). After cyclic prefix (CP) insertion, the serial symbols in time domain  $\tilde{x}_k$  are transmitted through the multipath fading channel.

At the Rx side, the received signals represented in equation (1) go through the inverse process of OFDM modulation before the MUD procedure.

$$r(j) = \sum_{k=1}^K \sum_{l=0}^L h_{k,l} \tilde{x}_k(j-l) + n(j), \quad j = 1, \dots, J+L-1. \quad (1)$$

We write

$$r(j+l) = h_{k,l} \tilde{x}_k(j) + \zeta_{k,l}(j), \quad (2)$$

where  $h_{k,l}$  is the channel impulse response for user  $k$  with channel length  $L$ ,  $n(j)$  is the additional white Gaussian noise (AWGN), and  $\zeta_{k,l}(j) = r(j+l) - h_{k,l} \tilde{x}_k(j)$  is the interference from other UEs to user  $k$  and the AWGN.

Elementary signal estimator (ESE) is applied to perform the chip by chip interference cancellation for each sub-carrier. The inputs of the ESE consist of the received signal in equation (2) and log-likelihood ratio  $L_{\text{ESE},k}^{(\text{in})}$  [6]. Log-likelihood ratio  $L_{\text{ESE},k}^{(\text{in})}$  is given by the decoder in the previous iteration and will be used to reestimate the transmitted signal in order to perform interference cancellation in the next iteration. The output of ESE  $L_{\text{ESE},k}^{(\text{out})}$  is soft information after interference cancellation, and the deinterleaved version  $L_{\text{DEC},k}^{(\text{in})}$  through  $\pi_k^{-1}$  is fed into the a posteriori probability (APP) decoder (DEC) module. The DEC despreads  $L_{\text{DEC},k}^{(\text{in})}$  and spreads the sequence again and then subtracts  $L_{\text{DEC},k}^{(\text{in})}$ , giving rise to  $L_{\text{DEC},k}^{(\text{out})}$ .  $L_{\text{DEC},k}^{(\text{out})}$  is interleaved again and fed into the ESE. The ESE and the DEC perform a turbo

process iteratively until the refined decoded bits are obtained in the final iteration.

## 3. Service Group Based FOFDM-IDMA Platform for IoT Connectivity

In this section, a multiuser system of service group based FOFDM-IDMA platform for IoT connectivity in the uplink is proposed. Then, the dedicated parameters are configured to support diverse service groups according to latency requirement.

*3.1. System Model for the Service Group Based FOFDM-IDMA Platform.* Figure 2 shows the block diagram of the service group based FOFDM-IDMA platform as depicted for user  $k$  in service group  $g$ . The IDMA encoder and decoder processes are the same as in the conventional OFDM-IDMA scheme, but the difference is that an alternative waveform of FOFDM is applied, taking advantage of scalable numerology, such as various transmission time intervals (TTI) and subcarrier spacing in the communication systems in order to meet various requirements of IoT applications. Moreover, this scheme can overcome typical OFDM weak points through a sub-band filter [19], including high peak-to-average power ratio (PAPR) and high side lobes in the frequency domain.

The transmitted signal is represented as

$$\tilde{x}_k^{(g)} = \sum_{i=1}^B F_{k,i}^{(g)} \cdot V_{k,i}^{(g)} \cdot x_{k,i}^{(g)}, \quad (3)$$

where  $x_{k,i}^{(g)}$  is the modulated symbol,  $V_{k,i}^{(g)}$  is the IFFT matrix, and  $F_{k,i}^{(g)}$  is the sub-band filter of the  $i^{\text{th}}$  sub-band with total  $B$  sub-bands for user  $k$  in group  $g$ .

Then, the received signal can be represented as

$$r(j) = h_{k,l} \tilde{x}_k^{(g)}(j) + \zeta_{k,l}(j), \quad (4)$$

where  $\zeta_{k,l}(j)$  is the distortion (including interference from other UEs and AWGN) in  $r(j)$  with respect to user  $k$  and can be approximated as a Gaussian variable according to the central limit theorem.

Therefore, the operational procedure for the service group based FOFDM-IDMA platform can be described in the following steps, considering that users are required to be served in the uplink.

*Step (1). User Grouping:*

Group the  $K$  UEs to be served in  $G_{\text{max}}$  subcategories  $\{G^{(g)}\}$ ,  $g \leq G_{\text{max}}$ , where  $G_{\text{max}}$  is the total number of service groups.

*Step (2). Assigning Parameter Configuration*

Assign the predefined parameter configuration suitable to the  $g^{\text{th}}$  service group,  $G^{(g)}$ , to apply to user  $k$ .

*Step (3). FOFDM-IDMA Tx Side Processing*

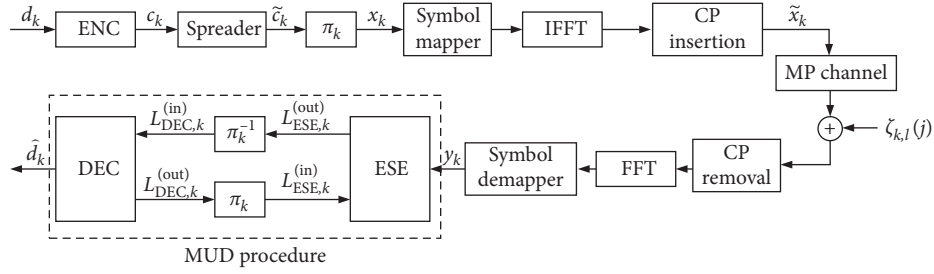
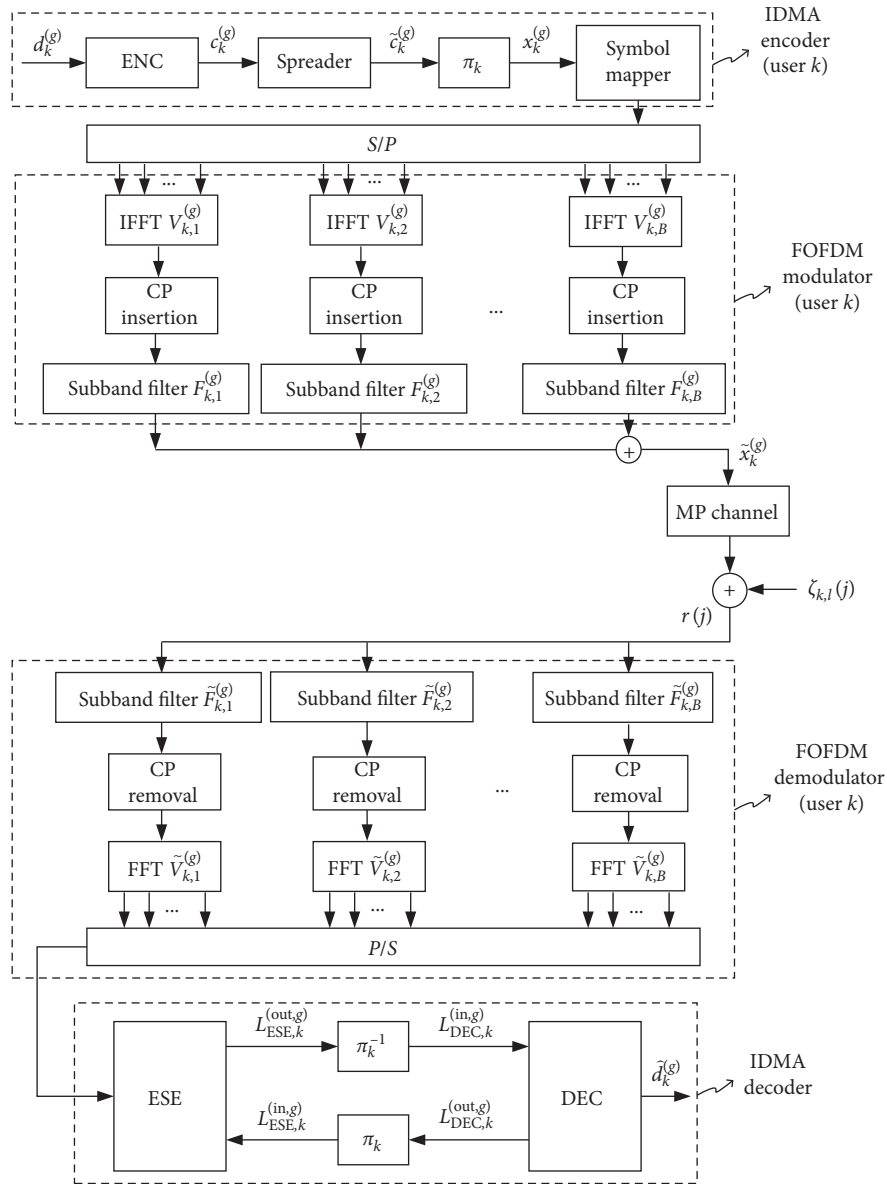

 FIGURE 1: Block diagram of OFDM-IDMA transceiver in the uplink for user  $k$ .


FIGURE 2: Block diagram of the service group based FOFDM-IDMA transceiver.

All  $K$  UEs belong to their relevant service groups with their specific predefined parameter configurations and perform IDMA encoding and FOFDM modulation procedures, as shown in Figure 2.

#### Step (4). FOFDM-IDMA Rx Side Processing

After the FOFDM demodulation procedure at the Rx side, MUD is performed by the ESE and DEC modules. The output of the ESE can be represented as

$$L_{\text{ESE},k}^{(\text{out},g)} = \sum_{l=0}^{L-1} \frac{2h_{k,l}(r(j+l) - E(\zeta_{k,l}(j)))}{\text{Var}(\zeta_{k,l}(j))}. \quad (5)$$

Also, the functions of the DEC module can be represented as

$$L(\tilde{d}_k^{(g)}) = \sum_{i=1}^S S_k(i) L_{\text{DEC},k}^{(\text{in},g)}, \quad (6)$$

$$L_{\text{DEC},k}^{(\text{out},g)} = S_k(i) L(\tilde{d}_k) - L_{\text{DEC},k}^{(\text{in},g)},$$

where  $S_k$  is the spreading code for user  $k$ .

Finally, the mean and variance of the transmitted signal are estimated by the ESE as

$$E(\tilde{x}_k^{(g)}(j)) = \tanh\left(\frac{L_{\text{ESE},k}^{(\text{in},g)}}{2}\right), \quad (7)$$

$$\text{Var}(\tilde{x}_k^{(g)}(j)) = 1 - E(\tilde{x}_k^{(g)}(j)).$$

It is noted that in Step 1, user  $k$  is grouped into the  $g^{\text{th}}$  group,  $G^{(g)}$ , according to the service requirement, and then in Step 2, a suitable parameter configuration is assigned to the service group. In Step 3, IDMA encoding and FOFDM modulation are performed. Hence, the first three steps show the flexibility of the FOFDM platform to enable the coexistence of various time-frequency granularities suitable to diverse service groups.

**3.2. Frame Structure and Parameter Configuration for FOFDM Platform.** Based on Section 3.1, a dedicated frame structure for the IoT environment is designed, and specific parameters are configured for the FOFDM platform. For most IoT applications, a longer TTI is required to enable large coverage and higher spectral efficiency in order to support massive connectivity (MC). On the other hand, a shorter TTI for shorter round-trip latency and low overhead for efficiently transmitting small packets are still required to support part of the UEs with higher low-latency (LL) requirement. Therefore, in this section, a flexible frame structure for two service types in the IoT environment is proposed, as shown in Figure 3. In addition, it is noted that the FOFDM platform enables various TTI and waveform numerology because sub-band based filtering is applied, so specific parameters are configured for the FOFDM platform, as shown in Table 1, by splitting the IoT applications into two subcategories with massive connectivity or low-latency requirement.

In Table 1, the bandwidth in long-term evolution for machine-type communications (LTE-M) [1] is employed, which restricts machine-to-machine transmissions to a small amount of the available bandwidth that is orthogonal to the broadband UEs. Parameter configuration for MC refers to a new random access technology (RAT) for 5G with a longer TTI and a CP longer than  $10 \mu\text{s}$ . Conversely, for low-latency service, the physical transmission should be performed using very small packets to enable one-way

physical layer transmission within  $100 \mu\text{s}$ ; thus, each packet cannot exceed a  $33 \mu\text{s}$  duration because of structural additional latency, including the encoding procedure at the transmitter and the detection and decoding procedure at the receiver [20]. Therefore, the  $30 \mu\text{s}$  symbol duration is configured. And then, the value of subcarrier spacing is obtained by taking the reciprocal of symbol duration. In addition, CP length configuration is considered in terms of overhead, which should be extremely small for low-latency applications [21].

## 4. Simulation and Performance Evaluation

In this section, we perform the simulations for the filtered orthogonal frequency division multiple access (FOFDMA), OFDM-IDMA, and the proposed FOFDM-IDMA with parameter configuration for MC.

The parameters for the waveforms are configured according to Table 1, and a convolutional code with 1/2 code rate followed by a length-8 spreading sequence is employed for each UE. The simulation is under a multipath fading channel applying an extended typical urban (ETU) model [22] with mobility of 1 km/h and employing perfect channel estimation. Ten subcarriers per sub-band are assigned, and ten iterations for the IDMA decoder are assumed to finally obtain the decoded bits for each UE.

The BER performance varying number of UEs of FOFDMA, OFDM-IDMA, and the proposed FOFDM-IDMA schemes when  $(E_b/N_o) = 8$  is shown in Figure 4. Figure 4 shows that the BER performance gets worse with the increasing number of supported UEs. When  $(E_b/N_o) = 8$  and the number of UEs equals to 64, the BER of FOFDMA, OFDM-IDMA, and FOFDM-IDMA is  $1.9 \times 10^{-2}$ ,  $4.83 \times 10^{-3}$ , and  $2.32 \times 10^{-3}$ , respectively. FOFDM-IDMA gives the best performance while FOFDMA gives the worst. It illustrates that the waveforms with IDMA are much more suitable to support massive connectivity.

The BER performance of the three schemes: FOFDMA, OFDM-IDMA with parameter configuration for MC, and the proposed FOFDM-IDMA (including two service groups with parameter configurations for both MC and LL) are further investigated in  $(E_b/N_o)$  perspective. Eight and sixteen UEs are assumed to share the resource. For the FOFDM-IDMA platform, we assume a small fraction of UEs with higher low-latency requirement, i.e., two UEs for LL, and six UEs for MC when eight UEs are considered. In addition, there are four UEs for LL and twelve UEs for MC when sixteen UEs are considered. BER performances for the three schemes are compared in Figure 5.

Figure 5 shows that conventional OFDM-IDMA gives better BER performance, about 2.2 dB better at the target BER of  $10^{-3}$ , compared to FOFDMA, which has the worst performance, because IDMA can potentially exploit frequency diversity due to wider frequency bandwidth employed for each user. Our proposed service group based FOFDM-IDMA platform gives the best performance, and the gain is 0.3 dB over the conventional OFDM-IDMA at the target BER of  $10^{-3}$ , which comes from the sub-band filter of the FOFDM to protect neighbor UEs from interference. Moreover, it simultaneously meets the service requirements

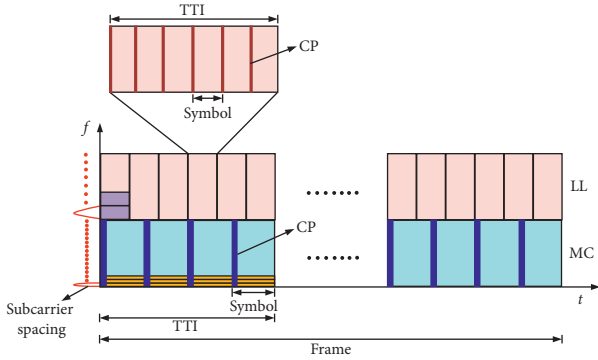


FIGURE 3: Flexible frame structure to support diverse IoT services of massive connectivity (MC) and low latency (LL).

TABLE 1: Parameter configuration for MC and LL.

Parameter	MC	LL
Bandwidth	1.4 MHz	
TTI length	1.2 ms	0.2 ms
Subcarrier spacing	3.75 kHz	33.33 KHz
FFT size	512	48
Symbol duration	266.67 $\mu$ s	30 $\mu$ s
# of symbols/TTI	4	6
CP length	10.6 $\mu$ s	2.2 $\mu$ s

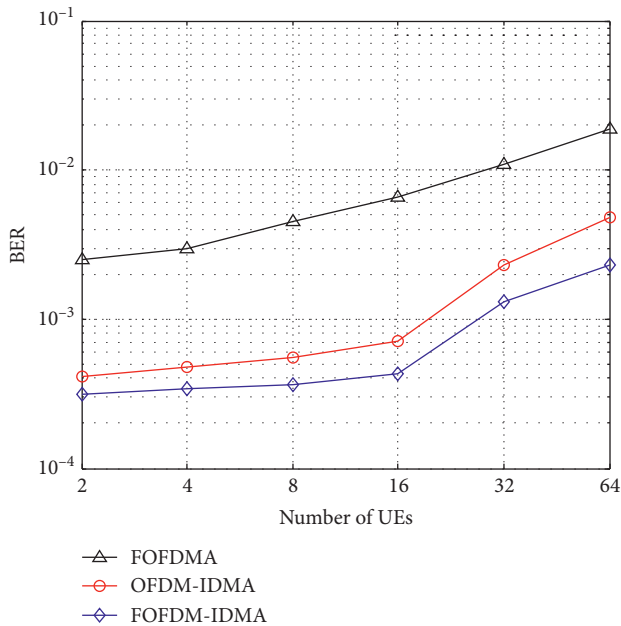


FIGURE 4: BER performance varying number of UEs of FOFDMA, OFDM-IDMA, and the proposed FOFDM-IDMA schemes.

for UEs in separate service groups, providing suitability with flexible parameters.

### 5. Conclusions

In this paper, FOFDM-IDMA is proposed, which has the capability of supporting massive connectivity and fulfilling

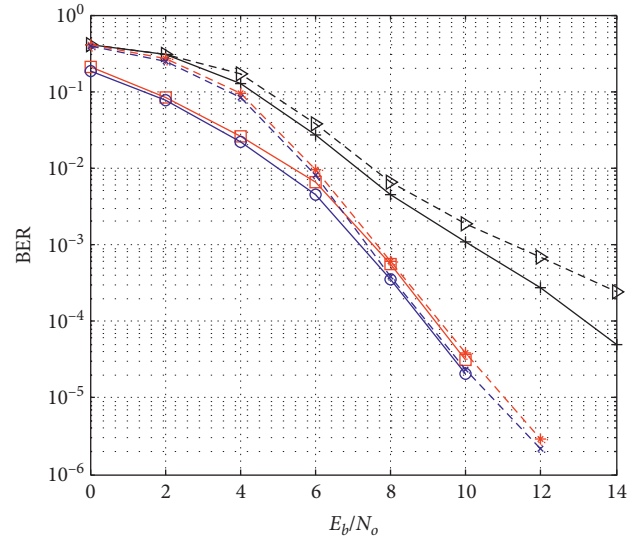


FIGURE 5: BER performance versus  $E_b/N_o$  of the proposed FOFDM-IDMA, OFDM-IDMA, and OFDMA schemes.

low-latency requirement when providing reliable communications in the IoT environment. Moreover, a dedicated frame structure for the IoT environment is proposed, and specific parameters are configured for the FOFDM platform. In addition, the proposed FOFDM-IDMA framework can simultaneously support the requirements of uRLLC and mMTC for the next generation communication systems. However, the 5G NR can only support the requirements of uRLLC and mMTC independently. The simulation results confirm that, compared with conventional OFDM-IDMA, the proposed scheme shows 0.3 dB SNR gain at the target BER of  $10^{-3}$ . Moreover, the proposed FOFDM-IDMA platform enables the coexistence of various time-frequency granularities suitable to diverse service groups.

### Data Availability

We are not supposed to share the data due to project privacy policy.

### Conflicts of Interest

The authors declare that there are no conflicts of interest regarding the publication of this paper.

### Authors' Contributions

Lin Shi proposed the idea of the service group based filtered orthogonal frequency division multiplexing (FOFDM) combined with interleaved division multiple access (IDMA), i.e., FOFDM-IDMA, in order to simultaneously support massive connectivity and fulfill the low-latency requirements

in the uplink (UL) IoT environment. Moreover, she wrote some technical aspects of the manuscript and also performed the simulations. Ishtiaq Ahmad made all the block diagrams of the manuscript and also drew the flexible frame structure to support diverse IoT services of massive connectivity and low latency. Moreover, he wrote some sections of the manuscript and also corrected all the English mistakes in the manuscript. YuJing He by discussion helped in proposing the FOFDM-IDMA scheme which has the capability of supporting massive connectivity and fulfilling low-latency requirement when providing reliable communications in the IoT environment. Moreover, she wrote some technical equations which helped in the analysis of the proposed scheme. KyungHi Chang was the technical leader of this manuscript. He suggested all the technical issues for the proposed FOFDM-IDMA scheme and also for simulation aspects. In addition, he corrected the whole simulation methodology of this manuscript and also corrected all the mistakes in the simulation environment as well as in the structure of the manuscript.

## Acknowledgments

This work was supported by an Institute for Information and Communications Technology Promotion (IITP) grant funded by the Korean Government Ministry of Science, ICT and Future Planning (MSIP) through Development of Fundamental Technologies for the Next Generation Public Safety Communications under Grant 2017-0-00316.

## References

- [1] Nokia Networks, "LTE-M—optimizing LTE for the internet of things white paper," 2014, <http://networks.nokia.com/>.
- [2] M. Simsek, A. Aijaz, M. Dohler, J. Sachs, and G. Fettweis, "5G-enabled tactile internet," *IEEE Journal on Selected Areas in Communications*, vol. 34, no. 3, pp. 460–473, 2016.
- [3] M. Khairnar and D. Vaishali, "V2V communication survey wireless technology," 2014, <https://arxiv.org/abs/1403.3993>.
- [4] 3GPP, "Technical specification 22.368, V13.0.0," 2014, <http://www.3gpp.org/>.
- [5] J. Abdoli, M. Jia, and J. Ma, "Filtered OFDM: a new waveform for future wireless systems," in *Proceedings of the 2015 IEEE Signal Processing Advances in Wireless Communications (SPAWC)*, pp. 66–70, IEEE, Stockholm, Sweden, June 2015.
- [6] L. Ping, L. Liu, K. Wu, and W. K. Leung, "Interleave-division multiple-access," *IEEE Transactions on Wireless Communications*, vol. 5, no. 4, pp. 938–947, 2006.
- [7] I. Mahafeno and C. Langlais, "OFDM-IDMA versus IDMA with ISI cancellation for quasi-static Rayleigh fading multipath channels," in *Proceedings of the 4th International Symposium on Turbo Codes and Related Topics*, pp. 140–144, Munich, Germany, April 2006.
- [8] I. Ahmad, W. Chen, and K. H. Chang, "LTE-railway user priority-based cooperative resource allocations schemes for coexisting public safety and railway networks," *IEEE Access*, vol. 5, pp. 7958–8000, 2017.
- [9] W. Chen, I. Ahmad, and K. Chang, "Co-channel interference management using eCIC/FeCIC with coordinated scheduling for the coexistence of PS-LTE and LTE-R networks," *EURASIP Journal on Wireless Communications and Networking*, vol. 2017, no. 1, p. 37, 2017.
- [10] I. Ahmad, Z. Kaleem, R. Narmeen, L. D. Nguyen, and D. B. Ha, "Quality-of-service aware game theory-based uplink power control for 5G heterogeneous networks," *Mobile Networks and Applications*, vol. 24, no. 2, pp. 556–563, 2019.
- [11] I. Ahmad and K. Chang, "Effective SNR mapping and link adaptation strategy for next-generation underwater acoustic communications networks: a cross-layer approach," *IEEE Access*, vol. 7, pp. 44150–44164, 2019.
- [12] I. Ahmad and K. Chang, "Mission critical user priority-based random-access scheme for collision resolution for coexisting PS-LTE and LTE-M networks," *IEEE Access*, vol. 7, pp. 115505–115517, 2019.
- [13] I. Ahmad and K. H. Chang, "Mission-critical user priority-based cooperative resource allocation schemes for multi-layer next-generation public safety networks," *Physical Communication*, vol. 38, Article ID 100926, 2020.
- [14] I. Ahmad and K. H. Chang, "Downlink power allocation strategy for next-generation underwater acoustic communications networks," *Electronics*, vol. 8, no. 11, p. 1297, 2019.
- [15] Z. Kaleem, M. Khaliq, A. Khan, I. Ahmad, and T. Duong, "PS-CARA: context-aware resource allocation scheme for mobile public safety networks," *Sensors*, vol. 18, no. 5, p. 1473, 2018.
- [16] I. Ahmad, Z. Kaleem, and K. Chang, "QoS priority-based femtocell user power control for interference mitigation in 3GPP LTE-A HetNet," *The Journal of Korean Institute of Communications and Information Sciences*, vol. 39B, no. 2, pp. 61–74, 2014.
- [17] J. Guo, I. Ahmad, and K. H. Chang, "Classification, positioning and tracking of drones by HMM using acoustic circular microphone array beamforming," *EURASIP Journal on Wireless Communications and Networking*, vol. 2020, no. 1, p. 9, 2020.
- [18] Y. He, I. Ahmad, L. Shi, and K. H. Chang, "SVM-based drone sound recognition using the combination of HLA and WPT techniques in practical noisy environment," *KSII Transactions on Internet and Information System*, vol. 13, no. 10, pp. 5078–5094, 2019.
- [19] X. Zhang, M. Jia, L. Chen, J. Ma, and J. Qiu, "Filtered-OFDM—enabler for flexible waveform in the 5th generation cellular networks," in *Proceedings of the 2015 IEEE GLOBECOM*, pp. 1–6, IEEE, San Diego, CA, USA, December 2015.
- [20] G. P. Fettweis, "The tactile internet: applications and challenges," *IEEE Vehicular Technology Magazine*, vol. 9, no. 1, pp. 64–70, 2014.
- [21] F. Schaich, T. Wild, and Y. Chen, "Waveform contenders for 5G—suitability for short packet and low latency transmissions," in *Proceedings of the 79th Vehicular Technology Conference*, pp. 18–21, IEEE, Seoul, South Korea, May 2014.
- [22] 3GPP, "Technical specification 36.104, V13.2.0," 2016, <http://www.3gpp.org/>.

## Research Article

# Formal Verification of Hardware Components in Critical Systems

Wilayat Khan <sup>1</sup>, Muhammad Kamran <sup>2</sup>, Syed Rameez Naqvi <sup>1</sup>,  
Farrukh Aslam Khan <sup>3</sup>, Ahmed S. Alghamdi,<sup>2</sup> and Eesa Alsolami<sup>2</sup>

<sup>1</sup>Department of Electrical and Computer Engineering, COMSATS University Islamabad, Wah Campus, Pakistan

<sup>2</sup>Department of Cyber Security, College of Computer Science and Engineering, University of Jeddah, Jeddah, Saudi Arabia

<sup>3</sup>Center of Excellence in Information Assurance (CoEIA), King Saud University, Riyadh, Saudi Arabia

Correspondence should be addressed to Wilayat Khan; wilayatk@gmail.com and Farrukh Aslam Khan; fakhan@ksu.edu.sa

Received 2 July 2019; Revised 10 January 2020; Accepted 16 January 2020; Published 20 February 2020

Guest Editor: Fadi Al-Turjman

Copyright © 2020 Wilayat Khan et al. This is an open access article distributed under the Creative Commons Attribution License, which permits unrestricted use, distribution, and reproduction in any medium, provided the original work is properly cited.

Hardware components, such as memory and arithmetic units, are integral part of every computer-controlled system, for example, Unmanned Aerial Vehicles (UAVs). The fundamental requirement of these hardware components is that they must behave as desired; otherwise, the whole system built upon them may fail. To determine whether or not a component is behaving adequately, the desired behaviour of the component is often specified in the Boolean algebra. Boolean algebra is one of the most widely used mathematical tools to analyse hardware components represented at gate level using Boolean functions. To ensure reliable computer-controlled system design, simulation and testing methods are commonly used to detect faults; however, such methods do not ensure absence of faults. In critical systems' design, such as UAVs, the simulation-based techniques are often augmented with mathematical tools and techniques to prove stronger properties, for example, absence of faults, in the early stages of the system design. In this paper, we define a lightweight mathematical framework in computer-based theorem prover Coq for describing and reasoning about Boolean algebra and hardware components (logic circuits) modelled as Boolean functions. To demonstrate the usefulness of the framework, we (1) define and prove the correctness of *principle of duality* mechanically using a computer tool and all basic theorems of Boolean algebra, (2) formally define the algebraic manipulation (step-by-step procedure of proving functional equivalence of functions) used in Boolean function simplification, and (3) verify functional correctness and reliability properties of two hardware components. The major advantage of using mechanical theorem provers is that the correctness of all definitions and proofs can be checked mechanically using the type checker and proof checker facilities of the proof assistant Coq.

## 1. Introduction

Hardware, software, and communication networks altogether make systems operating in the cyberspace such as Unmanned Aerial Vehicles (UAVs). UAVs operating in an uncertain, potentially hazardous, remote, and dynamic environment are extremely important but challenging to be reliable, robust, and secure. These flying vehicles are currently being used in mission-critical [1], industry-oriented [2], and Internet of Things (IoT) [3] applications, to name a few. To meet the high standards of safety and reliability of UAV-based mission-critical [1] or IoT [2, 3] applications, the UAVs in such systems must be studied and analysed using rigorous and formal techniques. Failure or unauthentic use of software and hardware systems of air vehicles

can lead to human losses [4, 5] and strategic losses [6, 7]. UAV-based human environment can be manipulated and controlled by a remote attacker using attacks such as *sensor input spoofing attack* [8]. Military UAVs have been and are currently the favourite target of attackers to gain cyber power [9], which has recently led towards a *drone war* [10].

To design fault-tolerant and secure air vehicles, conventional design and testing methods must be augmented with more robust and reliable tools and techniques called formal methods [11]. Formal methods have been successfully used to verify collision avoidance between UAVs [12], certify UAVs within civil airspace [13], and design resilient UAV systems [14]. As the security and reliability of UAVs depend upon the security and reliability of individual components, their correctness must be ensured in the design phase. In addition to

UAVs, the formal framework presented in this paper is equally applicable to any other computer system such as sensor networks [15–17] and hardware components, such as flash memory, of such systems [18]. In this paper, we address the formal specification and verification of hardware (logic) components, such as memory units and adders, designed at the logic gates level using Boolean algebra. This makes our formal model extremely important in the domain of critical system design in general and in UAVs in particular.

Boolean algebra [19] is the basic logic tool for the analysis and synthesis of (models of) logic circuits. This connection between Boolean algebra and logic circuits was established by Claude Shannon [20]. While different computer tools [21–25] and mathematical techniques [26, 27] are available to manipulate logic circuits modelled as Boolean functions, it must be ensured that such tools and techniques do not alter the intended interpretation (behaviour) of these circuits. To verify that the behaviour of the digital circuit (modelled as Boolean function) after the analysis is symmetric to the original behaviour, the Boolean function *before* the mathematical manipulation must be proven to be functionally symmetric to the function *after* the manipulation. This property of digital circuits is often referred to as functional equivalence [28]. Common examples of manipulation are mathematical manipulation [29], Karnaugh map [26], and tabulation method [27] used for the Boolean functions.

Boolean algebra is one of the most widely used mathematical techniques to model and analyse logic circuits. In the electronic design flow, the initial circuit design is often described at system level in high-level languages (e.g., MATLAB and C) and translated to register-transfer logic (RTL) representation in a description language (e.g., Verilog and VHDL) using high-level synthesis (hardware compilers) tools. The RTL representation of the circuit is transformed to gate-level representation (often as Boolean functions) using logic synthesis tools, which is finally fabricated to produce physical layout of the circuit. The gate-level representation described as Boolean functions is commonly used in techniques and frameworks [30–33] and in classrooms for the design and analysis of simple logic circuits [29].

*1.1. Research Challenges.* Boolean functions or logic circuits described as Boolean functions are normally manipulated through the error-prone pen-and-paper method using the basic theorems and postulates of Boolean algebra. To the best of our knowledge, neither the algebra nor the mathematical manipulation process has been formally defined in an interactive theorem prover and hence their correctness cannot be checked mechanically. There is no guarantee that the principle of duality indeed holds, the mathematical manipulation carried out is correct, or the logic circuits (described as Boolean functions) optimized for size, efficiency, and cost-effectiveness using K-map [26] or tabulation [24] methods are behaviourally symmetric.

*1.2. Solution Overview.* In order to formally reason about Boolean algebra and verify the correctness of digital components described at gate level as Boolean functions, we

define a formal model of the Boolean algebra using the calculus of construction in theorem prover Coq. The formal model of Boolean algebra defined enables one to define and prove all the basic theorems as well as the principle of duality. We extend our formal model of the Boolean algebra to represent combinational circuits. To assess the efficacy of our formal model, the proof facility of Coq is used to carry out proof of correctness of gate-level combinational circuits and reason about Boolean algebra. Among other numerous advantages (Section 2) of computer-aided verification using interactive theorem prover are the following: (a) all the formal definitions and proofs can be defined in the computer, and (b) the correctness of the proofs can be automatically checked by the computer [34].

The formal approach for checking correctness of Boolean functions and digital circuits is described in Figure 1. Formal models of the digital circuit under verification and the properties of interest as theorems are fed into an ITP engine (Coq system, in our case) and a formal proof that the (model of the) circuit holds the properties is carried out interactively. A proof engineer guides the tool by providing it proof commands, which becomes part of the proof script if accepted by the tool. The correctness of the proof script is automatically checked using the tool. The formal verification in Coq using the proposed formal model is demonstrated in Section 6 by proving equivalence, reversibility, and type safety properties of multiple circuits. In this context, the major contributions of this paper are the following:

- (i) A computer-based mathematical model for describing and reasoning about Boolean functions and gate-level combinational circuits is defined. Our formal model is novel as it enables, in addition to Boolean algebra and basic theorems, defining the principle of duality and logic circuits in a computer-based theorem prover. Furthermore, the model together with the basic theorems allows one to mechanize the mathematical manipulation process, which can be checked correctly using computer.
- (ii) Formal proofs of the principle of duality and basic theorems of Boolean algebra are carried out. In the literature, there is no computer-based proof of validity of the principle of duality and proof of basic theorems listed in most popular books such as [29, 36].
- (iii) Formal proofs of equivalence and reversibility of multiple combinational circuits are carried out. To reduce the propagation delay in a multibit adder, a look-ahead carry generator circuit is added using a step-by-step process; however, there is no proof that it does not alter the intended behaviour of the adder. We formally prove that the look-ahead carry generator preserves the functional behaviour of the adder.
- (iv) The performance of the Coq theorem prover over our model is evaluated.

The rest of the paper is organized as follows. In the next section, the significance of interactive theorem proving is highlighted. The tool Coq theorem prover and Boolean

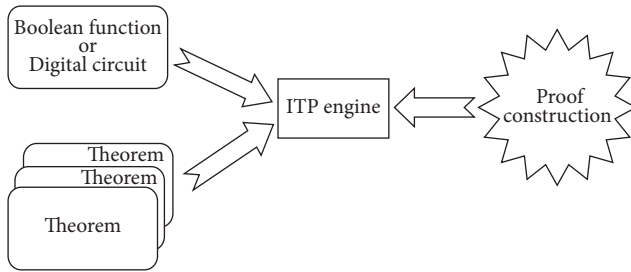


FIGURE 1: Formal verification of Boolean functions and digital circuits [35].

algebra are introduced in Section 3. The formal model based on Boolean algebra is defined in theorem prover in Section 4. Boolean algebra and logic circuits are reasoned about in Sections 5 and 6, respectively. Our formal model is evaluated and results are discussed in Section 7. A critical review of the related work is given in Section 8 and Section 9 concludes the paper. All the Coq source codes are available from our GitHub repository at <https://www.github.com/wilstef/booleanalgebra>.

## 2. Why Interactive Proof Assistant?

A common approach to check the two circuits (represented as Boolean functions) for functional equivalence is to extensively simulate them against many inputs and compare the results. Simulation-based testing is the most popular approach in industry because it is easy to use; however, it fails to ensure absence of faults in the system. Furthermore, simulating systems with large inputs are not computationally feasible; for instance, simulating a 256 bit memory chip would require testing it for  $2^{256}$  possible inputs. Another approach to check correctness of the digital circuits in general, or equivalence checking in particular, is to use formal methods based on computer-based mathematical tools and techniques. The prevailing advantages of formal tools and techniques are that they are rigorous and computer-aided and can be used to formally prove properties for all the possible inputs. Moreover, formal methods based techniques can be used to ensure the absence of faults in the system.

According to a recent survey [35], most of the formal verification methods and tools are based on model checking and automated theorem provers that are restricted by well-known state and memory explosion [37, 38] problems. Formal verification using model checking is popular in industry [39, 40] and well-studied domain by the research community [40–42]; however, the focus of this paper is on interactive theorem proving (ITP) [43–45] approach. In the ITP-based formal approach, a proof engineer guides a computer-based proof assistant, such as Coq and Isabelle/HOL [45], by providing proof commands during the proof process. The ITP-based formal verification, also referred to as semiautomated approach, combines the strengths of manual and automated proofs. This semiautomated ITP approach requires expertise and skills; however, it has been used in the past for investigating large case studies [46]. In

automated theorem proving, it is hard to get insights when a proof attempt fails, while ITP forces the designer to pay attention to even the minor details. This results in understanding the system under study more precisely.

The conventional mathematical proofs on pen and paper (informal) are error-prone and difficult to manage large and complex proofs. Computer-aided verification, on the other hand, is an effective, efficient, and rigorous way of formal specification and verification. Automated theorem provers are widely used in industry as they automatically create proofs without requiring human effort; however, they face problems such as state explosion [37, 38]. Human-assisted theorem provers, on the other hand, require human support to carry out mathematical proofs. A proof engineer guides the theorem prover by providing proof commands and interactively creating proofs. Coq is one such popular interactive proof assistant considered for defining our formal framework.

Mathematical proofs carried out in a human-assisted theorem prover are more organized because of the following reasons: (i) in mechanized theorem prover (such as Coq), the proofs can be divided into modules (to make proof handling easy); (ii) lemmas/theorems already proven can be easily invoked and applied; (iii) the Coq Language of Tactics (Ltac) can be used to combine complex set of proof commands (tactics) in a single tactic; (iv) the proofs can be read and checked by the computer using a proof checker; (v) a new proof can be opened inside an existing unfinished proof; (vi) large proof scripts can be checked for unproved lemmas just by using a single Coq command; and so on. In summary, the proofs in proof assistants such as Coq are more organized as compared to pen-and-paper proof methods and the correctness of the proof scripts can be checked by the computer.

## 3. Background

To mathematically prove the properties of Boolean algebra and verify correctness of digital circuits using computer, the algebra must be defined in the logic of a mechanical (computer-readable) proof assistant such as Coq. Such a formal definition of Boolean algebra is given in Section 4. To understand the formal definition, the Boolean algebra and the formal tool Coq used are introduced in this section. For an in-depth understanding of circuit modelling using Boolean algebra and Coq theorem prover, the readers are recommended to refer to books [29, 47], respectively.

**3.1. Coq Proof Assistant.** Coq [44] is an interactive theorem prover based on the calculus of inductive construction. It is available with a language of specification called Gallina, a type checker and a proof checker. The language, type checker and proof checker are used for creating formal specifications of the systems under test, checking the specifications for type errors, creating and checking formal proofs, respectively. To understand formalizing and proving systems using interactive theorem prover, we define a simple system of numbers using the proof assistant Coq and then give reasoning about the system.



We begin with formally defining numbers inductively as data type `Nat` using the Coq keyword `Inductive` with two constructors for generating elements of the type `Nat` (lines 1–3, Listing 1). The definition `Nat` in this listing states that `0` (for 0) is `Nat` and if `n` is `Nat`, `Succ n` is also `Nat`. The first constructor has no argument and simply states that `0` is a member of type `Nat`. The second constructor `Succ` has one argument of type `Nat` which states that `S` followed by a `Nat` (the `Nat` on left of the arrow) is also a `Nat` (the `Nat` on right of the arrow). The term `Succ (Succ (Succ 0))`, for example, is a `Nat` that corresponds to number 3.

To operate on numbers, we define a recursive function `Add` (lines 5–9) to add values of type `Nat`. The function returns the second argument `m` if the first argument is `0`; otherwise, it returns `Succ (Add n' m)`. A lemma `Add_N_0`, where `Add n 0 = n` holds for any value of `n`, is stated and proven in Listing 1 (lines 11–18). The proof of this lemma has been carried out by applying induction on the construction of the first argument `n`. While carrying out the proof, the Coq tool was interactively guided by giving proof commands called *tactics* (lines 13–17). Many other properties of the `Add` function, such as commutative and associative properties, may also be stated and proven mechanically using the Coq proof assistant.

**3.2. Boolean Algebra.** According to George Boole [19], Boolean algebra is an algebraic structure with a set of values, two binary operations “+” and “.” over the values in the set and proof of Huntington [48] postulates. Later on, Shannon [20] introduced a two-valued version of the algebra to represent properties of the switching circuits. In a two-valued algebra, the set of values include elements 1 and 0 and the two binary operations are conjunction (logical AND) and disjunction (logical OR). In addition, there is a unary operation called negation or complement (NOT).

Using Boolean functions in the two-valued Boolean algebra, logic circuits can be modelled. The function  $F = \bar{x} \cdot \bar{y}$  models a logic circuit where the AND gate represents the product operation and the NOT gate represents the complement operation. When logic circuits are represented with functions, they can be manipulated and reasoned about using tools and techniques developed for Boolean algebra. For example, the algebraic manipulation steps using postulates can be written down in and checked using Coq tool (see Section 5).

Shannon’s two-valued version of the Boolean algebra is defined in Coq theorem prover as described in Listing 2 [47]. The first part of Boolean algebra, a set of two elements, is represented with Coq type `bool` defined using the Coq keyword `Inductive` as shown in Listing 2 (line 1). The two values of the Boolean algebra defined are `true` and `false`.

The second part of Boolean algebra is to define two binary operations over the values of the Boolean type `bool`. The rules for the first operation + (sum) are defined as function `sum` on lines 3–7 in Listing 2. Using pattern matching, the function `sum` gets two values of type `bool` and returns value `false` if both input values are `false`; otherwise, it returns `true`. The rules for the second binary

operation . (product) are defined in function `prod` (lines 9–13, Listing 2). This function returns `true` only if the two input values are `true`; otherwise, it returns `false`. A unary operation `complement` on elements of Boolean set is defined in the function `not` on lines 15–19 in the listing. Given one value as the input, `not` returns the other value. Among these operations, the operation `¬` has the highest and `+` has the lowest precedence.

## 4. Formalizing Logic Circuits and Boolean Algebra

The Boolean algebra defined in Section 3 is extended and tailored towards combinational circuit definitions. To begin with, the set of notations in Listing 3 is extended with symbol  $\oplus$  (Listing 4) for xor operation with same precedence as (operation `prod`). The formal definitions of logic operations `sum`, `prod`, `xor`, and `not` model the basic logic components OR, AND, XOR, and NOT gates, respectively. After formally modelling these basic logic components, they are combined together to form combinational circuits. A combinational circuit is defined as a list of Boolean (functions) values (Listing 5).

The list “ $F^1 \ x \ y :: F^2 \ x \ y :: nil$ ” represents a combinational circuit with two inputs `x` and `y` and two outputs defined as two Boolean functions. To evaluate each Boolean function in the list to a Boolean value, an evaluation function `eval_cir` is defined in Listing 6. The function takes a combinational circuit as list of Boolean functions and returns a list of Boolean values (Listing 7).

The final requirement of Boolean algebra is to formalize the six Huntington postulates [29, 48] and prove the set of all basic theorems. Formal definitions of Huntington postulates are included in the Coq script available from our repository. Furthermore, the formal definitions of operation `sum`, `prod`, and `not` are sufficient to reason about Huntington postulates and all the basic theorems except principle of duality (discussed in Section 5). As the derivation in principle of duality requires operating on the Boolean expressions, the principle cannot be defined in the current setting. The existing definitions of expressions do not differentiate between variables and values (identity elements), which is the basic requirement of operation in the duality. To do this, a type `exp` for Boolean expressions is defined as shown in Listing 8. The first three constructors (line 2–4) correspond to the three logical operations `sum`, `prod`, and `not`, respectively. The last constructor converts a Boolean term, variable, or value to an expression.

All the postulates and basic theorems, except the *closure*, *involution*, and *consensus*, have two parts: one part is for the operation + (sum) and the other is for . (prod). According to the *principle of duality*, one part of the postulate/theorem can be derived from the other if the operators and the identity elements are interchanged. The duality principle is significant in proving the theorems using postulates and in algebraic manipulation. In particular, when the proof of one part of a theorem is given, the other can easily be carried out following the principle of

```

(1) Inductive Nat : Type :=
(2)   |O : Nat
(3)   |Succ : Nat → Nat.
(4) Fixpoint Add (n m : Nat) : Nat :=
(5)   match n with
(6)   |O ⇒ m
(7)   |Succ n' ⇒ S (Add n' m)
(8)   end.
(9) Lemma Add_N_O : ∀ n : Nat, Add n O = n.
(10) Proof.
(11)   induction n.
(12)   (*CASE 1: n is O*)
(13)     reflexivity.
(14)   (*CASE 2: n is (S n)*)
(15)     simpl. rewrite IHn. auto.
(16)   Qed.

```

LISTING 1: Example of interactive formal proof in Coq.

```

(1) Inductive bool : Type := true | false.
(2) Definition sum (x y : bool) : bool :=
(3)   match x, y with
(4)   | false, false ⇒ false
(5)   | _, _ ⇒ true
(6)   end.
(7) Definition prod (x y : bool) : bool :=
(8)   match x, y with
(9)   | true, true ⇒ true
(10)  | _, _ ⇒ false
(11)  end.
(12) Definition not (x : bool) : bool :=
(13)   match x with
(14)   | false ⇒ true
(15)   | true ⇒ false
(16)   end.
(17) Definition circuit := list bool.

```

LISTING 2: Formal definition of Boolean operations.

```

(1) Notation "x + y" := (sum x y)
(2)   (at level 50, left associativity) : bool_scope.
(3) Notation "x * y" := (prod x y)
(4)   (at level 40, left associativity) : bool_scope.
(5) Notation "¬x" := (not x) (at level 30, right associativity) : bool_scope.
(6) Notation "[ x ; .. ; y ]" := (cons x .. (cons y nil) ..).

```

LISTING 3: Shorthand notations.

```

(1) Notation "x ⊕ y" := (x * ¬y + ¬x * y)
(2)   (at level 40, left associativity) : bool_scope.

```

LISTING 4: Notation for operation xor.

```
(1) Definition circuit := list bool.
```

LISTING 5: Definition of circuit.

```
(1) Fixpoint eval_cir (c: circuit): list bool :=
(2) match c with
(3) | nil => nil
(4) | cons c tl => cons c (eval_cir tl)
(5) end.
```

LISTING 6: Function eval\_cir for evaluating circuit.

```
(1) Definition F(x y: bool): circuit := ¬x*¬y::nil.
```

LISTING 7: Example of circuit description in Coq notations.

```
(1) Inductive exp: Type :=
(2) | sumexp: exp → exp → exp
(3) | prodexp: exp → exp → exp
(4) | compexp: exp → exp
(5) | bexp: bool → exp.
```

LISTING 8: Definition of data type exp.

duality. The derivation carried out this way is believed to be valid according to the principle of duality in literature and textbooks [29]; however, no formal proof has been provided. We bridge this gap by providing a formal proof of duality principle.

A function `changeident` (Listing 9) is defined to interchange identity elements in the Boolean expression. It gets an expression and swaps the identity elements `true` and `false` and leaves the operators and variables unchanged. The keyword `Fixpoint` is used to define recursive functions. Another operation for interchanging operators is defined as a recursive function `changeop` in Listing 10. Similarly, the function `changeop` gets an expression and swaps the operators `sum` and `prod`.

## 5. Formal Proofs of Boolean Algebra

The formal definitions in Section 4 enable one to formally reason about both Boolean algebra and combinational circuits described as Boolean functions. This section contains proof of duality principle and demonstrates with examples that our formal setting mechanizes the informal algebraic manipulation used in textbooks on Digital Logic Design. Furthermore, all the basic theorems and postulates have been defined and proven in Coq and given in the Coq script available from our repository.

```
(1) Fixpoint changeident (e: exp): exp :=
(2) match e with
(3) | trueexp => falseexp
(4) | falseexp => trueexp
(5) | bexp e' => e
(6) | sumexp e1 e2 =>
(7)   sumexp (changeident e1) (changeident e2)
(8) | prodexp e1 e2 =>
(9)   prodexp (changeident e1) (changeident e2)
(10) | compexp e' => compexp (changeident e')
(11) end.
```

LISTING 9: Function changeident for interchanging identity elements.

```
(1) Fixpoint changeop (e: exp): exp :=
(2) match e with
(3) | sumexp e1 e2 => prodexp e1 e2
(4) | prodexp e1 e2 => sumexp e1 e2
(5) | _ => e
(6) end.
```

LISTING 10: Function changeop for interchanging operators.

*5.1. Principle of Duality.* The duality principle states that expressions derived from postulates by interchanging the operators (`+` and `.`) and identity elements (`0` and `1`) are valid. After defining the interchange operations over the Boolean expressions, the duality principle can now be stated as a lemma as shown in Listing 11. The lemma states that if a part of theorem holds (two arbitrary expressions are equal), then it implies that the second part of the theorem can be derived by changing the identity elements and operators. To check that the duality property can be used in proofs, given the first part of commutative property ( $x + y = y + x$ ), the second part of commutative property ( $x \cdot y = y \cdot x$ ) is proven (Listing 12) by applying the duality property.

*5.2. Mechanizing Algebraic Manipulation.* To get simplified logic circuit, the number of literals and terms must be reduced in the description of the circuit. The algebraic manipulation method is one of the most popular methods used in textbooks [29] for this purpose. This kind of manipulation is informal and hence is error prone. The formal structure including the postulates and basic theorems defined in previous sections can be applied, as in the informal algebraic manipulation, using Coq proof assistant. The main advantage of mechanizing algebraic manipulation in proof assistant is that proof scripts can be mechanically read, checked, and maintained.

To demonstrate that our formal framework is fit for mechanically checking correctness of algebraic manipulation, proof of the theorem `absorption_sum` has been listed in Listing 13. This proof is carried out by applying (using the `rewrite` tactic) the postulates and theorems. This proof

```

(1) Lemma duality:  $\forall$  lhs rhs,
(2)   lhs = rhs  $\longrightarrow$ 
(3)   changeop (changeident lhs) = changeop (changeident rhs).

```

LISTING 11: Lemma stating the duality property.

```

(1) Lemma duality_check:  $\forall$  x y,
(2)   sumexp (bexp x) (bexp y) = sumexp (bexp y) (bexp x)  $\longrightarrow$ 
(3)   prodexp (bexp x) (bexp y) = prodexp (bexp y) (bexp x).

```

LISTING 12: Example of proof using the duality property.

```

(1) Lemma absorption_sum:  $\forall$  x y,  $x + x * y = x$ .
(2)   Proof.
(3)     intros.
(4)     pattern x at 1.
(5)     rewrite  $\longleftarrow$  pos_identity_prod.
(6)     rewrite  $\longleftarrow$  pos_dist_over_sum.
(7)     rewrite  $\longleftarrow$  pos_comm_sum.
(8)     rewrite identity_sum_1.
(9)     rewrite pos_identity_prod.
(10)    auto.
(11)    Qed.

```

LISTING 13: Proof of absorption law (sum).

script is a mechanized version of the informal proof of Theorem 6 (a) in the textbook [29].

Proof of the second part `abroption_prod` of the same theorem is believed to hold by the duality principle. This principle has been proven to hold in the above section. Every postulate or basic theorem has two parts, where one is the dual of the other. This is interesting to show that, given step-by-step proof of one theorem, proof of the other (dual) part can be carried out by applying the dual of postulate/theorem applied at the corresponding step. The proof of the theorem `abroption_prod` (dual of theorem `absorption_sum`) has been listed in Listing 14. The postulates/theorems applied on lines 5–9 in both proofs are the dual of each other.

## 6. Describing and Verifying Combinational Circuits

UAVs or drones are like flying computers with Linux or Windows operating system, flight controllers, main boards, memory units, and thousands of lines of programmable code. Formal methods, and in particular our framework, can be applied to the analysis of UAVs in different ways. As mentioned, it is a complex computer system, and hence formal techniques can be used to verify the operating system, protocols, logic components, memory units, and any algorithm used in the UAV system. As arithmetic and logic components (e.g., adder and comparator) and memory (e.g.,

ROM) are the main components of any typical computer (including UAVs), we apply our formal framework to analyse a memory and an adder circuit. In this section, functional equivalence and reversibility properties of few combinational circuits are proven. Furthermore, it is also proven that all the described circuits hold the basic reliability property called type-safety.

*6.1. Verifying Equivalence of Memory Circuits.* To begin with, a 32×8 ROM memory chip with content *Trusted designs*, stored as the ASCII data on the first sixteen locations, is specified in a truth table as shown in Table 1 (entries for the first 16 inputs are defined and shown in the table. The rest of entries are *do not care* conditions.). The letters A–E represent the five-bit input (adders lines) and O<sub>7</sub>–O<sub>0</sub> show the eight-bit output (data lines) of the memory. The table specifies the input-output relationship: a five-bit input selecting any of the first sixteen locations; the chip returns ASCII code of a letter of the content *Trusted designs*.

To design the memory chip, first each output of the memory chip is defined as a Boolean function of the five input variables A–E. A function for each output is formed by combining (through operator +) all the minterms, where the value of the corresponding output column is 1. This would result in eight Boolean functions O<sub>7</sub> – O<sub>0</sub>, represented in *sum-of-minterms* [29, 36] forms, as shown in Listing 15 (the

```

(1) Lemma abroption_prod:  $\forall x y, x * (x + y) = x.$ 
(2) Proof.
(3)   intros.
(4)   pattern x at 1.
(5)   rewrite  $\leftarrow$  pos_identity_sum.
(6)   rewrite  $\leftarrow$  pos_dist_over_prod.
(7)   rewrite  $\leftarrow$  pos_comm_prod.
(8)   rewrite identity_prod_0 with (x := y).
(9)   rewrite pos_identity_sum.
(10)  auto.
(11)  Qed.

```

LISTING 14: Proof of absorption law (product).

TABLE 1: Truth table for  $32 \times 8$  ROM chip.

Address					Data								Symbol
A	B	C	D	E	O <sub>7</sub>	O <sub>6</sub>	O <sub>5</sub>	O <sub>4</sub>	O <sub>3</sub>	O <sub>2</sub>	O <sub>1</sub>	O <sub>0</sub>	
0	0	0	0	0	0	1	0	1	0	1	0	0	"T"
0	0	0	0	1	0	1	1	1	0	0	1	0	"I"
0	0	0	1	0	0	1	1	1	0	1	0	1	"u"
0	0	0	1	1	0	1	1	1	0	0	1	1	"s"
0	0	1	0	0	0	1	1	1	0	1	0	0	"t"
0	0	1	0	1	0	1	1	0	0	1	0	1	"e"
0	0	1	1	0	0	1	1	0	0	1	0	0	"d"
0	0	1	1	1	0	0	1	0	0	0	0	0	"d"
0	1	0	0	0	0	1	1	0	0	1	0	0	"e"
0	1	0	0	1	0	1	1	0	0	1	0	1	"s"
0	1	0	1	0	0	1	1	0	1	0	0	1	"i"
0	1	0	1	1	0	1	1	0	0	1	1	1	"g"
0	1	1	0	0	0	1	1	0	1	1	1	0	"n"
0	1	1	0	1	0	1	1	0	1	1	1	0	"s"
0	1	1	1	0	0	1	1	1	0	0	1	1	"s"
0	1	1	1	1	0	0	1	0	1	1	1	0	"."

product and sum terms of each function are given in the source code.). The  $32 \times 8$  ROM chip is defined (Listing 16) as list of seven Boolean functions in Listing 15. This is a  $5 \times 8$  combinational circuit with five inputs and eight outputs. The five-input bits of the chip identify one of the  $2^5$  memory locations and the output lines give the 8-bit ASCII code of the character stored at that location.

To design a simple and efficient memory chip, all the eight functions (for outputs  $O_7-O_0$ ) are simplified using K-map method to functions  $O_7-O_0$  as shown in Listing 17. The simplified Boolean functions have fewer literals and terms (Listing 17) as compared to original functions (Coq Definitions  $O_7-O_0$  in source code) and would produce a simple and efficient circuit layout (see Section 7 for a circuit layout example). The simplified Boolean functions in Listing 17 representing outputs of the memory chip are combined together in a list to form the simplified combinational circuit as shown in Listing 18.

The formal model of the combinational circuit in Listing 16 has been simplified following the well-known simplification method K-map to circuit in Listing 18; however, it is not guaranteed that the circuits are functionally equivalent. In other words, there is no mathematical guarantee that the

```

(1) Definition O7(A B C D E : bool) : bool := false.
(2) Definition O6(A B C D E : bool) : bool :=
(3)    $\sum(0-6, 8-14).$ 
(4) Definition O5(A B C D E : bool) : bool :=
(5)    $\sum(1-15).$ 
(6) Definition O4(A B C D E : bool) : bool :=
(7)    $\sum(0-4, 10, 14).$ 
(8) Definition O3(A B C D E : bool) : bool :=
(9)    $\sum(11, 13, 15).$ 
(10) Definition O2(A B C D E : bool) : bool :=
(11)   $\sum(0, 2, 4-6, 8, 9, 12, 13, 15).$ 
(12) Definition O1(A B C D E : bool) : bool :=
(13)   $\sum(1, 3, 10, 12-15).$ 
(14) Definition O0(A B C D E : bool) : bool :=
(15)   $\sum(2, 3, 5, 9-12, 14).$ 

```

LISTING 15: Boolean functions for ROM outputs  $O_7-O_0$ .

K-map simplification process has not altered the original behaviour of the circuit. The initial design built from the truth table specification serves as the "golden" or "reference" design. To prove the simplified circuit is functionally equivalent to the "golden" design, the individual functions are proven to be equivalent in Theorem 1 (this theorem corresponds to a set of eight lemmas `equiv_00' 0-equiv_v_00' 7` in Coq script.). Functional equivalence of the two circuits is checked in Theorem 2. The theorem states that the circuit *before* simplification is equivalent to the circuit *after* simplification, which guarantees that the simplification process preserves the functionality.

**Theorem 1 (Equivalence of Boolean Functions):** For any function  $O_i$ , where  $i=0, 1, 2, \dots, 7$ , Boolean function simplification operation  $S_f$  and functional equivalence relation  $\approx$ ,  $O_i \approx S_f(O_i)$ .

**Proof:** This theorem is proven using case analysis on the Boolean variables used. The Coq proof of this theorem is listed at our GitHub repository at <https://github.com/wilstef/booleanalgebra>.

**Theorem 2 (Functional Equivalence of Circuits):** The combinational circuit  $C$  described in Listing 16 and its simplified version  $C_s$  in Listing 18 are functionally equivalent. More formally,  $C \approx C_s$ , where  $C_s = S_{Kmap}(C)$  and  $S_{Kmap}$  is K-map simplification operation.

**Proof:** This theorem is proven by applying (rewriting) the eight lemmas already proven in Theorem 1. The Coq proof of this theorem is listed at our GitHub repository at <https://github.com/wilstef/booleanalgebra>.

## 6.2. Verifying Equivalence of Combinational Circuits.

Arithmetic component, such as adder, is an integral part of the arithmetic and logic unit (processor) of any micro-processor-based system. To design energy-efficient and fast components, their design description (normally in a description language) is often transformed and mathematically manipulated. However, it must be ensured that such transformations do not alter the intended behaviour of these components. This surety is even more necessary when the

```
(1) Definition ROM32x8_orig (A B C D E: bool): circuit :=
(2)   O7 A B C D E::O6 A B C D E::O5 A B C D E::O4 A B C D E::O3 A B C D E::O2 A B C D E::
(3)   O1 A B C D E::O0 A B C D E::nil.
```

LISTING 16: Formal definition of  $32 \times 8$  ROM chip.

```
(1) Definition O'7(A B C D E:bool) : bool := false.
(2) Definition O'6(A B C D E:bool) : bool :=
(3)    $\neg C + \neg D + \neg E$ .
(4) Definition O'5(A B C D E:bool) : bool :=
(5)    $B + C + D + E$ .
(6) Definition O'4(A B C D E:bool) : bool :=
(7)    $\neg B * \neg C + \neg B * \neg D * \neg E + B * D * \neg E$ .
(8) Definition O'3(A B C D E:bool) : bool :=
(9)    $B * C * E + B * D * E$ .
(10) Definition O'2(A B C D E:bool) : bool :=
(11)   $\neg B * \neg E + B * \neg D + C * \neg D + \neg D * \neg E + B * C * E$ .
(12) Definition O'1(A B C D E:bool) : bool :=
(13)   $\neg B * \neg C * E + B * C + B * D * \neg E$ .
(14) Definition O'0(A B C D E:bool) : bool :=
(15)   $\neg B * C * \neg D * E + \neg C * D + B * \neg C * E + B * C * \neg E$ .
```

LISTING 17: Simplified Boolean functions for ROM outputs.

```
(1) Definition ROM32x8_simpl (A B C D E: bool): circuit :=
(2)   O'7 A B C D E::O'6 A B C D E::O'5 A B C D E::O'4 A B C D E::O'3 A B C D E::O'2 A B C D E::O'1 A B C D E::O'0 A B C D E::nil.
```

LISTING 18: Formal definition of  $32 \times 8$  ROM chip (simplified).

component being designed is used in critical systems, such as UAVs. To demonstrate that our formal definitions can also be used to prove functional equivalence of two combinational circuits, we describe two versions of a Binary Coded Decimal (BCD) adder (Figure 2) in Coq. Such a BCD adder has been designed and described in the popular textbook [29] on the subject Digital Logic Design; however, no formal proof of equivalence has been provided.

A BCD adder adds two decimal digits and their sum results as a BCD number. A 4-bit BCD adder may be designed using two 4-bit binary parallel adders as shown in Figure 2 (right). The conventional 4-bit binary adder, comprised of four full adders, is a serial adder that adds two 4-bit binary numbers in serial fashion. Each full adder gets two bits (the augend and addend bits) and an input carry bit and gives a sum bit and an output carry bit. The output carry of one full adder is given as input carry to the next one and the input carry of the first (right most) adder is set to logic 0. The output carry of the last adder is the output carry of the 4-bit binary adder.

The initial carry, given as input to the first adder, propagates to the last adder, which results in a *propagation delay*. To avoid this propagation delay in the binary adder, a look-ahead carry generator [29] is used to predict the input

carries. The look-ahead carry generator is a small-scale integrated circuit added in front of the 4-bit adder to make it fast. The transformation avoids propagation delay; however, no formal proof that the functional properties of the adder are preserved is provided. In this section, we formally prove that two implementations of the BCD adder (Figure 2), one with and the other without look-ahead carry generator circuit, are functionally equivalent.

First, we design a BCD adder using binary adders without look-ahead carry generator. The 4-bit parallel full adder `FA4bit` is defined as a function in Listing 19. It applies the full-adder function `fa` to the 4-bit pairs of the two 4-bit numbers and input carry (inputs `D-A`, `d-a` and `e`), and returns a 5 bit tuple. The first bit in the tuple is the final carry and the next four bits are the sum bits. The binary adder `FA4bit` is used to implement the BCD adder as shown in Listing 20. The let-expressions on lines 2, 3, and 4 calculate the result of the first binary adder, output carry, and second binary adder, respectively. The additional circuitry between the two binary adders is needed to generate the output carry of the BCD adder and to adjust the sum of the first binary adder to BCD sum.

To generate a BCD adder with look-ahead carry generator, we must first design binary parallel adder with look-ahead

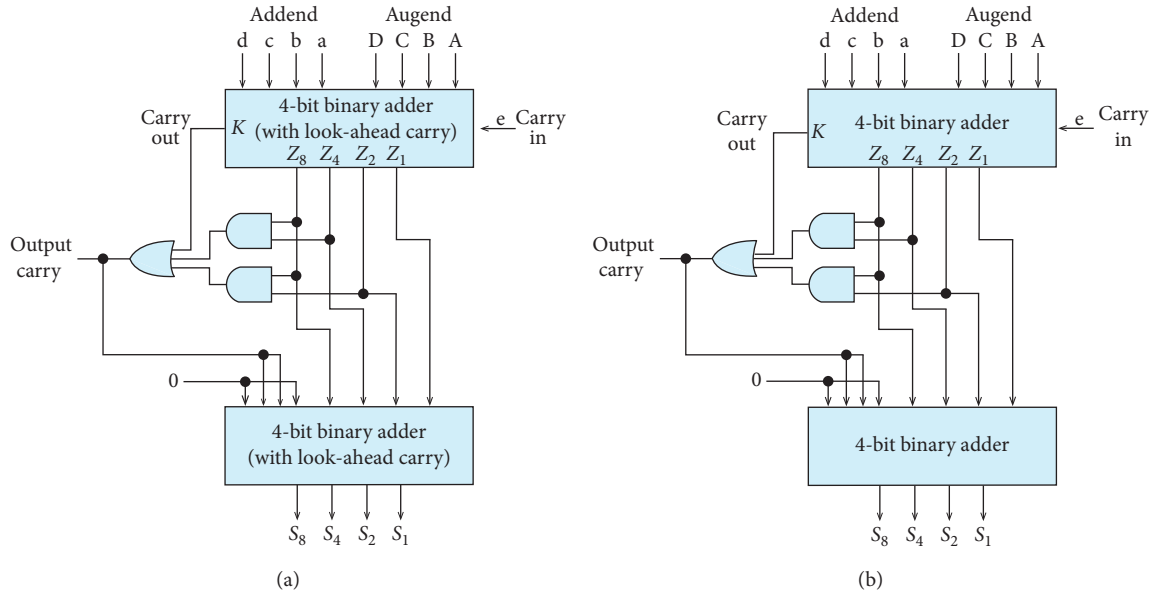


FIGURE 2: Block diagrams of two versions of a BCD adder. The BCD adder on the left is with look-ahead carry generator and the one on the right is without look-ahead carry generator [29].

```

(1) Definition fa (a A e: bool) : (bool * bool) :=
(2)   (A * a + (A ⊕ a) * e, A ⊕ a ⊕ e).
(3) Definition FA (f: bool → bool → bool → (bool * bool)) (a A e: bool)
(4) : (bool * bool) := fa a A e.
(5) Definition FA4bit (D C B A d c b a e: bool)
(6) : (bool * bool * bool * bool * bool) :=
(7) let ss1 := snd(FA fa a A e) in
(8) let cc1 := fst(FA fa a A e) in
(9) let ss2 := snd(FA fa b B cc1) in
(10) let cc2 := fst(FA fa b B cc1) in
(11) let ss3 := snd(FA fa c C cc2) in
(12) let cc3 := fst(FA fa c C cc2) in
(13) let ss4 := snd(FA fa d D cc3) in
(14) let cc4 := fst(FA fa d D cc3) in
(15) (cc4, ss4, ss3, ss2, ss1).

```

LISTING 19: Formal definition of 4-bit binary parallel adder (without look-ahead carry).

```

(1) Definition BCDadder (D C B A d c b a e: bool) : circuit :=
(2) let t1 := FA4bit D C B A d c b a e in
(3) let outcarry := FST t1 + (SND t1) * (TRD t1) + (SND t1) * (FRT t1) in
(4) let t2 :=
(5)   FA4bit (SND t1) (TRD t1) (FRT t1) (FFT t1) false outcarry outcarry false e in
(6) [outcarry; SND t2; TRD t2; FRT t2; FFT t2].

```

LISTING 20: Formal definition of 4-bit BCD adder (without look-ahead carry).

carry generator. Formal definition of a 4-bit binary parallel adder has been listed in Listing 21. The definitions C2–C5 (lines 1–7) calculate the four output carries of the four full adders in the binary adder. Unlike the adder FA4bit, every

internal output carry is independent of the output carry of the previous full adder. This allows every full adder to produce output sum simultaneously without waiting for the output carry from the previous adder. The definitions S1–S4

calculate the four sum bits in terms of the look-ahead carry bits C2–C5 and initial carry e. Finally, the 4-bit binary parallel adder with look-ahead carry generator is defined as a function `FA4bitLA` (lines 17–20). As in `BCDadder`, two instances of binary parallel adder `FA4bitLA` are combined together with the additional circuitry for output carry to form a BCD adder. The formal definition of 4-bit BCD adder with look-ahead carry generator has been shown in Listing 22. Readers are advised to refer to books [29, 36] for further details about BCD adder and look-ahead carry generator.

The formal definitions `BCDadderLA` and `BCDadder` model 4-bit BCD adders with and without look-ahead carries, respectively. Their functional equivalence is stated in theorem `check_equiv_BCD_adder` in Listing 23. The theorem states that both adders produce equal outputs for all equal inputs. This theorem is proven using case analysis on the input variables. The formal proof of Theorem `check_equiv_BCD_adder` demonstrates that our framework can effectively be used to check equivalence of combinational circuits other than memory circuits.

**6.3. Proof of Reversibility Property.** To demonstrate that our formal framework can also be used to verify properties other than equivalence, we formally verify reversibility of a simple circuit description. To this end, we prove that the circuit `Circuit` defined in Listing 24 is reversible. The theorem `reversible_circuit` states that, for all different (2-bit) inputs, the outputs are different. Additionally, this theorem also states that the numbers of inputs and outputs are the same. In this theorem, the lists `[w; x]` and `[y; z]` on line 4 in Listing 24 model the inputs.

## 7. Evaluation and Discussion

Automated tools, such as model checkers, sometimes stuck due to memory or state explosion problems [38] and never return. To evaluate the performance of Coq tool running over our framework, we tested the Coq proof checker to check proof scripts of functional equivalence of Boolean functions with multiple Boolean variables. The results in Figure 3 show that the Coq proof checker takes around 12 seconds to check proof scripts for functional equivalence with functions up to 45 variables (over a billion input cases).

The formal model developed in Coq provides a formal foundation for defining and reasoning about Boolean functions and logic circuits using the calculus of constructions behind the Coq theorem prover. The following is a list of the major advantages of our formal model:

- (i) Boolean function definitions or models of logic circuits can be automatically checked (for type errors) by the Coq type checker.
- (ii) The correctness of the mathematical manipulation used in the analysis of Boolean functions can be checked automatically.
- (iii) Properties, such as principle of duality, functional equivalence, and reversibility, of Boolean algebra

and (models of) logic circuits can be proven interactively using the Coq theorem prover.

- (iv) All the proofs carried out can be mechanically checked by the Coq proof checker using computer.

Formal verification using proof assistant is very tedious and requires expertise; however, many researchers have recently used proof assistants to build formal languages and frameworks for hardware verification [49–53]. Proof assistants include benefits of both manual and automated theorem provers and are more powerful and expressive [50]. Our framework allows defining Boolean functions and combinational circuits in a natural style similar to that used in many popular textbooks [29, 36] and most of the proofs can be carried out easily by applying Coq's `destruct` tactic.

## 8. Related Work

The most common approach to reliable digital circuit design is to test designs using simulators such as VCS [54] and Icarus [55] by providing all possible inputs. While simulation-based verification can show presence of errors, it fails to guarantee their absence [56]. Approaches based on formal verification [57], such as *model checking* [32, 58, 59] and *theorem proving* [49, 52, 53, 60, 61], are more popular in the literature. Readers are recommended to refer to [62] for a detailed comparison of simulation and formal method-based approaches. Tools based on model checking can be used to check equivalence of two functions (models); however, they are constrained by the popular *state explosion* [37, 38] problem. There is a body of research works in the literature on formal verification of software systems [63–65]; however, literature review of hardware verification and simulation tools for checking Boolean functions equivalence is included in this section.

**8.1. Formal Hardware Verification.** As mentioned earlier, tools and techniques based on formal methods can be used to prove absence of faults in hardware components. Osman et al. [51] defined a formal framework in the higher-order logic of HOL theorem prover for proving reliability property of combinational circuits. While their work is mainly tailored towards checking reliability property, our framework facilitates functional equivalence checking in a stronger and expressive logic calculus of inductive constructions of Coq theorem prover [50]. Kabat et al. [66] advocate the use of automated theorem provers for the synthesis of combinational logic. They used demodulation as the rewriting logic to simplify canonical circuit structures. Automated theorem provers are more popular in industry; however, they are not as powerful and expressive as proof assistants. Proof assistants, on the other hand, combine the benefits of automated and manual theorem provers and are currently investigated and encouraged for hardware verification [50, 51]. The work in [50] highlights the effectiveness and power of interactive theorem prover Coq in hardware verification which further supports our framework embedded in Coq for logic circuit verification. While their work is more focused towards synthesis based on Coq's code



```

(1) Definition C2(D C B A d c b a e: bool) := A * a + (A ⊕ a) * e.
(2) Definition C3(D C B A d c b a e: bool) :=
(3)   B * b + (B ⊕ b) * (A * a) + (B ⊕ b) * (A ⊕ a) * e.
(4) Definition C4(D C B A d c b a e: bool) :=
(5)   C * c + (C ⊕ c) * (B * b) + (C ⊕ c) * (B ⊕ b) * (A * a) + (C ⊕ c) * (B ⊕ b) * (A ⊕ a) * e.
(6) Definition C5(D C B A d c b a e: bool) :=
(7)   D * d + (D ⊕ d) * (C4 D C B A d c b a e).
(8) Definition S1(D C B A d c b a e: bool) := (A ⊕ a) ⊕ e.
(9) Definition S2(D C B A d c b a e: bool) :=
(10)  (B ⊕ b) ⊕ (C2 D C B A d c b a e).
(11) Definition S3(D C B A d c b a e: bool) :=
(12)  (C ⊕ c) ⊕ (C3 D C B A d c b a e).
(13) Definition S4(D C B A d c b a e: bool) :=
(14)  (D ⊕ d) ⊕ (C4 D C B A d c b a e).
(15) Definition FA4bitLA (D C B A d c b a e: bool)
(16) : (bool * bool * bool * bool * bool) :=
(17)  (C5 D C B A d c b a e, S4 D C B A d c b a e, S3 D C B A d c b a e,
(18)  S2 D C B A d c b a e, S1 D C B A d c b a e).

```

LISTING 21: Formal definition of 4-bit binary parallel adder (with look-ahead carry).

```

(1) Definition BCDadderLA (D C B A d c b a e: bool): circuit :=
(2)   let t1 := FA4bitLA D C B A d c b a e in
(3)   let outcarry := FST t1 + (SND t1) * (TRD t1) + (SND t1) * (FRT t1) in
(4)   let t2 :=
(5)     FA4bitLA (SND t1) (TRD t1) (FRT t1) (FFT t1) false outcarry outcarry false e in
(6)   [outcarry; SND t2; TRD t2; FRT t2; FFT t2].

```

LISTING 22: Formal definition of 4-bit BCD adder (with look-ahead carry).

```

(1) Theorem check_equiv_BCD_adder: forall D C B A d c b a e,
(2)   BCDadder D C B A d c b a e = BCDadderLA D C B A d c b a e.

```

LISTING 23: Proof of equivalence of BCD adders (with and without look-ahead carry).

```

(1) Definition Circuit(w x: bool): circuit := [¬w; ¬x].
(2) Theorem reversible_circuit: for all w x y z,
(3)   [w; x] <> [y; z] →
(4)   (Circuit w x) <> (Circuit y z)
(5)   ∧ length [w; x] = length (Circuit w x)
(6)   ∧ length [y; z] = length (Circuit y z).

```

LISTING 24: Proof of reversibility.

extraction feature, our work embeds Boolean algebra as a gate-level description language for circuit's description. Our gate-level description language provides a general framework for describing combinational circuits. Furthermore, we build metatheory for expressing and proving duality principle and carry out proofs of basic theorems of Boolean algebra.

Meredith et al. [67] defined executable semantics for Verilog by embedding it in the tool Maude [68] with

rewriting logic as the underlying logic. Inspired from [67], Wilayat et al. [49, 69] introduced a formal language, VeriFormal: a hardware description language with mathematical foundation. VeriFormal is a formal replica of description language Verilog deeply embedded in Isabelle/HOL theorem prover. VeriFormal and the formal simulator available with it were used later to prove functional equivalence of multiple logic circuits [70]. Braibant et al. [71] defined Fe-Si by deeply embedding the simplified version of functional

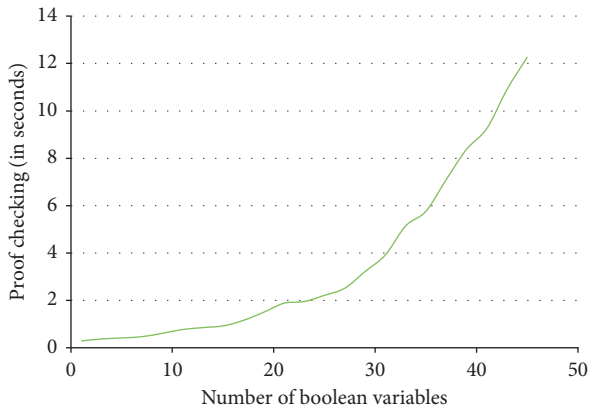


FIGURE 3: Performance evaluation.

hardware description language Bluespec in theorem prover Coq. Building upon the concepts behind proof-carrying code, Love et al. [72] implemented a framework by formalizing a synthesizable subset of Verilog in proof assistant Coq. Some researchers [52, 60] targeted programmable logic controllers by formalizing the semantics of the programming languages used in the controllers, while others specified circuits as operations on bit-vectors. Coquet [53] is a high-level specification of circuits using deep embedding; however, this level of abstraction is achieved through advanced types, such as parametric types, which makes the formal definitions of circuits short but with increased complexity. All these research contributions add formal verification at higher level of abstraction, while our work analyses the circuits at gate level. Formal verification at higher levels, such as register-transfer level, is equally important but the main focus of this paper is to target circuits at gate level. Furthermore, in addition to reasoning about digital circuits, our Coq framework can effectively be used to reason about Boolean algebra as well.

**8.2. Boolean Equivalence Checking Tools.** There are a number of other tools developed specifically for Boolean functions manipulation. Ronjom et al. [23] developed an online database of Boolean functions. Their tool can be used to check different properties of a Boolean function and convert between different representations. The WolframAlpha computational engine [21] translates logical function as input to a truth table and different minimal forms. Moreover, the tool generates a Venn diagram and logic circuit for the input function. The WolframAlpha engine has been included as Boolean algebra calculator by the company TutorVista. Another tool [22] was developed to minimize Boolean functions using Karnaugh maps [26]. The function can be entered as a sequence of notations or as a truth table (up to six variables).

Among the most recent tools is 32x8 [25] which has been built for logic circuit simplification. It accepts a function (up to eight variables) in the form of a truth table and returns a Karnaugh map, Boolean function (as sum of product or product of sums), truth table, and logic circuit for the input. Lean and Marxel developed a solver, QMSolver [24], based on Quine-McCluskey algorithm for simplification of Boolean functions. The solver gets number of minterm indices

(separated by spaces) and returns a simplified function. All these tools manipulate circuits at gate level; however, none of them have formal foundation and hence the manipulation of circuit designs cannot be proven correct.

## 9. Conclusions

When (model of) a logic circuit is transformed or mathematically manipulated (most often for optimization purposes), it must be guaranteed that the transformation does not alter the desired behaviour of the circuit. In this paper, a formal framework for describing and verifying Boolean functions and logic circuits at gate level was defined in the Coq theorem prover. To demonstrate the significance of the framework, basic theorems of the Boolean algebra and the duality principle were proven. Furthermore, multiple basic hardware components were described in the formal notations and functional equivalence and reversibility properties were verified. Our formal developments can be used to describe other logic components used in critical systems and can be formally proven correct using the Coq theorem prover tool.

As a future work, we plan to build a translator to automatically translate circuit designs as Boolean functions in a natural style to the formalized (in Coq) Boolean algebra. Furthermore, to complete a formal electronic design flow, we intend to build a logic synthesis tool for translation from formal register-transfer level representation of the circuit (e.g., in VeriFormal, [49, 69]) to gate-level representation as Boolean functions.

## Abbreviations

ROM:	Read-only memory
RTL:	Register-Transfer Logic
ITP:	Interactive theorem proving
HOL:	Higher Order Logic
ASCII:	American Standard Code for Information Interchange
HDL:	Hardware description language
BCD:	Binary-coded decimal
S:	K-map simplification operation
$\approx$ :	Function equivalence relation.

## Data Availability

The Coq script data used to support the findings of this study have been deposited in the GitHub repository at <https://github.com/wilstef/booleanalgebra>.

## Conflicts of Interest

The authors declare that there are no conflicts of interest regarding the publication of this article.

## Acknowledgments

The authors would like to extend their sincere appreciation to the Deanship of Scientific Research at King Saud University, Saudi Arabia, for partially funding this

research through the Research Group Project no. RGP-214.

## References

- [1] F. Al-Turjman, "A novel approach for drones positioning in mission critical applications," *Transactions on Emerging Telecommunications Technologies*, p. e3603, 2019.
- [2] F. Al-Turjman and S. Alturjman, "5G/IoT-enabled UAVs for multimedia delivery in industry-oriented applications," *Multimedia Tools and Applications*, vol. 78, pp. 1–22, 2018.
- [3] F. Al-Turjman, M. Abujubbeh, A. Malekloo, and L. Mostarda, "UAVs assessment in software-defined IoT networks: an overview," *Computer Communications*, vol. 150, pp. 519–536, 2020.
- [4] V. Arumugham, *Vaccine Safety: Learning from the Boeing 737 MAX Disasters*, CERN European Organization for Nuclear Research, Geneva, Switzerland, 2019.
- [5] P. Robison, *Boeing's 737 Max Software Outsourced to USD9-An-Hour Engineers*, The Guardian, Bloomberg, London, UK, 2019.
- [6] D. P. Shepard, J. A. Bhatti, and T. E. Humphreys, "Drone hack: spoofing attack demonstration on a civilian unmanned aerial vehicle," *GPS World*, vol. 23, no. 8, pp. 30–33, 2012.
- [7] S. M. Giray, "Anatomy of unmanned aerial vehicle hijacking with signal spoofing," in *Proceedings of the 2013 6th International Conference on Recent Advances in Space Technologies (RAST)*, pp. 795–800, IEEE, Istanbul, Turkey, June 2013.
- [8] D. Davidson, H. Wu, R. Jellinek, V. Singh, and T. Ristenpart, "Controlling UAVs with sensor input spoofing attacks," in *Proceedings of the 10th USENIX Workshop on Offensive Technologies (WOOT 16)*, Austin, TX, USA, August 2016.
- [9] K. Hartmann and K. Giles, "UAV exploitation: a new domain for cyber power," in *Proceedings of the 2016 8th International Conference on Cyber Conflict (CyCon)*, pp. 205–221, IEEE, Tallinn, Estonia, May–June 2016.
- [10] S. Center, *Drone Wars—The Yemen Review*, Sana'a Center for Strategic Studies, Sana'a, Yemen, June 2019.
- [11] J. M. Wing, "A specifier's introduction to formal methods," *Computer*, vol. 23, pp. 8–22, 1990.
- [12] E. Adler and J. B. Jeannin, "Formal verification of collision avoidance for turning maneuvers in UAVs," in *Proceedings of the AIAA Aviation 2019 Forum*, p. 2845, Dallas, Texas, USA, June 2019.
- [13] M. Webster, M. Fisher, N. Cameron, and M. Jump, "Formal methods for the certification of autonomous unmanned aircraft systems," in *Proceedings of the International Conference on Computer Safety, Reliability, and Security*, pp. 228–242, Springer, Naples, Italy, September 2011.
- [14] A. M. Madni, M. W. Sievers, J. Humann, E. Ordoukhanian, B. Boehm, and S. Lucero, "Formal methods in resilient systems design: application to multi-UAV system-of-systems control," in *Disciplinary Convergence in Systems Engineering Research*, pp. 407–418, Springer, Berlin, Germany, 2018.
- [15] S. Jo, M. Ikram, I. Jung, W. Ryu, and J. Kim, "Power-driven image compression in wireless sensor networks," *Mobile and Wireless*, vol. 42, pp. 28–33, 2013.
- [16] S. K. Jo, M. Ikram, I. Jung, W. Ryu, and J. Kim, "Power efficient clustering for wireless multimedia sensor network," *International Journal of Distributed Sensor Networks*, vol. 10, Article ID 148595, 2014.
- [17] M. A. H. Chowdhury, M. Ikram, and K. H. Kim, "Secure and survivable group communication over MANET using CRTDH based on a virtual subnet model," in *Proceedings of the 2008 IEEE Asia-Pacific Services Computing Conference*, pp. 638–643, IEEE, Yilan, Taiwan, December 2008.
- [18] H. Redwan, M. A. H. Chowdhury, M. Ikram, and K. H. Kim, "Survey of indexing schemes for information retrieval on flash memory based wireless sensor networks," in *Proceedings of the 2009 Conference on Information Science, Technology and Applications*, pp. 14–21, ACM, Kuwait, March 2009.
- [19] G. Boole, *Investigation of the Laws of Thought*, Dover, Downers Grove, IL, USA, 1854.
- [20] C. E. Shannon, "A symbolic analysis of relay and switching circuits," *Electrical Engineering*, vol. 57, pp. 713–723, 1938.
- [21] WolframAlpha computational knowledge engine," February 2018, <https://www.wolframalpha.com/>.
- [22] Online minimization of Boolean functions," February 2018, [https://www.tma.main.jp/logic/index\\_en.html/](https://www.tma.main.jp/logic/index_en.html/).
- [23] R. Sondre, A. Mohamed, Lars, and D. Eirik, "Online database of Boolean functions," February 2018, <http://www.ii.uib.no/~mohamedaa/odbf/index.html>.
- [24] R. Lean, Kryle, and M. Marxel, "QMSolver," February 2018, <http://agila.upm.edu.ph/kmmolina/qms/index.html>.
- [25] Logic circuit simplification (SOP and POS)," February 2018, <http://www.32x8.com/>.
- [26] M. Karnaugh, "The map method for synthesis of combinational logic circuits," *Transactions of the American Institute of Electrical Engineers, Part I: Communication and Electronics*, vol. 72, pp. 593–599, 1953.
- [27] T. K. Jain, D. S. Kushwaha, and A. K. Misra, "Optimization of the Quine-Mccluskey Method for the Minimization of the Boolean Expressions," in *Proceedings of the ICAS 2008 Fourth International Conference on Autonomic and Autonomous Systems*, pp. 165–168, IEEE, Anchorage, AK, USA, September 2008.
- [28] A. Kuehlmann, V. Paruthi, F. Krohm, and M. K. Ganai, "Robust Boolean reasoning for equivalence checking and functional property verification," *IEEE Transactions on Computer-Aided Design of Integrated Circuits and Systems*, vol. 21, pp. 1377–1394, 2002.
- [29] M. M. Mano, *Digital Logic and Computer Design*, Pearson Education India, Delhi, India, 2017.
- [30] O. Lhoták, "Program analysis using binary decision diagrams," vol. 68, A thesis submitted to McGill University, McGill University, Montreal, Canada, 2006.
- [31] J. Whaley, D. Avots, M. Carbin, and M. S. Lam, "Using datalog with binary decision diagrams for program analysis," in *Proceedings of the Asian Symposium on Programming Languages and Systems*, pp. 97–118, Springer, Tsukuba, Japan, November 2005.
- [32] J. R. Burch, E. M. Clarke, K. L. McMillan, D. L. Dill, and L. J. Hwang, "Symbolic model checking:  $10^{20}$  states and beyond," *Information and Computation*, vol. 92, no. 98, pp. 142–170.
- [33] B. L. SYNTHESESIS, "ABC: a system for sequential synthesis and verification, release 70930," 2007.
- [34] A. Mulhern, C. Fischer, and B. Liblit, "Tool support for proof engineering," *Electronic Notes in Theoretical Computer Science*, vol. 174, pp. 75–86, 2007.
- [35] T. Grimm, D. Lettner, and M. Hübner, "A survey on formal verification techniques for safety-critical systems-on-chip," *Electronics*, vol. 7, no. 6, p. 81, 2018.
- [36] M. M. Mano and M. D. Ciletti, *Digital Design: With an Introduction to the Verilog HDL, VHDL, and System Verilog*, Pearson, Boston, MA, USA, 2018.

- [37] A. Valmari, "The state explosion problem," *Lectures on Petri Nets I: Basic Models*, pp. 429–528, Springer, Berlin, Germany, 1998.
- [38] E. M. Clarke, W. Klieber, M. Nováček, and P. Zuliani, "Modelchecking and the state explosion problem," in *Tools for Practical Software Verification*, Springer, pp. 1–30, 2012.
- [39] J. L. Boulanger, *Industrial Use of Formal Methods: Formal Verification*, John Wiley & Sons, Hoboken, NJ, USA, 2013.
- [40] M. Kwiatkowska, G. Norman, and D. Parker, "PRISM 4.0: verification of probabilistic real-time systems," in *Proceedings of the International Conference on Computer Aided Verification*, Springer, pp. 585–591, Snowbird, UT, USA, July 2011.
- [41] J. B. Almeida, M. J. Frade, J. S. Pinto, and S. M. de Sousa, "An overview of formal methods tools and techniques," *Rigorous Software Development*, pp. 15–44, Springer, London, UK, 2011.
- [42] D. Kroening and M. Tautschnig, "CBMC–C bounded model checker," in *Proceedings of the International Conference on Tools and Algorithms for the Construction and Analysis of Systems*, Springer, pp. 389–391, London, UK, October 2014.
- [43] Y. Bertot and P. Castéran, *Interactive Theorem Proving and Program Development: Coq'Art: The Calculus of Inductive Constructions*, Springer Science & Business Media, 2013.
- [44] B. Barras, S. Boutin, C. Cornes et al., *The Coq proof assistant reference manual: version 6.1*, Ph.D. thesis, Inria, 1997.
- [45] T. Nipkow, L. C. Paulson, and M. Wenzel, *Isabelle/HOL: A Proof Assistant for Higher-order Logic*, vol. 2283, Springer Science & Business Media, Berlin, Germany.
- [46] W. Ahrendt, B. Beckert, R. Hähnle et al., *Integrating Automated and Interactive Theorem Proving*, Kluwer Academic Publisher, Amsterdam, Netherlands, 1998.
- [47] B. C. Pierce, C. Casinghino, M. Gaboardi et al., "Software foundations," 2010, <http://www.cis.upenn.edu/bcpierce/sf/current/index.html>.
- [48] E. V. Huntington, "New sets of independent postulates for the algebra of logic, with special reference to Whitehead and Russell's Principia Mathematica," *Transactions of the American Mathematical Society*, vol. 35, pp. 274–304, 1933.
- [49] K. Wilayat, T. Alwen, and S. David, "VeriFormal: an executable formal model of a hardware description language. A systems approach to cyber security," in *Proceedings of the 2017 2nd Singapore Cyber Security R&D Conference SGCSC*, pp. 19–36, Singapore, February 2017.
- [50] S. Coupet-Grimal and L. Jakubiec, "Coq and hardware verification: a case study," in *Proceedings of the International Conference on Theorem Proving in Higher Order Logics*, pp. 125–139, Springer, Turku, Finland, August 1996.
- [51] O. Hasan, J. Patel, and S. Tahar, "Formal reliability analysis of combinational circuits using theorem proving," *Journal of Applied Logic*, vol. 9, pp. 41–60, 2011.
- [52] S. O. Biha, "A formal semantics of PLC programs in Coq," in *Proceedings of the 2011 IEEE 35th Annual Computer Software and Applications Conference (COMPSAC)*, IEEE, pp. 118–127, Munich, Germany, July 2011.
- [53] T. Braibant, "Coquet: a coq library for verifying hardware," in *Proceedings of the International Conference on Certified Programs and Proofs*, pp. 330–345, Springer, Kenting, Taiwan, December 2011.
- [54] Icarus Verilog," December 2016, <http://www.icarus.com/eda/verilog/>.
- [55] G. J. Pace and J. He, "Formal reasoning with verilog HDL," in *Proceedings of the Workshop on Formal Techniques for Hardware and Hardware-like Systems*, Marstrand, Sweden, June 1998.
- [56] S. Y. Huang and K. T. T. Cheng, *Formal Equivalence Checking and Design Debugging*, vol. 12, Springer Science & Business Media, Berlin, Germany.
- [57] E. M. Clarke, O. Grumberg, and D. Peled, *Model Checking*, MIT Press, London, UK, 1999.
- [58] A. Biere, A. Cimatti, E. M. Clarke, O. Strichman, and Y. Zhu, "Bounded model checking," *Advances in Computers*, vol. 58, pp. 117–148, 2003.
- [59] L. Xiaoa, M. Li, M. Gu, and J. Sun, "The modelling and verification of PLC program based on interactive theorem proving tool Coq," in *Proceedings of the International Conference on Computer Science and Information Technology (ICCSIT)*, Hong Kong, China, December 2012.
- [60] L. Arditi and S. Antipolis, "Formal verification of micro-processors: a first experiment with the Coq proof assistant," Technical report, Research report, I3S, Université de Nice–Sophia Antipolis, Nice, France, 1996.
- [61] W. K. Lam, *Hardware Design Verification: Simulation and Formal Method-Based Approaches (Prentice Hall Modern Semiconductor Design Series)*, Prentice Hall PTR, Upper Saddle River, NJ, USA, 2005.
- [62] W. Khan, M. Kamran, A. Ahmad, F. A. Khan, and A. Derhab, "Formal analysis of language-based android security using theorem proving approach," *IEEE Access*, vol. 7, pp. 16550–16560, 2019.
- [63] W. Khan, H. Ullah, A. Ahmad et al., "CrashSafe: a formal model for proving crash-safety of android applications," *Human-centric Computing and Information Sciences*, vol. 8, no. 1, p. 27, 2018.
- [64] M. Bugliesi, S. Calzavara, R. Focardi, and W. Khan, "CookiExt: patching the browser against session hijacking attacks," *Journal of Computer Security*, vol. 23, no. 4, pp. 509–537, 2015.
- [65] W. C. Kabat and A. S. Wojcik, "Automated synthesis of combinational logic using theorem-proving techniques," *IEEE Transactions on Computers*, vol. C-34, no. 7, pp. 610–632, 1985.
- [66] P. Meredith, M. Katelman, J. Meseguer, and G. Roşu, "A formal executable semantics of Verilog," in *Proceedings of the 2010 8th IEEE/ACM International Conference on Formal Methods and Models for Codesign (MEMOCODE)*, pp. 179–188, IEEE, Grenoble, France, July 2010.
- [67] M. Clavel, F. Durán, J. Hendrix, S. Lucas, J. Meseguer, and P. Ölveczky, "The Maude formal tool environment," in *Proceedings of the International Conference on Algebra and Coalgebra in Computer Science*, pp. 173–178, Springer, Bergen, Norway, August 2007.
- [68] W. Khan, D. Sanan, Z. Hou, and L. Yang, "On embedding a hardware description language in Isabelle/HOL," *Design Automation for Embedded Systems*, vol. 23, no. 3-4, pp. 123–151, 2019.
- [69] W. Khan, A. Basim, S. Noman, K. Abdul Moeed, and S. Ahtisham, "Formal verification of digital circuits using simulator with mathematical foundation," *Applied Mechanics and Materials*, vol. 892, pp. 134–142, 2019.
- [70] T. Braibant and A. Chlipala, "Formal verification of hardware synthesis," in *Proceedings of the International Conference on Computer Aided Verification*, Springer, pp. 213–228, St. Petersburg, Russia, July 2013.
- [71] E. Love, Y. Jin, and Y. Makris, "Proof-carrying hardware intellectual property: a pathway to trusted module acquisition," *IEEE Transactions on Information Forensics and Security*, vol. 7, no. 1, pp. 25–40, 2012.

## Research Article

# A Proposal for Routing Protocol for FANET: A Fuzzy System Approach with QoE/QoS Guarantee

Jorge Souza <sup>1</sup>, José Jailton <sup>2</sup>, Tássio Carvalho,<sup>2</sup> Jasmine Araújo <sup>2</sup> and Renato Francês<sup>2</sup>

<sup>1</sup>Ciberespacial Institute, Federal Rural University of the Amazon (UFRA), Belém, PA, Brazil

<sup>2</sup>Institute of Technology, Federal University of Pará (UFPA), Belém, PA, Brazil

Correspondence should be addressed to Jorge Souza; jams.souza@gmail.com

Received 21 May 2019; Revised 30 September 2019; Accepted 4 November 2019; Published 23 November 2019

Guest Editor: Zeeshan Kaleem

Copyright © 2019 Jorge Souza et al. This is an open access article distributed under the Creative Commons Attribution License, which permits unrestricted use, distribution, and reproduction in any medium, provided the original work is properly cited.

The flying ad hoc network (FANET) has emerged as an alternative access technology for regions that have no fixed infrastructure or are hard to reach. This new type of network is composed of devices called unmanned aerial vehicles (UAVs) that communicate with each other, but there is no specific routing protocol to FANET applications that allows efficient communication between these devices. This paper proposes a FANET adaptive routing protocol based on the fuzzy system. The validation of the FANET adaptive protocol was performed through simulation using Network Simulator version 2 (NS-2) and, it was assessed by quality of service (QoS) and quality of experience (QoE) metrics.

## 1. Introduction

In recent years, there has been a great deal of motivation in the search for new wireless communication mechanisms, with great growth due to new technologies or configurations in aerial technologies, to monitoring hard-to-reach areas or in case of disaster situations. In this context, FANETs (flying ad hoc networks) emerged, which are a type of ad hoc network configuration consisting of unmanned aerial vehicles (UAVs). UAVs are responsible for monitoring a specific area by capturing images and sending them to a base ground station [1] in a process known as UAV-to-ground (U2G) communication.

In this context of FANETs, new challenges arise unlike the traditional infrastructure and cable challenges: (1) positioning the UAVs in a most appropriated way to monitor regions, minimizing costs and maximizing the performance of network; (2) reduce the negative effects of UAVs high mobility; and (3) traditional routing protocols are not capable of handling, in an efficient fashion, the flying networks, especially flying ad hoc networks, due to features such as high node mobility and topology changes. This can compromise communication between UAVs and network performance. Due to this, it is important to define a strategy to

ensure adequate communication under these conditions, providing resources that guarantee satisfactory and intelligent performance to reduce the selected challenges [2].

Another important point to consider in FANET/UAV scenarios is that most mobile devices have an average flight time of approximately 30 minutes [3, 4] due to limited battery capacity. This fact draws the following conclusion: a node, with a low battery charge, will stop being part of the aerial network due to its “death,” requiring the network to autoconfigure and restructure and reorganize its topology, avoiding damages that could affect aerial wireless communication. Because of this, it is necessary to determine and/or predict which devices have low flight autonomy or are close to being incapacitated, in order to minimize the impacts on communication quality.

UAVs need to have sensors attached to them to capture real-time images of a certain area, and because of this, it is necessary to evaluate the quality of the data and video collected, which can be done by using QoE (quality of experience), that have equivalent direct measurements related to the evaluation of multimedia streams, from the user perception point of view, corroborating and complementing traditional QoS (quality of service) metrics, which evaluate objective measurements from the network point of view as

throughput, delay, etc., but do not reflect the final user experience with the video streams nor the final quality of the received video [5].

As already commented, flight range and mobility are influential factors that can severely alter the topology of the aerial network. Because of this, it is of fundamental importance to build a new routing protocol that can consider these factors and exert a mutual interaction between them and the topological changes of the network, especially since currently there are no specific routing protocols for these ad hoc network scenarios beyond traditional routing protocols that date back to the emergence of the Internet such as Ad-hoc On Demand Distance Vector (AODV) and optimized link state routing (OLSR) that are neither adequate nor efficient in these scenarios [6].

Taking the numerous problems encountered in FANETS and air network scenarios, this paper proposes a routing protocol adapted and implemented for these scenarios created through a fuzzy system to enable the best communication path between UAVs (a process known as UAV-to-UAV communication—U2U). The new routing protocols will find the best route, with the best connection and longest durability, improving network performance.

The paper is distributed as follows: Section 1, presented here, contextualized the work and introduced its contribution. Section 2 discusses the related works and compares them. Section 3 presents the state of the art of FANET applications. Section 4 describes the proposed new routing protocol and the details of the implemented system. Section 5 discusses the performance evaluation of the proposed routing protocol, which is sequentially complemented by Section 6 which concludes the work and presents its main contributions.

## 2. Related Work

This section examines the related work on the routing protocol flying ad hoc networks (FANETs). The aim is to demonstrate some gaps in related work and how the proposed routing protocol addresses them.

In paper [7], through simulations in Network Simulator 3 (NS-3), performance of AODV, OLSR, and HWMP protocols in FANETs was compared. The protocols were evaluated using the QoS metrics and Gauss–Markov mobility model. Despite the comparison, the paper proposed no improvement to the protocols.

In paper [8], the authors devise a new mechanism for data routing based on localization in GPS-denied or GPS-challenged areas. This mechanism relies on a weighted centroid localization technique, where the position of unknown UAV nodes is calculated by means of fuzzy logic. This paper does not take into account that changes in topology require new packet routing or the flight autonomy of each drone.

In paper [9], the authors investigated a routing protocol called predictive OLSR (P-OLSR), which is an extension of the traditional OLSR protocol. The authors compared the P-OLSR with OLSR by means of QoS metrics. However, although the paper put forward a new routing protocol, it

did not compare it with the other routing protocols and failed to evaluate it with the QoE metrics.

In paper [10], the authors recommended an energy-efficiency algorithm for drones that included the parameters of the communication channel. This system reduced energy consumption, but even though there were a number of changes in the topology, the network was unable to identify new routes in an effective way and thus maintain the required level of quality.

In paper [11], the authors carried out a survey of the routing protocols for VANET and FANET. Their paper discusses the use of optimization techniques (particle swarm optimization, ant colony optimization, and bee colony optimization) to improve the routing performance but did not employ flight autonomy as a parameter or take QoE metrics into account.

In paper [12], the authors discuss the use of hop-by-hop communication between the drones as a means of increasing the network coverage area. However, the paper does not discuss to what extent the changes in the topology can have an effect on the quality of transmission, while also failing to address the need for an efficient routing protocol.

In paper [13], the authors introduced the use of the multiple path OLSR (MP-OLSR) routing protocol into FANET applications, especially in wildfires, to increase the chances of rescuing victims. The work considered scenarios with different speed ranges but did not address the flight autonomy problem.

In paper [14], the authors proposed the use of continuous Hopfield neural network (CHNN) to optimize the routes found by the dynamic source routing (DSR) protocol so that they would adapt to the high-speed movement of the FANET nodes. Simulation using NS-3 showed that the optimized DSR protocol improved the indicators such as end-to-end average delay, throughput, and packet delivery ratio. The authors did not address QoE and QoS metrics.

The authors in [7–14] examine the techniques that are used in FANET, but none of them set out a routing protocol that provides an effective response to the changes in the network topology. These papers do not address flight autonomy of the drones either and do not use a computer intelligence system for decision-making.

The proposed routing protocol, unlike those addressed in the related work presented in the literature, considers the needs and challenges of a FANET. Table 1 shows the related work that broadly addresses FANET routing and its solutions. This paper proposes an alternative approach to routing protocols already used in FANET by adopting fuzzy systems. The proposed routing protocol was validated by QoE metrics.

## 3. Flying Ad Hoc Network (FANET)

The increasing use of mobile ad-hoc networks (MANETs), vehicular ad hoc networks (VANETs), and wireless sensor networks, has led them to use new devices capable of moving and flying autonomously, generating more complex systems.

In FANET, the devices are generally referred to as unmanned aerial vehicles (UAVs). The use of UAVs has

TABLE 1: Related work.

Proposal	Flight autonomy	Decision strategy	Proposal focus
[7]	No	Using the Gauss–Markov mobility model	Evaluate the traditional routing protocol in FANETs
[8]	No	Mechanism for data routing based on localization	The position for UAV device
[9]	No	Extension of the OLSR protocol called P-OLSR	Compare P-OLSR with OLSR
[10]	No	Energy-efficiency algorithm	Reduce the energy consumption
[11]	No	Survey of the routing protocols	Discuss the use of optimization techniques to improve the routing performance
[12]	No	Discuss the hop-by-hop communication	Number of UAVs necessary to network coverage area
[13]	No	Routing based on multiple paths	Prove the efficiency of MP-OLSR in monitor wildfire areas to increase the saving chances of people victims of them
[14]	No	CHNN-DSR protocol	Optimize routes to adapt them to high-speed movement of nodes
Current proposal	Yes	Routing protocol with fuzzy logic system	Select the best routing communication considering flight autonomy with mobility and RSSI (received signal strength indicator)

created new ways of operating innovative applications, by introducing a new type of network paradigm known as FANETs.

The networks differ from their traditional predecessors (MANETs in this case) as a result of the high mobility of UAVs, their greater connectivity, expansion in application areas, etc. In this respect, FANETs can generalize and extrapolate the topologies from 2D to 3D through a free-motion scheme, owing to the ability of the drones to fly independently in three-dimensional space. This new context has attracted researchers and industry as well as providing a driving force for real-life applications.

FANETs are generally used to provide connectivity to hard-to-reach places in regions where there have been natural disasters or even for military applications. After a catastrophic event (such as an earthquake, hurricane, tsunami, and dam breach), traditional network infrastructures can suffer damage and be subject to automatic shutdowns. However, through a FANET configuration, they could be employed to restore and provide sufficient connection and communication to the network in isolated areas. Besides, UAVs could be equipped with cameras and other types of sensors and devices to provide a constant aerial view and thus help rescue crews and firefighters to save lives.

In extensive coverage areas, it may be impracticable to establish direct communication from the UAVs to the base station on the ground at certain times. However, this problem can be overcome through hop-by-hop communication, which requires the use of a routing protocol to discover the best route/path from the source to the final destination [15].

*3.1. Problem Statement and Major Contributions.* The high mobility of UAVs means that network topology can change over time, so discovering and maintaining routes becomes one of the main issues to address [16]. For this reason, the

focus of this paper is to establish a specific FANET protocol that can perform this task more efficiently.

Routing protocols are responsible for finding, establishing, and maintaining routes between two nodes that wish to communicate. These protocols should minimize overhead and bandwidth consumption.

A routing protocol that targets FANETs is more complex than fixed network protocols; this is due to several features of these networks such as their dynamic topology algorithm, mutual interference, restricted power, and the limited resources available in the UAVs.

In a FANET, given UAV mobility, it may happen that one aircraft is not close enough to another to establish communication, so it will need to use routing information to choose an alternate route. This communication can be done in multiple hops through the collaboration of intermediate nodes; that is, communication is not restricted to the radius of action of each device individually, but the sum of the radius of action of all devices (Figure 1).

The mobility of UAVs and their spatial arrangement are also very important for determining the communication routes. As a result of the movement, these routes are usually rearranged so that the interconnection between the UAVs can be continued. For this reason, the routing must be carried out dynamically by increasing the autonomy of the UAVs and reducing the delay in data delivery between a source node and a destination node [17].

Another main contribution of this paper is the adoption of a new communication network model used to provide connectivity in regions that are difficult to reach on land (especially regions after natural disasters). FANETs are easily established, as they are easily moved to a new region.

The frequent updating of the control information can ensure more accurate information; however, there is a need for a greater use of energy since this reduces the autonomy of the nodes. For this reason, this paper proposes a specific routing protocol for FANETs where the received signal

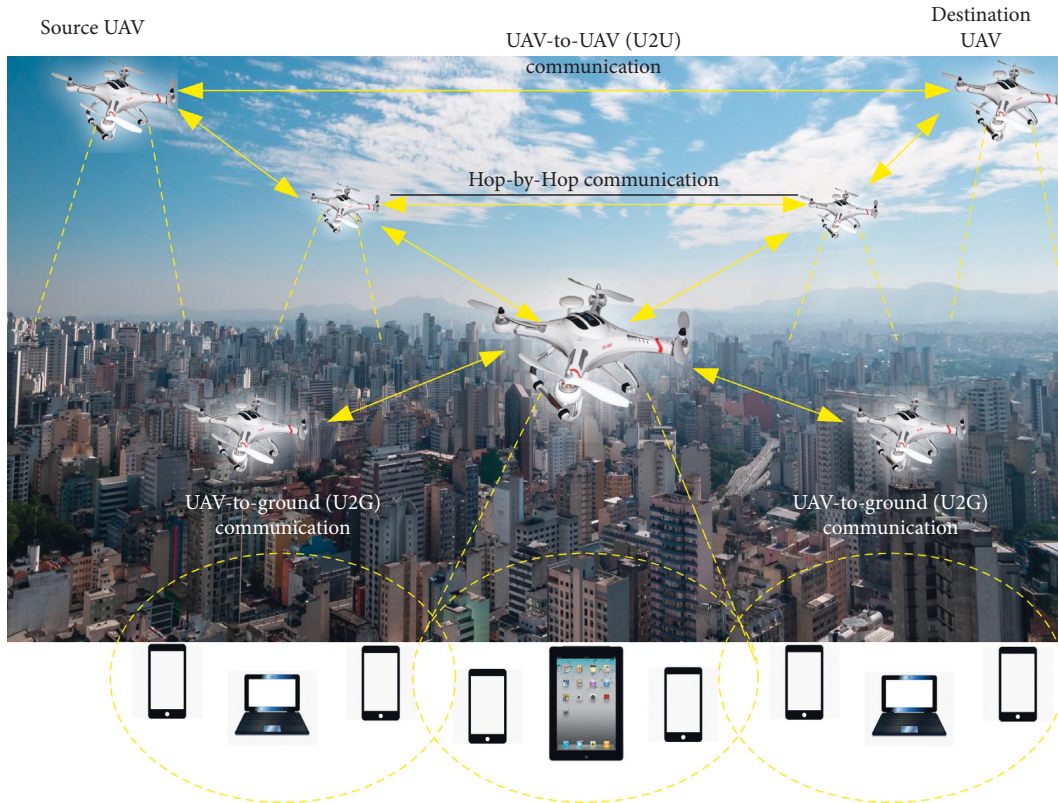


FIGURE 1: Hop-by-hop communication in FANET.

strength indicator (RSSI), mobility level, and in particular the flight autonomy of each UAV are employed as decision-making metrics to ensure quality of service and quality of experience for the network.

This paper also proposes, as a contribution, the use of a fuzzy system for the implementation of the routing protocol, with a set of inputs composed of information collected, in real time, from the network itself. The pieces of information collected are flight autonomy, mobility level, and RSSI. Based on such information, it is possible to establish communication routes that will remain active for a longer period. The objective is to discover routes with high flight autonomy (longer service life), low mobility (fewer changes in the topology), and better RSSI (better condition for data transmission).

FANETs are commonly employed to monitor regions by using sensors to capture images and/or videos. Therefore, it is very important that the quality of the video stream can be assessed using QoE metrics to ensure that, in fact, good data communication reflects a good user experience. Therefore, this paper performs a cross-layer evaluation involving the network and application layers to verify it.

#### 4. A Fuzzy Routing Protocol System

The fuzzy system is a special kind of a knowledge-based system that works through dynamic and inaccurate sets of measurements. Fuzzy sets express the meaning of linguistic values related to a linguistic variable. A linguistic variable can be associated with a set of linguistic values, and that are

associated with fuzzy sets that express the corresponding degree of relevance (truth value) of a linguistic variable. Fuzzy sets are used to quantify the corresponding degrees of uncertainty in evaluating a given concept (instance). Elements that belong to the fuzzy set may have degrees of relevance in the range of  $[0,1]$ .

These systems are widely used in dynamic scenarios, such as vehicular network scenarios, being terrestrial or aerial because, as the dynamics occur in the scenarios, the values are changed, and, consequently, new solutions for the network are found. This paper considers three input metrics (language variables in the fuzzy system): mobility level, flight autonomy, and RSSI.

The level of mobility is linked to the speed metric, which is an important measure as it can affect the quality of communication/transmission because this measure indicates how fast the drones are moving, consequently changing the network topology as approach or distance from a particular area. For the variable, three linguistic values were defined: low speed (range 0 to 5 m/s), average speed (range 4 to 13 m/s), and high speed (when velocity is greater than 11 m/s).

Another important metric is the flight autonomy, directly linked to the battery capacity of the device; In this case, which is related to the time that the UAV will be able to fly over and monitor a particular region. The greater the battery capacity, the longer the flight range, and therefore, the longer the route, and network topology will remain active. This metric is divided into three linguistic values within this set: low range (0 to 600 seconds), medium



range (600 to 1200 seconds), and high range (over 1200 seconds).

The third and last metrics used are linked to the signal strength, which can also represent the signal quality and is represented by the RSSI. The better the RSSI, the better the communication between two or more drones. Inversely, the worse the RSSI is, the worse is the signal quality between airborne devices, and the worse is the communication between them. In this metric, three language variables were defined for RSSI (dBi): low RSSI (-125.1 to -102.1 dBi), average RSSI (-111.1 to 63.1 dBi), and high RSSI (greater than -71.1).

With the support of the fuzzy system and the rule set used, accurate results will handle inaccurate and vague entries of input language variables, interpreted and classified as follows: terrible path, regular path, good path, and excellent path. When the drone detects a new path/route, it will provide the input variables collected for the embedded fuzzy system, which after applying the inference equation and the diffusion process, will indicate the quality level of the detected paths/routes, qualifying the best for the routing process of the air network.

In this paper, a Gaussian fuzzifier was used due to its inherent ability to reduce the noise of input variables [18]. Fuzzification is the mapping of input variables to a set of ranges that will be analyzed by a fuzzy rule base, the inference machine, and their respective membership functions of a set of linguistic variables, identifying which set it belongs to. After 100 interactions of the simulation process, it was concluded that the value of 0.6 would be considered for good or excellent paths. In certain situations, an inference value can be a part of two or more fuzzy sets at the same time (such as 0.55). In this case, the metric that has the most relevance according to the relevance function will be decisive in identifying the output set (Figure 2).

For the implementation and construction of this fuzzy system and after a set of tests and simulations, it was concluded that the ideal communication between drone devices would be in a scenario with high flight autonomy, high signal strength (RSSI), and low mobility level because in this scenario/topology, the route is kept longer so that the transmission stays longer and with fewer communication problems. The greater the distance from this ideal scenario, the fuzzy system can fetch the results that are closest to the context, based on a table of rules and the inference machine that can be dynamic and realistic in intelligent decision-making.

Table 2 shows a set of fuzzy system rules defined for performing this role. Through this set of rules and in conjunction with the implemented inference engine, the system finds the most appropriate decision to select the route/path that will remain active for the longest, improving and maintaining network performance with the best path (Table 2), mostly choosing the EXCELLENT and GOOD paths and very rarely the REGULAR and BAD paths.

The final decision is made according to the fuzzy system set inference values which qualify the highest inference value for the choice. During the implementation of the fuzzy system, it was observed that inference values equal to or

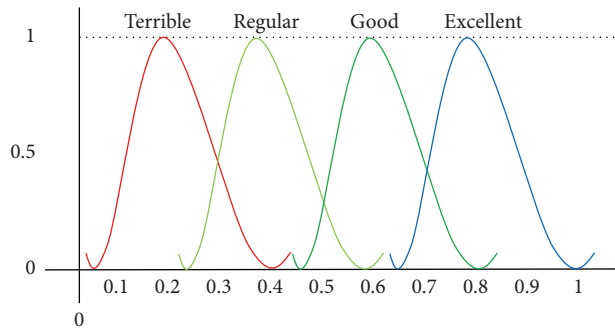


FIGURE 2: Output of the fuzzy system.

TABLE 2: A fuzzy rule-based system.

Mobility	Flight autonomy	RSSI	Output
Low	Low	Low	Terrible
Low	Low	Medium	Regular
Low	Low	High	Regular
Low	Medium	Low	Regular
Low	Medium	Medium	Good
Low	Medium	High	Excellent
Low	High	Low	Regular
Low	High	Medium	Good
Low	High	High	Excellent
Medium	Low	Low	Terrible
Medium	Low	Medium	Regular
Medium	Low	High	Regular
Medium	Medium	Low	Regular
Medium	Medium	Medium	Good
Medium	Medium	High	Excellent
Medium	High	Low	Regular
Medium	High	Medium	Good
Medium	High	High	Excellent
High	Low	Low	Terrible
High	Low	Medium	Terrible
High	Low	High	Terrible
High	Medium	Low	Terrible
High	Medium	Medium	Regular
High	Medium	High	Regular
High	High	Low	Terrible
High	High	Medium	Regular
High	High	High	Regular

higher than 0.6 represented the best way in these scenarios and therefore those with the highest probability of being chosen (Figure 3).

In the 3D graphic image of Figure 4, the yellow areas represent the routes/paths most likely to be chosen, as they correspond to routes where drones have high flight autonomy, low mobility, and high RSSI. The green-shaded chart area corresponds to the average speed, average RSSI, and average flight range drones, and in this situation, there is little chance of the drone being chosen as the communication route. The last region, represented by the blue color on the chart, represents a drone with high mobility, low RSSI, and low flight range, in which case the drone will not be chosen as the communication route (Figure 4).

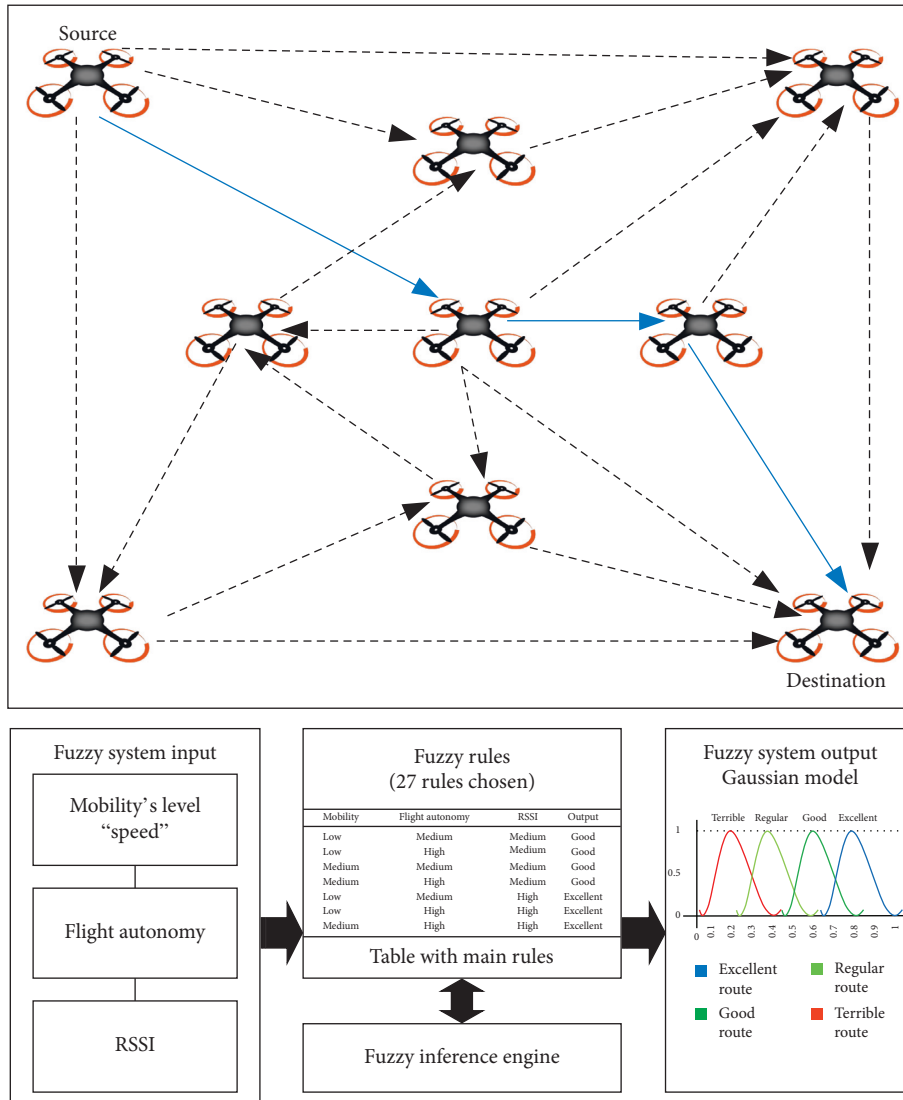


FIGURE 3: Schematic representation of the proposal.

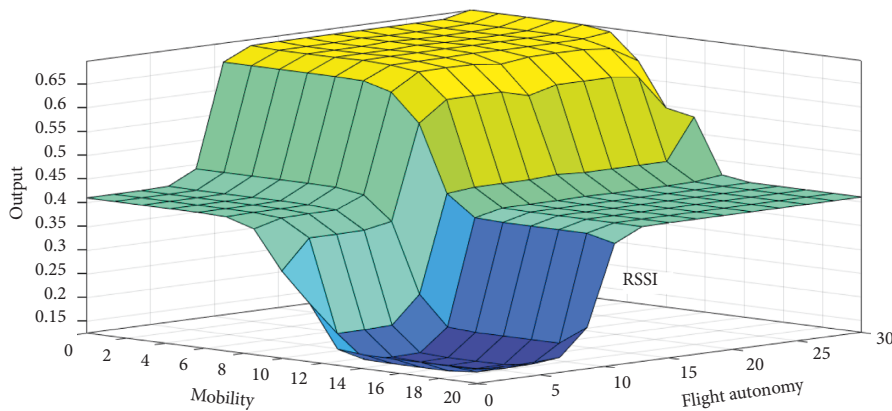


FIGURE 4: Fuzzy inference system.

### 5. Results

This section evaluates the performance of the FANET protocol by proving the benefit of the proposed routing

protocol when compared to AODV (reactive protocol) and OLSR (proactive protocol). The results were performed by simulation through the network simulator version 2 and multimedia applications. The video used was the "Sintel"

TABLE 3: NS-2 simulation parameters.

Drones	10
Access technology	IEEE 802.11 g
Propagation model	Shadowing
Mobility type	Random waypoint
Query	Droptail
Number of simulations	100
Confidence interval	95%
Frequency	2.4 GHz
Area	200 m $\times$ 200 m

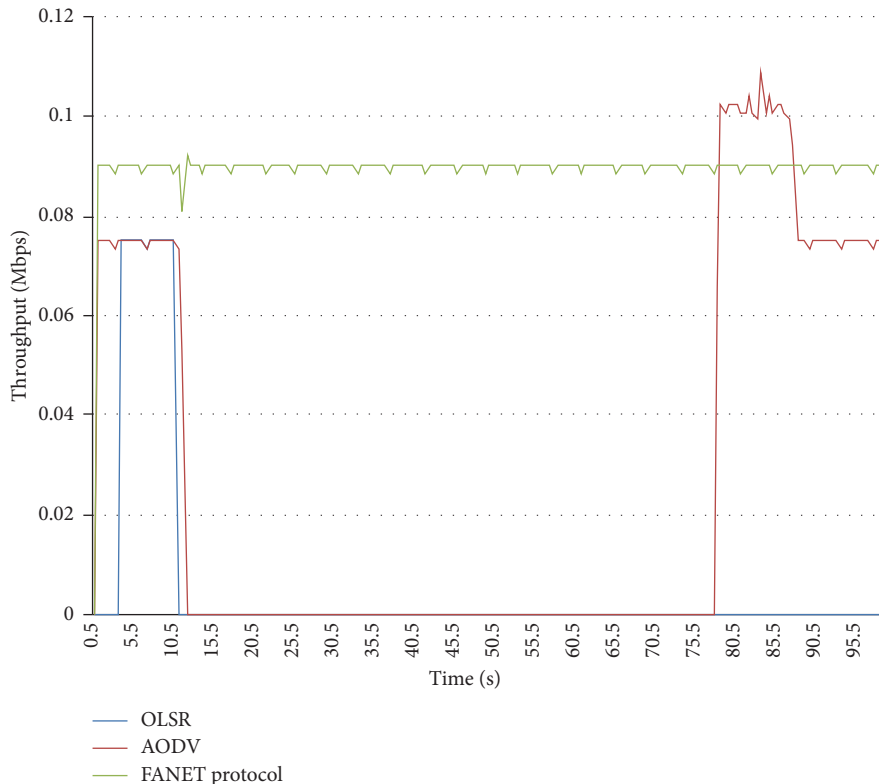


FIGURE 5: Throughput over time.

which is high definition (HD 1280  $\times$  7200p) with 1200 frames.

The propagation model used in the simulations was shadowing because it is more realistic in signal attenuation than the free-space model and two-ray ground models (propagation models available in NS-2) [19]. The simulator does not support three-dimensional scenarios, so it is assumed that drones are at similar heights and with a line of sight of communication. Table 3 shows the simulation parameters used for scenarios with 10 drones with random mobility (random way point) and speed range from 2 m/s to 20 m/s in an area of 200 m  $\times$  200 m.

Due to the drones' random mobility, they can fly closer or farther from each other, considering the speed drones can also get closer or fly slower or faster from each other. Changes in the network topology due to drone mobility require a fast response from routing protocols; if this response does not occur efficiently, network performance will be degraded.

The FANET adaptive protocol outperformed other protocols as shown in Figure 5. The AODV and OLSR protocols, due to network topology changes, did not update their routing tables quickly and efficiently and were unable to maintain an active route, and consequently, both protocols interrupted their transmissions during the part of the simulation. Unlike the others, the FANET adaptive protocol updated its routing table quickly and efficiently always keeping an active route for transmission and consequently avoiding connection breakdown.

The throughput average also shows that the FANET adaptive protocol performed better when compared to AODV and OLSR protocols. The proposed routing protocol performed approximately 300% better than the other two protocols, as shown in Figure 6.

In addition to evaluating through quality of service metrics, this paper also evaluated the FANET adaptive protocol using the quality of experience metric. The three main QoE metrics are peak signal-to-noise ratio (PSNR),

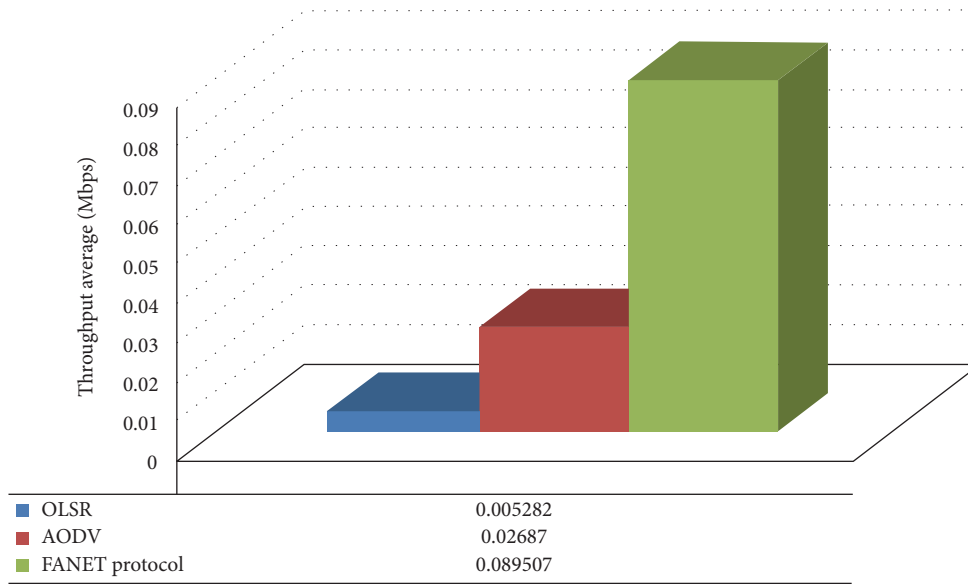


FIGURE 6: Average throughput.

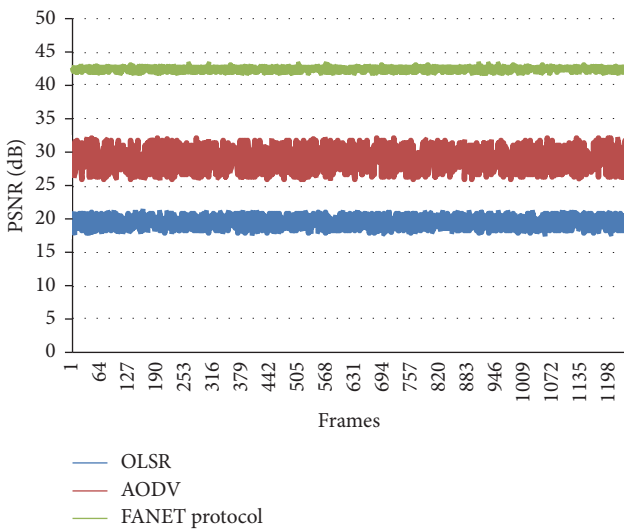


FIGURE 7: PSNR values.

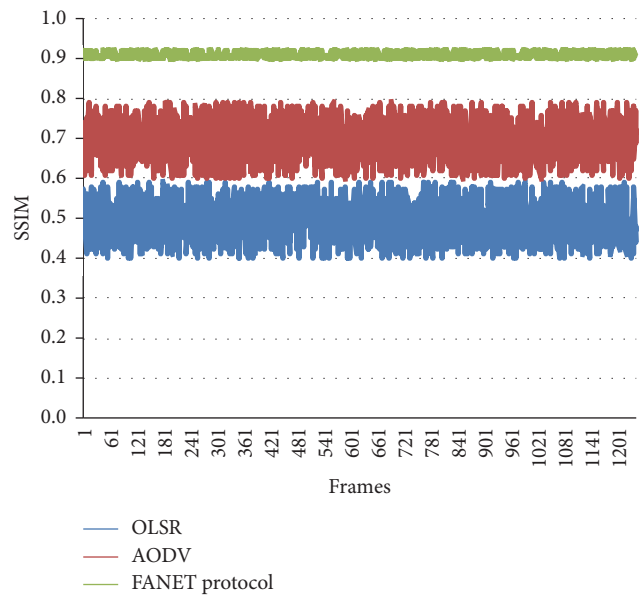


FIGURE 8: SSIM values.

structural similarity (SSIM), and video quality metric (VQM). PSNR evaluates the signal-to-noise ratio of the video considering features such as brightness, noise, and color. Figure 7 shows that the OLSR protocol had a PSNR average of 18 dB (rated as the poor video), the AODV protocol had a PSNR average of 28 dB (rated as the regular video), and the FANET adaptive protocol had an average PSNR of 42 dB (rated as the excellent video).

The FANET adaptive protocol also outperformed OLSR and AODV when evaluated using the SSIM metric. The metric evaluates the video considering features such as brightness, color, and contrast. The SSIM metric has a value scale from 0 to 1, the closer to value 1, the better the video quality. The OLSR protocol had an average SSIM of 0.43 (considered a bad video), the AODV protocol had an average SSIM of 0.61 (considered a regular video), and the

FANET adaptive protocol had an average SSIM of 0.91 (considered an excellent video), as shown in Figure 8.

The comparison between the three protocols was also made using the VQM metric, which also showed the superiority of the FANET adaptive protocol. The VQM metric has a scale from 0 to 5, in which case the closer to 0, the better the video quality. The metric evaluates the video considering features such as color, brightness, intensity, and frame distortion. The OLSR protocol had a VQM average of 4.1, the AODV protocol had a VQM average of 3.3, and the FANET adaptive protocol had a VQM average of 1.4 as shown in Figure 9.

This paper also evaluated the protocols by visually comparing frames received using the MSU Video Quality

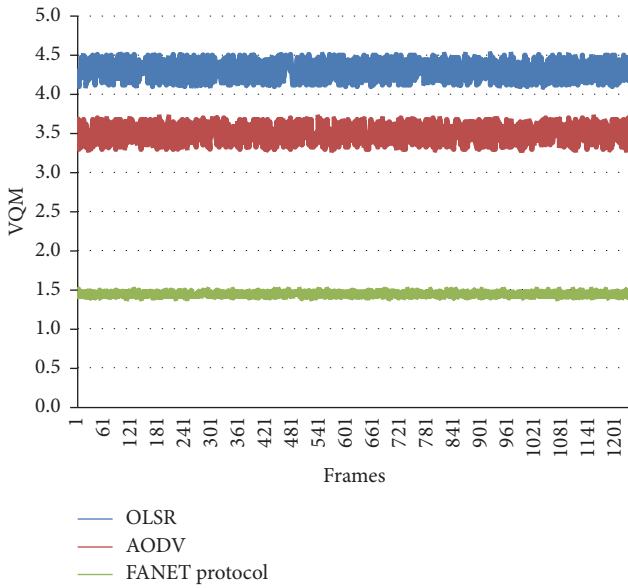


FIGURE 9: VQM values.



FIGURE 10: Frame received by OLSR.



FIGURE 11: Frame received by AODV.

Measurement Tool software [20]. Visual comparison of frames transmitted by each protocol also showed better performance of the FANET adaptive protocol. Figure 10 shows a video frame transmitted by the OLSR protocol in which it is possible to observe that the frame is distorted and has pixel flaws.



FIGURE 12: Frame received by the fuzzy system-based routing protocol.

Figure 11 shows a video frame transmitted by the AODV protocol, in which there was a quality improvement when compared to the previous frame. However, the video cannot be rated as of excellent quality, and it has minor distortions and flaws, so it is classified as a regular quality video.

The video frame transmitted by the FANET adaptive protocol has a better quality when compared to AODV and OLSR protocols. Figure 12 shows that the frame has no distortions or flaws being rated as an excellent quality video.

## 6. Conclusion

FANETs provide several benefits (as cited earlier), but there are still some challenges to be studied, such as routing between UAVs in the air network. For this reason, the flying networks have been a research topic.

There is no specific routing protocol for air networks, so this paper proposes a routing protocol for FANETs that uses a fuzzy system to improve the route discovery process. The FANET adaptive protocol takes into account RSSI, mobility level, and flight autonomy.

The FANET adaptive protocol was compared with AODV and OLSR protocols (traditional ad hoc routing protocols). The comparison was carried out by simulation using QoS and QoE metrics, and the proposed routing protocol had a better performance (around 35%) than the other two routing protocols.

In future paper, the authors intend to develop new artificial intelligence techniques and include new parameters for decision machine, as well as use a new wireless technologies (i.e., long-term evolution—LTE) and new propagation models (i.e., air-to-ground path loss for low-altitude platforms and air-to-ground path loss for high-altitude platforms).

## Data Availability

The data used to support the findings of this study are available from the corresponding author upon request.

## Conflicts of Interest

The authors declare that they have no conflicts of interest.

## References

- [1] E. Cruz, "A comprehensive survey in towards to future FANETs," *IEEE Latin America Transactions*, vol. 16, no. 3, 2018.
- [2] O. Burdakov, P. Doherty, K. Holmberg, J. Kvarnström, and P.-M. Olsson, "Relay positioning for unmanned aerial vehicle surveillance," *The International Journal of Robotics Research*, vol. 29, no. 8, pp. 1069–1087, 2018.
- [3] Phantom 4 user manual V 1.6, 2017, [https://dl.djicdn.com/downloads/phantom\\_4/20170706/Phantom\\_4\\_User\\_Manual\\_v1.6.pdf](https://dl.djicdn.com/downloads/phantom_4/20170706/Phantom_4_User_Manual_v1.6.pdf).
- [4] Mavic 2 pro zoom user manual V 2.0, 2019, [https://dl.djicdn.com/downloads/Mavic\\_2/20190417/Mavic\\_2\\_Pro\\_Zoom\\_User\\_Manual\\_v2.0\\_en.pdf](https://dl.djicdn.com/downloads/Mavic_2/20190417/Mavic_2_Pro_Zoom_User_Manual_v2.0_en.pdf).
- [5] S. Winkler, "Perceptual video quality metrics—a review," in *Digital Video Image Quality and Perceptual Coding*, CRC Press, Boca Raton, FL, USA, 2005.
- [6] Z. Zheng, A. Sangaiah, and T. Wang, "Adaptive communication protocols in flying ad hoc network," *IEEE Communications Magazine*, vol. 56, no. 1, pp. 136–142, 2018.
- [7] D. S. Vasiliev, D. S. Meitis, and A. Abilov, "Simulation-based comparison of AODV, OLSR and HWMP protocols for flying ad hoc networks," in *Proceedings of the Internet of Things, Smart Spaces, and Next Generation Networks and Systems NEW2AN 2014*, S. Balandin, S. Andreev, and Y. Koucheryavy, Eds., pp. 245–252pp. 245–, St. Petersburg, Russia, August 2014.
- [8] F. Khelifi, A. Bradai, K. Singh, and M. Atri, "Localization and energy-efficient data routing for unmanned aerial vehicles: fuzzy-logic-based approach," *IEEE Communications Magazine*, vol. 56, no. 4, pp. 129–133, 2018.
- [9] A. Nayyar, "Flying adhoc network (FANETs): simulation based performance comparison of routing protocols: AODV, DSDV, DSR, OLSR, AOMDV and HWMP," in *Proceedings of the International Conference on Advances in Big Data, Computing and Data Communication Systems (icABCD)*, pp. 1–9, Durban, South Africa, August 2018.
- [10] P. Kaur and A. Singh, "Nature-inspired optimization techniques in VANETs and FANETs: a survey," in *Advanced Computational and Communication Paradigms. Advances in Intelligent Systems and Computing*, S. Bhattacharyya, N. Chaki, D. Konar, U. Chakraborty, and C. Singh, Eds., vol. 706, Springer, Singapore, 2018.
- [11] G. A. Litvinov, A. V. Leonov, and D. A. Korneev, "Applying static mobility model in relaying network organization in mini-UAVs based FANET," in *Proceedings of the 2018 Systems of Signal Synchronization, Generating and Processing in Telecommunications (SYNCHROINFO)*, pp. 1–7, Minsk, Belarus, July 2018.
- [12] O. S. Oubbati, A. Lakas, F. Zhou, M. Güneş, and M. B. Yagoubia, "A survey on position-based routing protocols for Flying Ad hoc Networks (FANETs)," *Vehicular Communications*, vol. 10, pp. 29–56, 2017.
- [13] D. Radu, A. Cretu, B. Parrein et al., "Flying ad hoc network for emergency applications connected to a fog system," in *Advances in Internet, Data & Web Technologies*, pp. 675–686, Fev, Aachen, Germany, 2018.
- [14] H. Yang and Z. Liu, "An optimization routing protocol for FANETs," *J Wireless Com Network*, vol. 2019, no. 1, p. 120, 2019.
- [15] W. Zafar and B. Khan, "Flying ad-hoc networks: technological and social implications," *IEEE Technology and Society Magazine*, vol. 35, no. 2, pp. 67–74, 2016.
- [16] S. Rosati, K. Kruzelecki, G. Heitz, D. Floreano, and B. Rimoldi, "Dynamic routing for flying ad hoc networks," *IEEE Transactions on Vehicular Technology*, vol. 65, no. 3, 2016.
- [17] B. Yang, M. Liu, and Z. LI, "Rendezvous on the fly: efficient neighbor discovery for autonomous UAVs," *IEEE Journal on Selected Areas in Communications*, vol. 36, no. 9, 2018.
- [18] Z. Ju and H. Liu, "Fuzzy Gaussian mixture models," *Pattern Recognition*, vol. 45, no. 3, 2012.
- [19] The ns manual (formerly ns notes and documentation), 2011, [https://www.isi.edu/nsnam/ns/doc/ns\\_doc.pdf](https://www.isi.edu/nsnam/ns/doc/ns_doc.pdf).
- [20] MSU quality measurement tool, 2016, [https://www.compression.ru/video/quality\\_measure/vqmt\\_download.html](https://www.compression.ru/video/quality_measure/vqmt_download.html).

## Research Article

# IoT System Integrating Unmanned Aerial Vehicles and LoRa Technology: A Performance Evaluation Study

**J.-M. Martinez-Caro**  and **M.-D. Cano** 

*Department of Information Technologies and Communication, Universidad Politécnica de Cartagena, Cartagena 30202, Spain*

Correspondence should be addressed to J.-M. Martinez-Caro; [josem.martinezcaro@upct.es](mailto:josem.martinezcaro@upct.es)

Received 26 July 2019; Revised 1 October 2019; Accepted 9 October 2019; Published 3 November 2019

Guest Editor: Zeeshan Kaleem

Copyright © 2019 J.-M. Martinez-Caro and M.-D. Cano. This is an open access article distributed under the Creative Commons Attribution License, which permits unrestricted use, distribution, and reproduction in any medium, provided the original work is properly cited.

Nowadays, the popularity of the unmanned aerial vehicles (UAVs) is high, and it is expected that, in the next years, the implementation of UAVs in day-to-day service will be even greater. These new implementations make use of novel technologies encompassed under the term Internet of Things (IoT). One example of these technologies is Long-Range (LoRa), classified as a Low-Power Wide-Area Network (LPWAN) with low-cost, low-power consumption, large coverage area, and the possibility of a high number of connected devices. One fundamental part of a proper UAV-based IoT service deployment is performance evaluation. However, there is no standardized methodology for assessing the performance in these scenarios. This article presents a case study of an integrated UAV-LoRa system employed for air-quality monitoring. Each UAV is equipped with a set of sensors to measure several indicators of air pollution. In addition, each UAV also incorporates an embedded LoRa node for communication purposes. Given that mobility is key when evaluating the performance of these types of systems, we study eight different mobility models, focusing on the effect that the number of UAVs and their flying speed have on system performance. Through extensive simulations, performance is evaluated via multiple quality dimensions, encompassing the whole process from data acquisition to user experience. Results show that our performance evaluation methodology allows a complete understanding of the operation, and for this specific case study, the mobility model with the best performance is Pathway because the LoRa nodes are distributed and move orderly throughout the coverage area.

## 1. Introduction

The Internet of Things (IoT) is gaining momentum. IoT represents a heterogeneous network scenario with virtually unlimited uses [1, 2]: Smart-Homes, Smart-Cities, Industry 4.0, Smart-Grids, etc. At the same time, unmanned aerial vehicles (UAV), also known as drones, are becoming a very interesting tool for traffic surveillance, crop monitoring, border patrolling, disaster management, remote areas control, or wildfire monitoring, and among others [3]. Examining the characteristics of both, IoT and UAVs, it can be presumed that UAVs could become a natural symbiotic element of the Internet of Things (IoT) [1]. Let us delve into this idea.

On the one hand, UAVs can be classified in terms of several features such as size, communication capacity, flight

mode, and wing types. UAVs can work isolated or in groups, giving rise to a new type of communication network called Flying Ad hoc Networks (FANETs) [4]. FANET can be seen as an extension of Mobile Ad hoc Networks (MANETs) with singular features in terms of mobility, topology, wave propagation, and energy constraints. In contrast to other communication networks as MANET or Vehicular Ad hoc Networks (VANETs), the UAVs move freely in the air, including a third axis ( $z$ ) to the mobility of the devices ( $x, y$ ) considered so far. Mobility models used for UAVs are usually classified according to its nature and are either created for other networks and then adapted to this new environment or specifically introduced as mobility models [5]. Mobility models are key for an optimal UAV deployment [6]. Numerous factors have a notable effect on the trajectory of UAVs such as energy constraints, collision

avoidance, flight time, ground users' demands, and the specific service in use. For instance, UAVs employed for extension coverage of wireless telecommunications network (better connectivity to terrestrial networks) will need to consider the Quality of Service (QoS) as a key element to optimize their performance [7].

On the other hand, it is a common practice in IoT to use small (and sometimes low cost) sensor devices to capture data from multiples sources. Then, these data are usually sent by means of wireless technology to a gateway that provides Internet connectivity to the cloud, where network servers are located. Network servers are responsible for collecting and processing the data and also making decisions or defining specific actions to be carried out. Although there are several technologies being used for the wireless part of this general IoT communication architecture, Low-Power Wide-Area Network (LPWAN) solutions are standing out [8]. Among their benefits, we can highlight the following: energy efficiency, low cost, possibility of dense deployments, and high performance in a wide coverage area. However, it is important to note that the low data rate (DR) and the duty cycle constraint (1%) make this technology not appropriate for time-sensitive traffic. One of the most popular LPWAN technologies is Long-Range (LoRa) [9]. LoRa uses a proprietary modulation algorithm patented by Semtech [10] as a derivative of chirp spread spectrum (CSS), operating in the industrial, scientific, and medical (ISM) band and spreading a narrowband signal over a wider channel bandwidth. The communication architecture of LoRa (layers and protocols) is defined by LoRaWAN [11, 12].

Consequently, these small sensors used in IoT together with their communications capabilities could be easily embedded in UAVs (e.g., Figure 1). By doing so, the UAVs provide a new framework to deploy IoT-based services. Although the maturity level of UAVs and LoRa/LoRaWAN for IoT is higher and higher, there are some important unsolved issues. From the UAV perspective, mobility is a challenge. Specific mobility models have been proposed in the scientific literature for UAVs and FANETs. However, how to select the best mobility pattern for a given service is still an open issue. From the IoT perspective, there is not yet a standardized methodology for performance evaluation in terms of quality [13].

In this paper, we address these two questions using a case study. Particularly, we evaluate the performance of an IoT air-quality monitoring system that integrates LoRa/LoRaWAN and UAVs. Each UAV incorporates an IoT device that has sensors, which measure the quality of the air, and a LoRa node for sending these data to a gateway. Eight different UAV mobility models are tested, namely, Random Walk (RW), Random Waypoint (RWP), Random Direction (RD), Gauss–Markov (GM), Reference Point Group Mobility (RPGM), Pathway, Semi-Random Circular Movement (SRCM), and Smooth Turn (ST). Performance is measured using four quality components, namely, Quality of Data (QoD), Quality of Information (QoI), Quality of user Experience (QoE), and Quality Cost (QC). These quality components encompass the whole process from data acquisition to user experience and were introduced in previous

works [14, 15]. Observe that, for each mobility model, we will measure the effect on performance of both the number of UAVs, equivalent to the number of IoT end-nodes, and the UAVs' flying speed. Through intensive computer simulations, we find out the best mobility model to be used for this IoT system. Results show that the mobility models that orderly cover all the areas obtain the best performance for the service under study.

The rest of the paper is organized as follows. A review of the state-of-the-art literature is included in Section 2. Section 3 describes the materials and methods used in this study. Simulation results are shown and discussed in Section 4. The paper ends with a conclusion in Section 5.

## 2. Related Work

There are many proposals in the scientific literature addressing the trade-off between resource optimization and performance in UAV deployments. It is well known that the mobility model is one of the key factors with a high impact of performance. Therefore, in this section, we first review previous works related to optimal location, distribution, and trajectories of UAVs. Then, we focus on studies that analyzed the impact of UAV mobility in the performance of the system in terms of quality metrics. Finally, we explore those works that have proposed the combined use of IoT wireless communication technologies, e.g., Wireless Sensor Networks (WSN) or LoRa, and UAVs.

In [3, 16], authors studied mobility models in UAVs. The goal was to identify the best mobility model in order to achieve higher WLAN coverage without decreasing performance. They took into account the qualitative and quantitative communications needs and used the number of drones as the main investigated parameter. Similarly, Chen et al. [17] suggested maximizing QoE at the expense of minimizing the total transmitted power by each UAV considering the channel communication constraints between the deployed devices and the base station (or base stations). Gao et al. [18] proposed a high energy-efficient resource allocation scheme considering the mobility of the UAVs and measuring the performance of devices in terms of QoE in dynamic aerial channel conditions and different transmission DR. Vashisht et al. [19] analyzed the impact of the increase of peripherals into UAVs; the idea was that only needed peripherals should be fixed in drones with limited resources to perform all the tasks in an energy-efficient way and increasing as much as possible the flight time.

Cheng et al. [20] proposed a security alternative regarding UAV trajectories and time scheduling with an iterative algorithm solving a convex optimization problem. Similarly, Zhao et al. [21] solved an optimization problem for UAV trajectories and Non-Orthogonal Multiple Access (NOMA) precoding by erasing the interference from the base station to UAVs or minimizing to a given threshold. Also coupling with QoE, contributions [17, 22, 23] resolved different optimization problems to guarantee the QoE requirement using the minimum transmission power in the UAV. In this case, the goal was to provide wider coverage for all nodes in a particular area maintaining QoS requirements



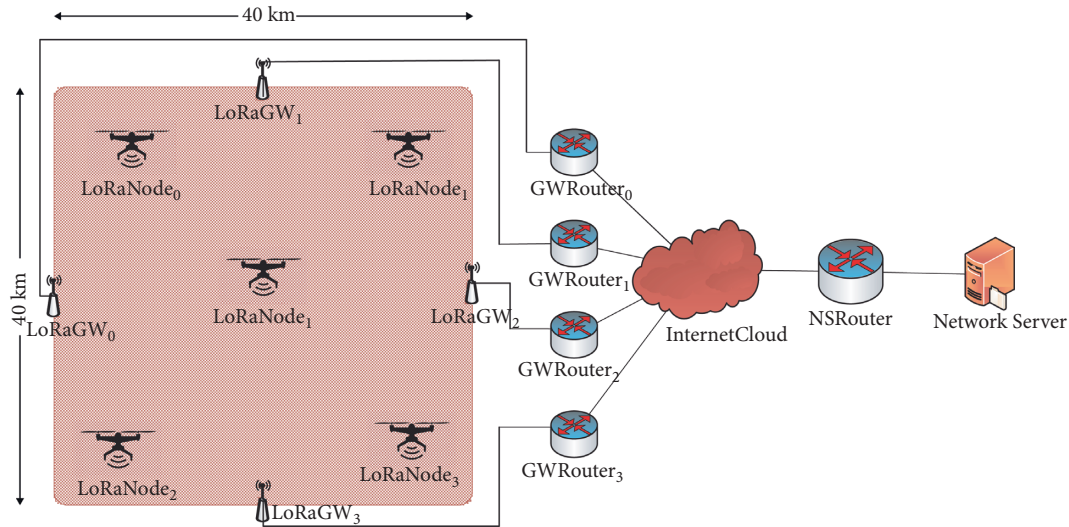


FIGURE 1: Example of an IoT deployment integrating LoRa/LoRaWAN and UAVs.

in the 3D deployment or maximizing the number of nodes in the coverage area but always being aware of energy efficiency. Other studies [18, 19, 24] addressed different challenges such as high node mobility, fluid topology, or low node density. As an example, Bouachir et al. [24] studied the Random Waypoint (RWP) mobility pattern, having a great impact on QoS metrics, mainly due to interference and packet collisions [25].

Regarding the combination of UAVs and IoT, several studies are addressing the use of WSN in these scenarios. For instance, in [3], the authors studied the features and conditions in a UAV network using different metrics to guarantee connectivity, security, and scalability. Other authors [26–29] evaluated the use of WSN to acquire raw data from the environment and employed LoRa/LoRaWAN to transmit the data to the server, assuming that LoRa covers a range up to 30 km. In [30, 31], the authors integrated WSN with UAVs and proposed an optimal trajectory design, minimizing the total path length, passing close to the main interesting points, and ensuring a minimal delay in the communication. Sharma et al. [32] tested a LoRaWAN network using UAVs for urban surveillance focusing on stress areas, being able to preserve 40% of the network energy consumption.

From a more complete perspective, Yuan et al. [1] assessed and compared the performance in rural and urban environments of UAVs equipped with LoRa, WiFi, and Long-Term Evolution (LTE) networks; results showed that LoRa achieved the best performance with greater swarm density and longer coverage range when LTE was not supported. Kirichek and Kulik [33] addressed the use of different elements in the networks as WSN acquiring data from terrestrial segments. In their proposal, LoRa/LoRaWAN devices transmitted the data acquired from the WSN to a UAV gateway. Then, the UAV acting as a gateway and/or as a repeater forwarded the data to reach the LoRa base station, which, in turn, forwarded the data to a network server. Finally, Trasviña-Moreno et al. [34] developed a

complete system with buoys equipped with WSN for marine-coastal environment monitorization and transmitted the acquired data using LoRa technology. This provided an easy-to-use and low-power solution with a large coverage area, one of the main features of LoRa. In parallel, a UAV with LoRa technology acted as a gateway to collect the data up to forwarding to the server that processes it. Finally, security is also one important concern because these devices could be an easy target. Some contributions addressed this issue using an efficient resource management and planning the strategy in accordance with QoS [19, 35, 36].

Despite existing many contributions that evaluated the performance of different mobility models in UAV or the incorporation of LoRa to UAV deployments, they have based the performance analysis only on two quality components, namely, QoS and QoE. For QoS, the examined metrics are the classic ones: delay, jitter, throughput, and packet losses. However, the QoE component does not have a standardized model for IoT services. Consequently, the metrics used to assess QoE in the state of the art are extremely unlike. With this paper, we verify a proposal that harmonizes the performance evaluation of IoT services using a complete UAV/LoRa/LoRaWAN deployment as a case study. The novelty resides on the use of multiple quality dimensions (QoD, QoI, QoE, and QC).

### 3. Materials and Methods

In this section, we describe the main features of the mobility models used in UAV deployments. Then, we describe the characteristics of the simulation framework that we have used in this study as well as the performance evaluation methodology.

*3.1. Mobility Models.* Dynamic topology, high mobility, etc., are significant challenges in the design of UAV networks and services. Taking into account that testing with real devices is

costly and depends on region restrictions, Camp et al. [25] suggested the use of mobility models under simulation to assess the performance of UAV networks and FANETs. The mobility of UAVs is largely different to the mobility of vehicles placed in the ground, so in most cases the MANET models are not directly applied. According to [5], two primary groups can be found for mobility models in this scenario: adapted mobility models and specific models defined for FANETs.

On the one hand, Xie et al. [5] adapted and extended traditional MANET mobility models from 2D to 3D classifying them into five categories: random, temporal dependency, spatial dependency, geographic dependency, and hybrid mobilities.

The first category encompasses Random Mobility, which, in turn, includes three models, namely, Random Walk (RW), Random Waypoint (RWP), and Random Direction (RD). In RW, the node randomly chooses the orientation and speed during a time interval, and before it ends, it chooses a new random orientation and speed for the next period reflecting or wrapping from the boundaries. In RWP, each node randomly selects a target in the coverage area and the travelling speed. When the node achieves the target, it waits for a random time; then, it chooses a new target and a new speed to reach the new target. Finally, in RD, the node chooses a course and speed moving to the border, where it rests and after that chooses a new direction to go. The difference among RD and RW is the travelling duration, being constant or random, respectively. In contrast, the aim of RWP model is to measure the influence of the range, speed, the number of hops, and the density of nodes in a FANET. Observe that despite the random mobility, the destination position is always in the constrained area range.

The second category is the temporally dependent mobility models that claim to avoid sudden changes in direction and speed, such as the Gauss–Markov (GM) [37] for tracking trajectories of targets. The GM equations are found in [5] and depend on heading speed, direction, and pitch, avoiding abrupt changes close to the borders. The GM model has been largely used for network performance evaluation. Smooth Random Mobility correlates the behavior of the vehicles in the ground by the Stop-Turn-Go model.

The third group is space-dependent, where the mobility of a node depends on the available space and the behavior of the closest nodes. One example is Reference Point Group Mobility (RPGM) that follows the master-slave model, where the members of a group follow the group leader [38]. Another example is Spatially Correlated Mobility, where the behavior of a node depends on the actions of the other nodes.

The fourth category is the geographical dependence classification, including the models with trajectory restrictions due to pathways or obstacles in the way [39]. Lastly, the hybrid models share at least two features of different categories as the Free-way Mobility model that relies on the present context (temporally dependent) and the position of surrounding nodes restricted to lanes on highways (space-dependent). Another case is the Disaster-Area model where many mobility models are included [5].

On the other hand, many mobility models have been specifically created for FANETs. First, in the Semi-Random Circular Movement (SRCM) model, all UAVs are placed around a fixed center and turn around it with a radius, speed, and initial angle. This model is not suitable in MANETs because these conditions are not feasible on ground due to geographical or item restrictions. But it is possible in FANET because of the available free space in the air. Second, the Three-Way Random Mobility assumes the heading speed and three possible states defined on a Markov chain: going straight, turning right, and turning left. Third, the Pheromone Repel model splits the area into small grids trying to cover all the available networks. The behavior of Three-Way Random and Pheromone Repel models close to the border is similar to GM model, choosing to turn completely the direction of the UAV pointing to the interior of the area. Fourth, the Smooth Turn (ST) captures the free-space mobility of the nodes making smooth trajectories with a large radius as aircrafts in 2D and 3D. In the second case, the 3D model has two versions,  $z$ -dependent and  $z$ -independent, which vary in the correlation along  $z$ -dimension and the plane  $(x, y)$ . Fifth, the Flight-Plan (FP) mobility defines flights where the initial and final point are known beforehand (e.g., regular and commercial), not suitable for autonomous UAVs. Finally, the Multi-Tier Mobility model use different aircraft types that flight at diverse heights. Figure 2 contains a brief summary of the mobility models mentioned in [5].

*3.2. Performance Evaluation in LoRa.* The simulation is carried out using OMNeT++ [40], INET framework [41], FLoRa framework [42], and Crypto++ [43]. The simulated scenario is composed of one server (called for this purpose Network Server, NS), four LoRa gateways (LoRaGWs), and a variable number of LoRa nodes ranging from five to twenty in the LoRa network. The scenario is depicted in Figure 1. Each UAV incorporates a set of sensors, so that the UAV can act as a mobile air-quality station. Specifically, each UAV includes nine pollution metrics.

During simulations, the UAVs will move around the coverage area at different speeds (10, 25, and 50 km/h). In addition, given the favored characteristic of LoRa nodes, these are also embedded into the UAVs to send the collected data to the LoRaGW. In our scenario, we employ four LoRaGWs to cover the complete area (40 km  $\times$  40 km), thus maximizing the coverage area, but considering that duplicated packets might be received. Behind the LoRaGWs, four GWRouters (one for each LoRaGW), one InternetCloud, one NSRouter, and one Network Server compose the backhaul network (Figure 1). When a LoRaGW receives a frame, it forwards it through the cloud to the Network Server. This element processes the packet and obtains valuable information for decision-making. In summary, each UAV in the topology represents an air-quality station with sensors that acquire data from the environment where the UAV is flying, and the embedded LoRa node transmits the raw data to the Network Server through a LoRaGW. Each LoRa node generates packets randomly using an

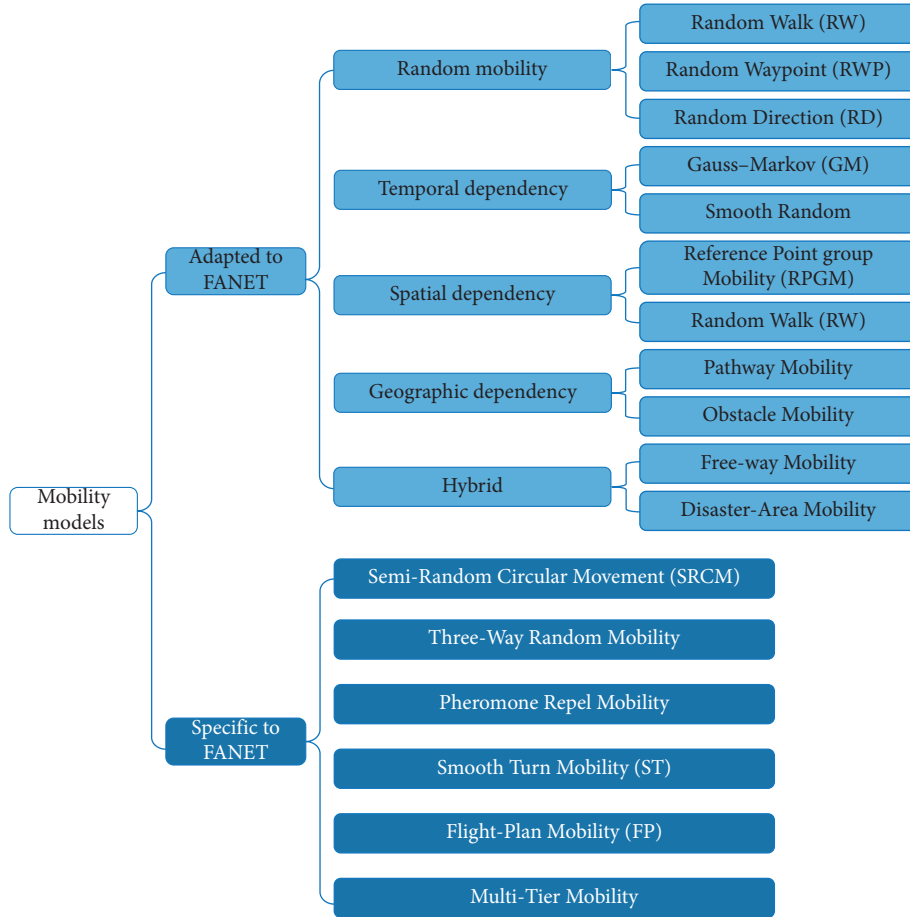


FIGURE 2: Mobility model classification.

exponential distribution with mean 100 seconds. For a better understanding, sensor measurements are obtained from a real dataset [44] that corresponds to a suburban area. Table 1 and Figure 3 show the configuration parameters used in the simulations.

Our goal is to evaluate the performance of eight different mobility models: RW, RWP, RD, GM, RPGM, Pathway, SRCM, and ST. For each model, we analyze the effect of the number of LoRa nodes (i.e., the number of UAVs) and also their motion speed. The evaluation is carried out using four quality components introduced in [14, 15], each one covering a different dimension of the performance, and thus avoiding overlapping. In this sense, these four quality components are divided into two magnitudes: profit (QoD, QoI, and QoE) and cost (QC). Each component assesses one dimension:

- (1) QoD: it measures the quality of raw data as acquired by sensors. It is calculated as shown in (1) and it refers to the precision of the sensor reading, the truthfulness of the measurement (it is within range), and the completeness of the measured data (if all sensors work properly).
- (2) QoI: it measures the quality of the obtained information after raw data have been processed in the server. It includes seven metrics dealing with the

TABLE 1: LoRa parameters used in simulations.

Parameter	Values
Spreading factor (SF)	Random (7, 12) uniform distribution
Transmission power (TP)	Random (2, 14 dBm) uniform distribution
Bandwidth (BW)	125 kHz
Coding rate (CR)	4/5
Time to first/next packet	Exponential (100 s)
Number of grids	5 × 5
$d_{\max}$ , $d_{\min}$ suburban	{12148.93 m, 999.71 m}

quality of the processed data, from the amount of data received to the accuracy of these data. It is obtained as shown in (2).

- (3) QoE: it measures network performance (i.e., classical QoS values) and the user experience. Initially, only the use of the network interface of the LoRa gateway is considered as a metric different from the well-known QoS metrics used for performance evaluation (delay, jitter, packet loss, and throughput). It is calculated as shown in (3).
- (4) QC: it measures the cost in terms of resources, e.g., energy consumption, computation capacity, and duty cycle limitation (1%). Its expression is depicted in (4).

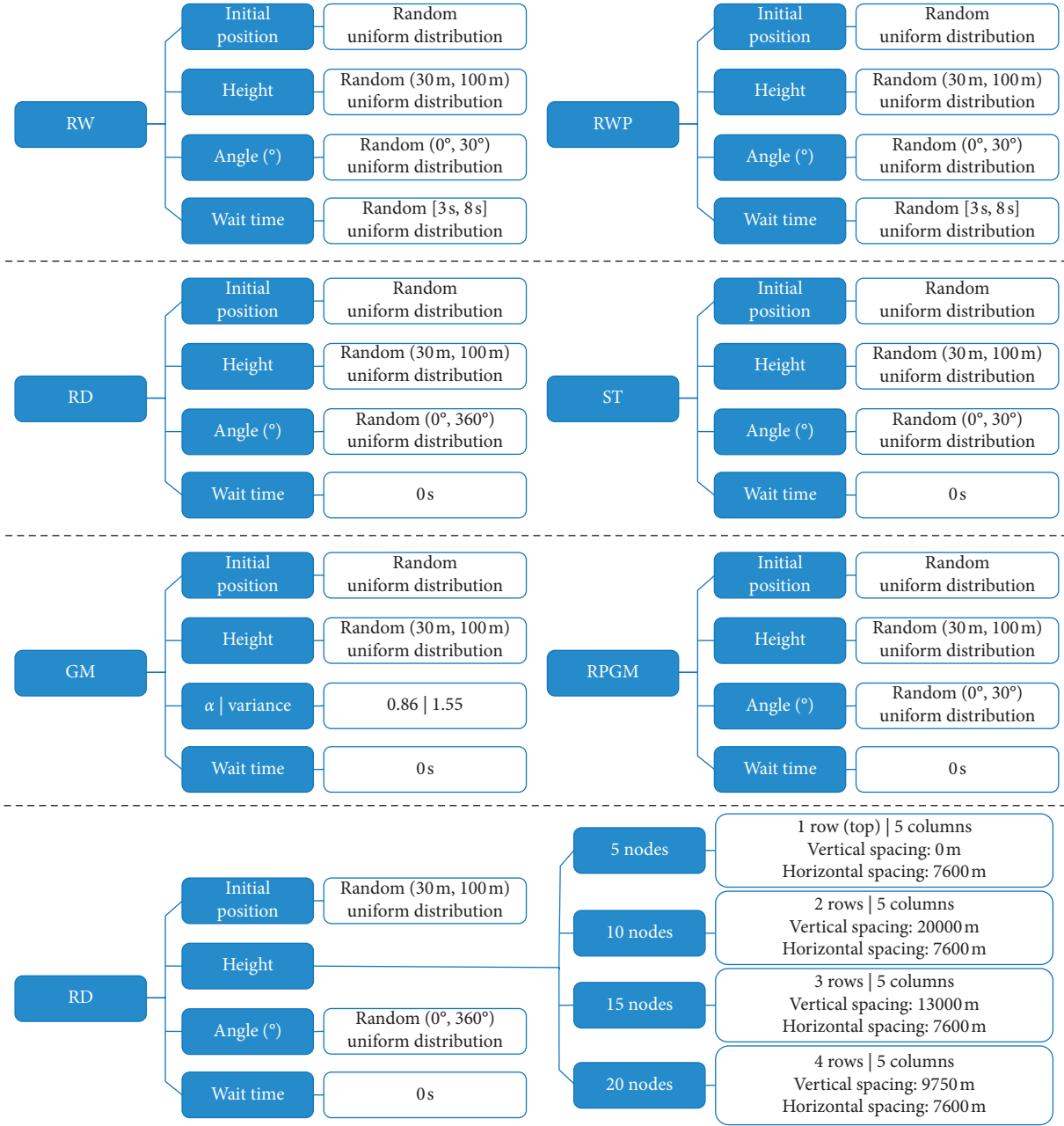


FIGURE 3: Specific parameters used in simulations for the mobility models.

$$\text{QoD} = \text{completeness} \cdot \text{precision} \cdot \text{truthfulness}, \quad (1)$$

$$\text{QoI} = \text{quantity} \cdot \text{precision} \cdot \text{recall} \cdot \text{accuracy} \cdot \text{timeliness} \cdot \text{detail} \cdot \text{validity}, \quad (2)$$

$$\text{QoE} = \text{jitter} \cdot \text{delay} \cdot \text{packet delivery rate} \cdot \text{throughput}_{\text{bps}} \cdot \text{gateway}_{\text{availability}}, \quad (3)$$

$$\text{QC} = \text{energy consumption} \cdot \text{interface usage}. \quad (4)$$

It is important to observe that each quality component is the product of several metrics, previously normalized, as

shown in (1)–(4). Therefore, QoD, QoI, QoE, and QC are also normalized values [0-1], being 1 the best possible performance and 0 the worst one. Quality components will be calculated at time intervals, called  $T_{\text{eval}}$ , at the network server. This evaluation period ( $T_{\text{eval}}$ ) is customized according to the monitoring needs. In this paper, we use  $T_{\text{eval}} = 500$  s.

#### 4. Results and Discussion

In this section, we show the results obtained after extensive simulations. The eight mobility models have been tested with a variable number of UAVs/LoRa nodes {5, 10, 15, and 20} and different speeds {10, 25, and 50 km/h}. Results are

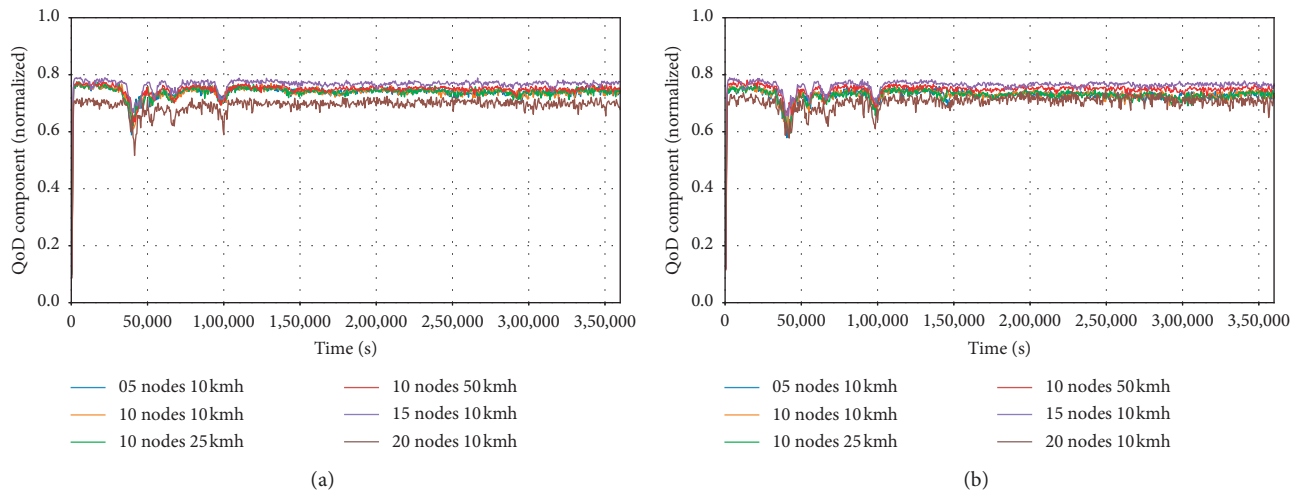


FIGURE 4: (a) RW and (b) RPGM models obtain the best QoD.

obtained for QoD, QoI, QoE, and QC. The term QoX will be used in this section to refer to any of these quality components.

Generally, the performance in terms of quality components QoX improves as the number of LoRa nodes/UAVs increases. This result applies to all the evaluated mobility models. The only exception is for RPGM because all flying nodes are usually located into a small part of the studied area; therefore, at each  $T_{eval}$ , the system only receives packets from one or two grids. This entails the worst value for QoI when the number of LoRa nodes/UAVs is higher in RPGM. In the situation where the number of flying devices is constant and we only change the speed of the devices, the different mobility models obtain similar results with a slight performance enhancement as the speed increases. As we commented previously, the QoI component of the RPGM model is highly affected by mobility, due to the coverage; therefore, the faster the movement, the best the results for this model.

Now, we discuss the particular results for each QoX component. In relation to the data acquisition process, we have measured the quality of the raw data obtained by the UAV-incorporated sensors. Because we are focusing on collecting data, the QoD component penalizes pollution measurements that are not taken. If we observe how QoD varies as a function of the number of nodes, we can see that, in general, the more the number of UAVs, the better the performance (Figure 4). In the scenario with 5 nodes, the raw data obtained by the first LoRa node ( $node_0$ ) is weaker because it has not all the sensors to obtain all the air-quality values. This fact penalizes the QoD in this scenario. As the number of UAVs increases, this “poor” UAV goes unnoticed because the rest of UAVs collect a high number of measurements, thus increasing the value of QoD. The QoD value is practically the same with a constant number of UAVs, though with a certain variance due to the random message generation by each UAV. On this component, the speed at which the UAV moves within the coverage area does not have any influence on

the results. Lastly, the scenario with 20 UAVs is slightly better than others in terms of QoD for all mobility models because the effect of that “poor” UAV is lower. The performance for all mobility models are quite similar because the QoD metrics only depend on the raw data, which is obtained from the same dataset that is shared by all the tested mobility models. The best performance is acquired by RPGM and RW models (Figure 4) and the worst by RWP and RD (Figure 5).

After the data acquisition process, the QoI component measures the quality of the obtained information. QoI depends on seven metrics, as shown in (2), which make it very volatile. In other words, mobility has a higher impact on QoI than in QoD. To this particular case, the better the performance, the faster the nodes because the Network Server receives packets from all grids (i.e., more data are available to monitor all grids in the studied area). The recall metric is responsible for measuring this effect on QoI. The mobility model with the best performance for this quality component is Pathway Mobility due to the orderly arrangement of the UAVs in the coverage area (Figure 6). This means that once processed the data, the Network Server assesses information from all the monitored areas, which is very important for decision-making.

The use of four LoRaGWs guarantees that there are no hidden or “blank” areas without LoRa coverage. Therefore, the performance in terms of QoE is very similar for all the mobility models. The only metric that varies a little bit more is  $gateway_{availability}$ , see (3). The reason is that this metric evaluates how busy is the gateway because of the need for sending data, which could create a bottleneck in specific congested scenarios (which is not the case). All mobility models obtain similar results with RD as the best one (Figure 7); this is because this model looks for the edge of the area to change the direction, coinciding with the location of LoRaGWs, so the ratio of delivery packets is higher than in other mobility models. The speed of the flying LoRa nodes/UAVs does not affect performance in the QoE quality component.

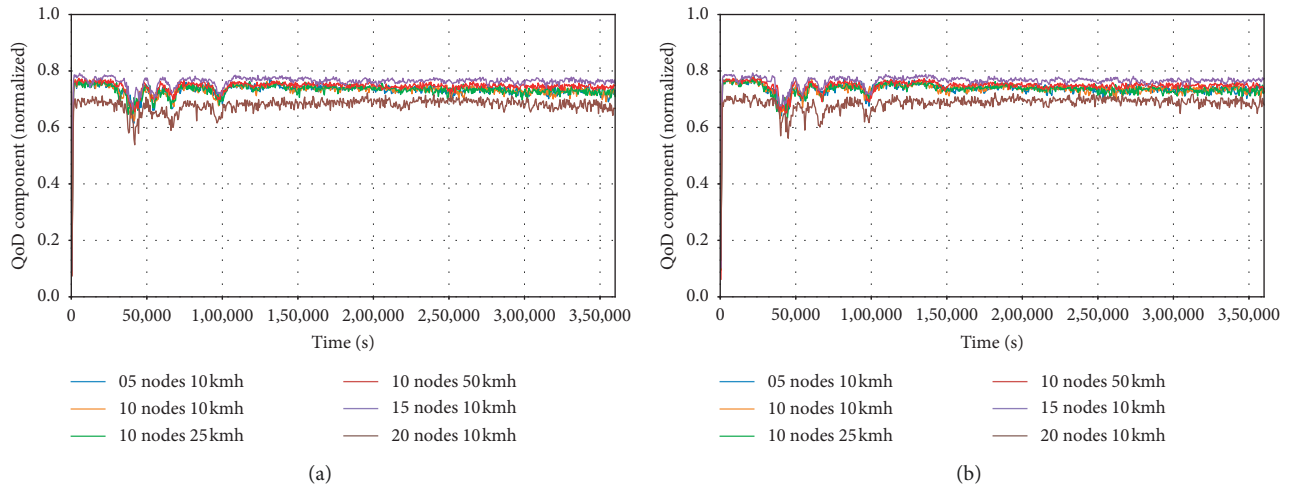


FIGURE 5: (a) RWP and (b) RD mobility models obtain the worst QoD.

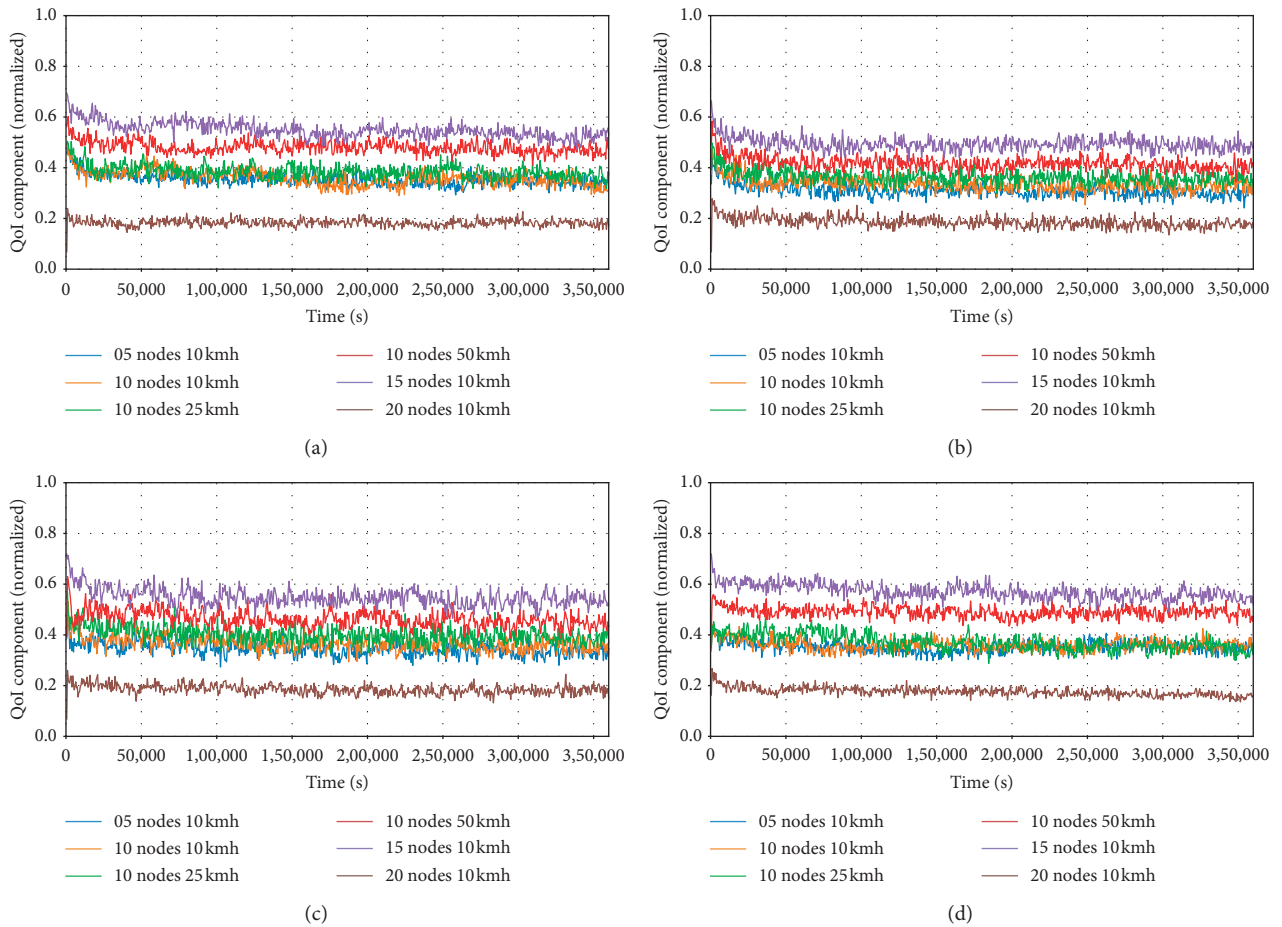


FIGURE 6: Continued.

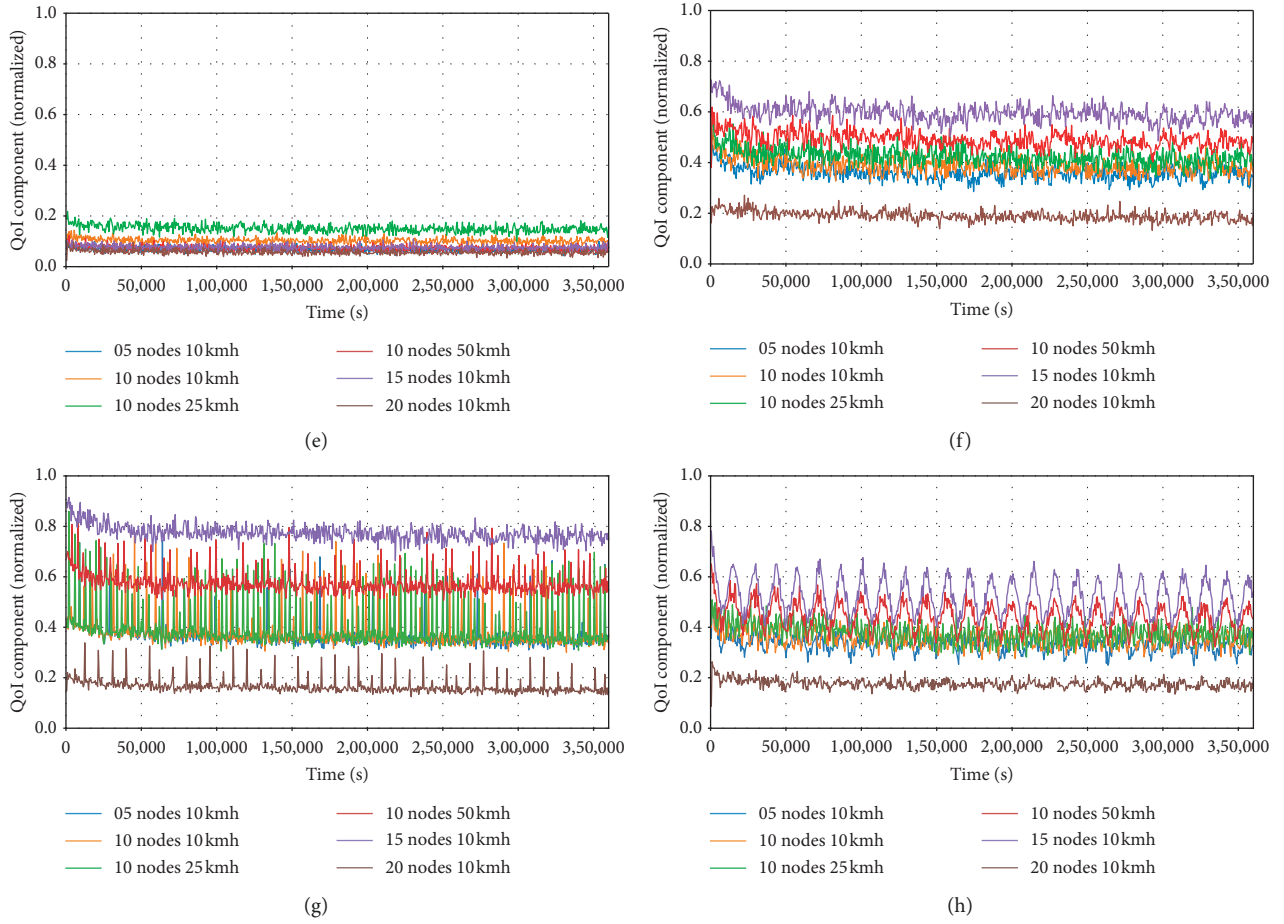


FIGURE 6: Performance results of the eight mobility models for the QoI quality component: (a) ST, (b) SRCM, (c) RWP, (d) RW, (e) RPGM, (f) RD, (g) Pathway, and (h) GM mobility models.

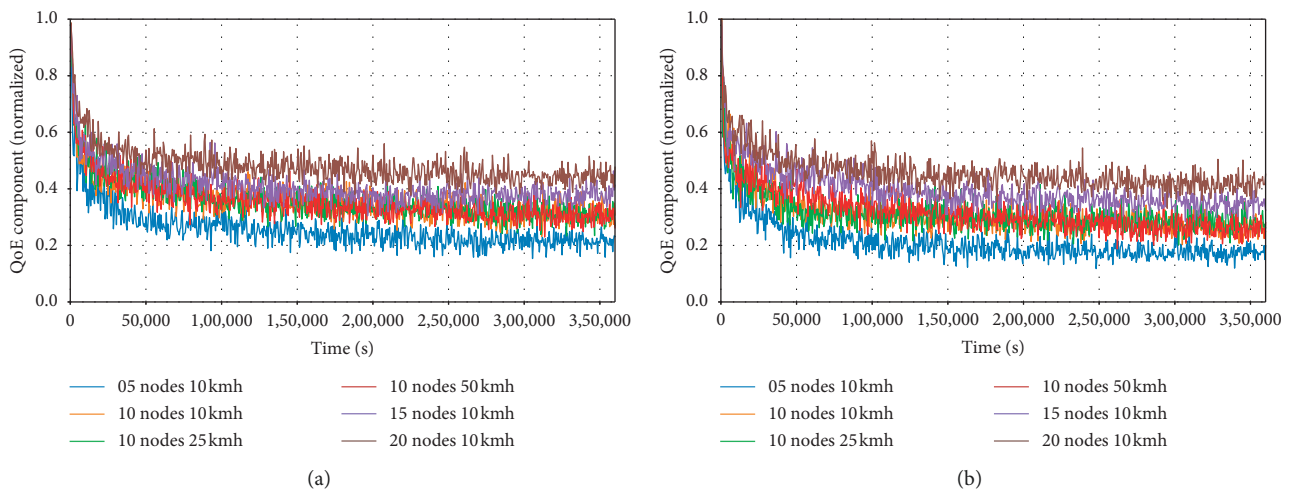


FIGURE 7: Performance results of the best ((a) RD) and the worst ((b) RPGM) mobility models for the QoE quality component.

Finally, we discuss the QC quality component. The energy consumption depends on the state of the transceiver (higher consumption in transmitting state). Due to a

random message generation when the number of UAVs is lower, the number of times that transceiver is in transmitting mode is different for each  $T_{eval}$ . This fact makes this

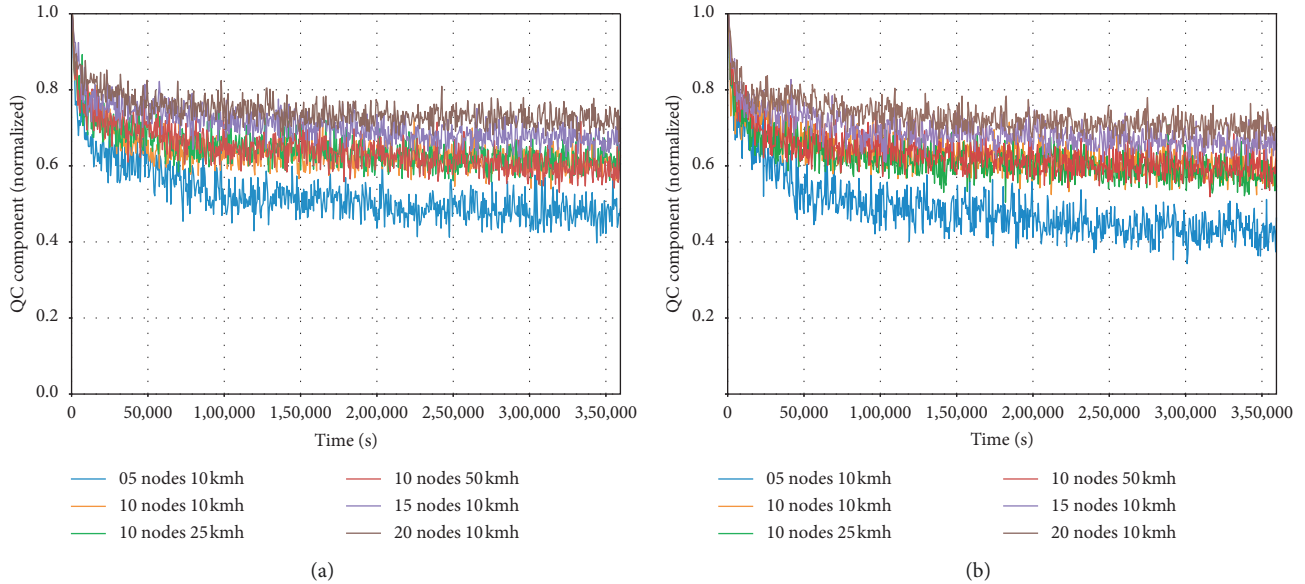


FIGURE 8: Performance results of the best ((a) GM) and the worst ((b) RPGM) mobility models for the QC quality component.

component unstable because the consumption is highly fluctuating between two time intervals  $T_{eval}$ . The best result is obtained for the GM model and the worst for RPGM model (Figure 8), although the difference is small.

## 5. Conclusion

The combination of technologies to design a multifaceted system is a current trend with greater impact on future smart services. UAVs, as well as LoRa, is a very flexible technology with an increasing number of applications. However, today, there is still not a standard to evaluate the performance of these technologies (or combination of them). Therefore, we used a model based on different quality components that address different dimensions of the operation of the service. We compared the results obtained for eight mobility models (Random Walk, Random Waypoint, Random Direction, Gauss–Markov, Reference Point Group Mobility, Pathway Mobility, Semi-Random Circular Movement, and Smooth Turn). From the results, we found out that whereas QoD and QC components hardly vary among models because these quality components do not depend on communication factors, some variation is perceived in terms of QoI and QoE. These two quality components, QoI and QoE, depend on wireless and wired network conditions, and thus, the provision and the movement of the flying nodes across the network have a direct impact on performance. On the one hand, the QoI component achieves a better performance for those mobility models whose UAVs move orderly through the network. On the other hand, QoE relies on network conditions and the best results were achieved for the RD mobility model which minimizes network metrics such as delay, jitter, and packet delivery rate. As future work, we plan to improve the quality model to find out the best relationship among quality components.

## Data Availability

The data used to support the findings of this study is open access and cited at relevant places within the text as references [44].

## Conflicts of Interest

The authors declare that there are no conflicts of interest regarding the publication of this paper.

## Acknowledgments

This work was supported by the AEI/FEDER-UE Project grant (TEC2016-76465.C2-1-R) (AIM).

## References

- [1] Z. Yuan, J. Jin, L. Sun, K.-W. Chin, and G.-M. Muntean, "Ultra-reliable IoT communications with UAVs: a swarm use case," *IEEE Communications Magazine*, vol. 56, no. 12, pp. 90–96, 2018.
- [2] A. Al-Fuqaha, M. Guizani, M. Mohammadi, M. Aledhari, and M. Ayyash, "Internet of things: a survey on enabling technologies, protocols, and applications," *IEEE Communications Surveys & Tutorials*, vol. 17, no. 4, pp. 2347–2376, 2015.
- [3] S. Hayat, E. Yanmaz, and R. Muzaffar, "Survey on unmanned aerial vehicle networks for civil applications: a communications viewpoint," *IEEE Communications Surveys & Tutorials*, vol. 18, no. 4, pp. 2624–2661, 2016.
- [4] A. Guillen-Perez and M. D. Cano, "Flying ad hoc networks: a new domain for network communications," *Sensors (Switzerland)*, vol. 18, no. 10, p. 3571, 2018.
- [5] J. Xie, Y. Wan, J. H. Kim, S. Fu, and K. Namuduri, "A survey and analysis of mobility models for airborne networks," *IEEE Communications Surveys & Tutorials*, vol. 16, no. 3, pp. 1221–1238, 2014.



- [6] M. Mozaffari, W. Saad, M. Bennis, Y.-H. Nam, and M. Debbah, "A tutorial on UAVs for wireless networks: applications, challenges, and open problems," *IEEE Communications Surveys & Tutorials*, vol. 21, no. 3, pp. 2334–2360, 2019.
- [7] A. Guillen-perez, R. Sanchez-iborra, and M. Cano, "WiFi networks on drones," in *Proceedings of the 2016 ITU Kaleidoscope: ICTs for a Sustainable World (ITU WT)*, Bangkok, Thailand, November 2016.
- [8] U. Raza, P. Kulkarni, and M. Sooriyabandara, "Low power wide area networks: an overview," *IEEE Communications Surveys & Tutorials*, vol. 19, no. 2, pp. 855–873, 2017.
- [9] LoRa Alliance, 2019, <http://lora-alliance.org/>.
- [10] Semtech, 2019, <http://www.semtech.com>.
- [11] LoRa Alliance, *LoRaWAN—What Is It?. A Technical Overview of LoRa and LoRaWAN*, LoRa Alliance, Fremont, CA, USA, 2015.
- [12] A. Lavric and V. Popa, "A LoRaWAN: Long range wide area networks study," in *Proceedings of the 2017 11th International Conference on Electromechanical and Power Systems*, vol. 2017, pp. 417–420, Iasi, Romania, October 2017.
- [13] Q. Wu, G. Ding, Y. Xu et al., "Cognitive internet of things: a new paradigm beyond connection," *IEEE Internet of Things Journal*, vol. 1, no. 2, pp. 129–143, 2014.
- [14] J.-M. Martinez-Caro and M.-D. Cano, "A holistic approach to evaluate the performance of applications and services in the internet of things," *International Journal of Communication Systems*, 2019.
- [15] J.-M. Martinez-Caro and M.-D. Cano, "Simulación y análisis de rendimiento en dispositivos LoRa sobre drones," in *Proceedings of the Jornadas de Ingeniería Telemática JITEL'19*, pp. 1–8, Zaragoza, Spain, January 2019.
- [16] J. Braga, A. Alessandretti, A. P. Aguiar, and J. Sousa, "A feedback motion strategy applied to a UAV to work as an autonomous relay node for maritime operations," in *Proceedings of the International Conference on Unmanned Aircraft Systems (ICUAS)*, no. 642153, pp. 625–632, Miami, FL USA, June 2017.
- [17] M. Chen, M. Mozaffari, W. Saad, C. Yin, M. Debbah, and C. S. Hong, "Caching in the sky: proactive deployment of cache-enabled unmanned aerial vehicles for optimized quality-of-experience," *IEEE Journal on Selected Areas in Communications*, vol. 35, no. 5, pp. 1046–1061, 2017.
- [18] A. Gao, Y. Hu, W. Liang, Y. Lin, L. Li, and X. Li, "A QoS-oriented scheduling scheme for energy-efficient computation offloading in UAV cloud system," *IEEE Access*, vol. 7, pp. 68656–68668, 2019.
- [19] S. Vashist and S. Jain, "Location-aware network of drones for consumer applications: supporting efficient management between multiple drones," *IEEE Consumer Electronics Magazine*, vol. 8, no. 3, pp. 68–73, 2019.
- [20] F. Cheng, G. Gui, N. Zhao, Y. Chen, J. Tang, and H. Sari, "UAV-relaying-Assisted secure transmission with caching," *IEEE Transactions on Communications*, vol. 67, no. 5, pp. 3140–3153, 2019.
- [21] N. Zhao, X. Pang, Z. Li et al., "Joint trajectory and precoding optimization for UAV-assisted NOMA networks," *IEEE Transactions on Communications*, vol. 67, no. 5, pp. 3723–3735, 2019.
- [22] Z. Zhu, L. Li, and W. Zhou, "QoS-aware 3D deployment of UAV base stations," in *Proceedings of the 10th International Conference on Wireless Communications and Signal Processing (WCSP)*, pp. 1–6, Xi'an, China, October 2018.
- [23] M. Alzenad, A. El-keyi, F. Lagum, and H. Yanikomeroglu, "3D placement of an unmanned aerial vehicle base station (UAV-BS) for energy-efficient maximal coverage," *IEEE Wireless Communications Letters*, vol. 6, no. 4, pp. 434–437, 2017.
- [24] O. Bouachir, F. Garcia, N. Larrieu, and T. Gayraud, "Ad hoc network QoS architecture for cooperative unmanned aerial vehicles (UAVs)," in *Proceedings of the IFIP Wireless Days*, pp. 1–4, Venice, Italy, October 2013.
- [25] T. Camp, J. Boleng, and V. Davies, "A survey of mobility models for ad hoc network research," *Wireless Communications and Mobile Computing*, vol. 2, no. 5, pp. 483–502, 2002.
- [26] S. Subashini, R. Venkateswari, and P. Mathiyalagan, "A study on LoRaWAN for wireless sensor networks," *Advances in Intelligent Systems and Computing*, Springer, Singapore, 2018.
- [27] W.-K. Lee, M. J. W. Schubert, B.-Y. Ooi, and S. J.-Q. Ho, "Multi-source energy harvesting and storage for floating wireless sensor network nodes with Long range communication capability," *IEEE Transactions on Industry Applications*, vol. 54, no. 3, pp. 2606–2615, 2018.
- [28] J. Petäjäjärvi, K. Mikhaylov, A. Roivainen, T. Hänninen, and M. Pettissalo, "On the coverage of LPWANs: range evaluation and channel attenuation model for LoRa technology," in *Proceedings of the 14th International Conference on ITS Telecommunications (ITST)*, pp. 55–59, Copenhagen, Denmark, December 2015.
- [29] C. A. Trasviña-Moreno, R. Blasco, R. Casas, and Á. Asensio, "A network performance analysis of LoRa modulation for LPWAN sensor devices carlos," in *Ubiquitous Computing and Ambient Intelligence*, pp. 174–181, Gran Canaria, Spain, December 2016, [https://link.springer.com/chapter/10.1007/978-3-319-48799-1\\_21](https://link.springer.com/chapter/10.1007/978-3-319-48799-1_21).
- [30] D. Popescu, C. Dragana, F. Stoican, L. Ichim, and G. Stamatescu, "A collaborative UAV-WSN network for monitoring large areas," *Sensors (Switzerland)*, vol. 18, no. 12, 2018.
- [31] Y. Zeng, R. Zhang, and T. J. Lim, "Throughput maximization for UAV-enabled mobile relaying systems," *IEEE Transactions on Communications*, vol. 64, no. 12, pp. 4983–4996, 2016.
- [32] V. Sharma, I. You, G. Pau, M. Collotta, J. D. Lim, and J. N. Kim, "LoRaWAN-based energy-efficient surveillance by drones for intelligent transportation systems," *Energies*, vol. 11, no. 3, 2018.
- [33] R. Kirichek and V. Kulik, "Distributed computer and communication networks," in *Proceedings of the International Conference on Distributed Computer and Communication Networks*, vol. 919, pp. 442–453, Moscow, Russia, September 2018.
- [34] C. A. Trasviña-Moreno, R. Blasco, Á. Marco, R. Casas, and A. Trasviña-Castro, "Unmanned aerial vehicle based wireless sensor network for marine-coastal environment monitoring," *Sensors (Switzerland)*, vol. 17, no. 3, pp. 1–22, 2017.
- [35] C. Lin, D. He, N. Kumar, K.-K. R. Choo, A. Vinel, and X. Huang, "Security and privacy for the internet of drones: challenges and solutions," *IEEE Communications Magazine*, vol. 56, no. 1, pp. 64–69, 2018.
- [36] L. Gupta, R. Jain, and G. Vaszkun, "Survey of important issues in UAV communication networks," *IEEE Communications Surveys & Tutorials*, vol. 18, no. 2, pp. 1123–1152, 2016.
- [37] S. Shirazipourzad, P. Ghosh, and A. Sen, "On connectivity of airborne networks with unpredictable flight path of aircrafts," in *Proceedings of the first ACM MobiHoc workshop on Airborne Networks and Communications—Airborne'12*, vol. 1, Hilton Head, SC, USA, June 2012.

- [38] X. Hong, M. Gerla, G. Pei, C. Chiang, and L. Angeles, "A group mobility model for ad hoc wireless networks," in *Proceedings of the 2nd ACM International Workshop on Modeling, Analysis and Simulation of Wireless and Mobile Systems*, Seattle, WC, USA, August 1999.
- [39] P. Johansson, T. Larsson, N. Hedman, B. Mielczarek, and M. Degermark, "Scenario-based performance analysis of routing protocols for mobile ad-hoc networks," in *Proceedings of the 5th Annual ACM/IEEE International Conference on Mobile Computing and Networking*, pp. 195–206, Seattle, WC, USA, August 1999.
- [40] OMNeT++ Simulator, 2019, <http://omnetpp.org/>.
- [41] INET Framework, 2019, <http://inet.omnetpp.org/>.
- [42] FLoRa Framework, 2019, <http://flora.aalto.fi/>.
- [43] Crypto++ Library 8.0, 2019, <http://www.cryptopp.com/>.
- [44] Euskadi Air Quality (2018), 2019, <http://opendata.euskadi.eus/catalogo/-/calidad-aire-en-euskadi-2018/>.

## Research Article

# Experiments with a LoRaWAN-Based Remote ID System for Locating Unmanned Aerial Vehicles (UAVs)

Ali Ghubaish , Tara Salman, and Raj Jain

Computer Science & Engineering, Washington University in St. Louis, St. Louis 63130, USA

Correspondence should be addressed to Ali Ghubaish; [aghubaish@wustl.edu](mailto:aghubaish@wustl.edu)

Received 24 May 2019; Revised 19 September 2019; Accepted 26 September 2019; Published 20 October 2019

Guest Editor: Zeeshan Kaleem

Copyright © 2019 Ali Ghubaish et al. This is an open access article distributed under the Creative Commons Attribution License, which permits unrestricted use, distribution, and reproduction in any medium, provided the original work is properly cited.

Federal Aviation Administration (FAA) of the United States is considering Remote ID systems for unmanned aerial vehicles (UAVs). These systems act as license plates used on automobiles, but they transmit information using radio waves. To be useful, the transmissions in such systems need to reach long distances to minimize the number of ground stations to capture these transmissions. LoRaWAN is designed as a cheap long-range technology to be used for long-range communication for the Internet of Things. Several manufacturers make LoRaWAN modules, which are readily available on the market and are, therefore, ideal for the UAVs Remote IDs at a low cost. In this paper, we present our experiences in using LoRaWAN technology as a communication technology. Our experiments to identify and locate the UAV systems uncovered several issues of using LoRaWAN in such systems that are documented in this paper. Using several ground stations, we can determine the location of a UAV equipped with a LoRaWAN module that transmits the UAV Remote ID. Hence, it can help identify UAVs that unintentionally, or intentionally, fly into restricted zones.

## 1. Introduction

According to the Federal Aviation Administration (FAA), around seven million unmanned aerial vehicles (UAVs) will be sold in the United States by 2020 [1]. UAVs have great potential in many civilian and military applications. Nevertheless, they can hinder public safety and privacy when flying in unauthorized areas. Governments may restrict or forbid UAVs flying in certain areas without prior permission. Such areas include airports, borders, and many others. In 2016 alone, around 1,800 violations were reported, including UAVs approaching airplanes and disturbing their safety [2–4]. This number has increased by more than one-third compared to 2015. Although no catastrophic accident has happened, it is essential to find a solution to reduce these violations.

Many solutions have been proposed for UAV surveillance such as the mandatory registrations in the FAA registry, geolocation systems, drone guns, signal jammers, sound recognition systems, and visual perception systems. The FAA started a UAV registry in 2015 to locate the owners

of UAVs violating any rules [5, 6]. UAV manufacturers use the global positioning system (GPS), which is a satellite-based navigation system owned by the United States, to detect the UAV's location and prevent it from flying in restricted areas [7, 8]. Two drone guns, "Dronegun" and "DroneDefender," have been offered by two different companies to bring down UAVs causing problems [9, 10]. These guns are used to override the signal between the UAV and its remote control, and the UAV is then controlled by the gun controller. However, drone guns require the UAV to be in the line of sight (LoS) of a human with the gun to find the same frequency used by the UAV's remote control to control it. Signal jammers have been used to prevent UAVs from being controlled by their owners when the UAVs enter restricted areas. This forces the UAVs to go back to their configured home point if they lose their control signal. However, jamming affects other wireless devices that use the same frequency band that the UAVs use. This includes 2.4 GHz used by Wi-Fi, which makes this approach inconvenient in most places. UAVs can also be detected by their propeller sound; hence, two different UAV sound

recognition systems were purposed by Shi et al. and Anwar et al. [11, 12]. The issue with these systems is that it may not efficiently work if an audio jammer device is attached to the UAV. Visual perception systems like humans' vision, cameras, and proper monitoring may be easier to enforce security in the restricted areas, but these come with cost and maintenance difficulties.

One of the solutions that are being considered by the FAA is to require all the UAVs to have a Remote ID [13, 14]. These IDs will serve as license plates that transmit information to allow authorities to determine the owners of the UAVs and may detect their locations. Remote ID transmission needs a long-haul wireless technology that is cheap enough for low-cost UAVs but still reaches several miles. We believe LoRaWAN is one such technology that can reach from 9 to 18 miles (15 to 30 kilometers) in optimal cases [15, 16]. Hence, deploying a system that uses LoRaWAN protocol can help track the UAVs.

We have developed a prototype and have experimented with LoRaWAN protocol on UAVs. Our goal was to find the feasibility of using this protocol to locate and identify the UAVs. Finding the location of any UAV required us to determine the 3-dimensional (3-D) location of the UAV using several ground stations (GSs) listening to the ID broadcasts from the UAV. Upon reception, each GS estimates the distance between itself and the UAV. A minimum of four GSs are required to estimate the location of the UAV in 3-D. A system like this can help law enforcement to be alerted when any UAV flies in a restricted area. We found several issues with using the LoRaWAN protocol in such systems. These issues include the variability of using different LoRaWAN modules, the module's antenna direction, and the battery capacity to run these modules.

The rest of the paper is organized as follows: Section 2 provides background and related work; Section 3 discusses system architecture; and Section 4 shows the experimental implementation and results in detail. The critical issues discovered by our experiments are discussed in Section 5. Finally, conclusions and future work are presented in Section 6.

## 2. Background and Related Work

This section gives a brief background on the technologies used in the paper. Besides, we discuss some of the earlier related works.

**2.1. LoRaWAN.** A UAV is controlled by a ground-based remote controller via a radio frequency (RF) communication protocol [17]. RF technologies such as LoRaWAN, Zigbee, and 6LoWPAN can be used for communications [18–21]. LoRaWAN is a relatively new technology that is suitable for UAV communications due to its low power, low cost, and long-range reachability. The medium access control (MAC) protocol for LoRaWAN has been standardized by the LoRa Alliance. It uses the LoRa physical layer that enables it to reach long ranges with low-power consumption using the chirp spread spectrum modulation [18, 22]. We selected

LoRaWAN for location estimation due to its low cost and long-range reachability. Further description of LoRaWAN can be found in [15].

**2.2. Distance and Location Estimation.** Different methods have been explored in the literature for distance estimation. These methods include the time of arrival (ToA), time of flight (ToF), and received signal strength indication (RSSI) [23–26]. ToA method uses elapsed time between sending and receiving a signal between two nodes to measure the distance between them. For instance, GPS uses the ToA between a client node and a satellite to measure the distance between them [8]. The ToF method measures the time for radio signals to bounce back to the GS after being sent to the UAV. This method has been used in aircraft since 1950 [27].

RSSI is a measure of the quality of the signal and can be used for distance estimation. It measures the power level of the received signal [28]. Its value is measured in decibel (dB) and has multiple applications in wireless communication. One of these applications is distance estimation between two nodes, such as the UAV and the GS [29].

Location estimation of any UAV requires knowing its distance from several GSs with known coordinates. For locating the UAV in 2-dimension (2-D), distances from at least 3 GSs are required. For location estimation in 3-D, distances from four GSs are required. Given the coordinates of the required number of GSs and by estimating the distance using one of the previously stated methods, the location of the UAV can be estimated. For example, the ToA method is being used in GPS, which consists of around 31 satellites [8]. Each satellite broadcasts its location and time. By knowing how far the UAV is from one satellite, the UAV knows its distance from that satellite and knows that it is located on a sphere with the estimated distance as a radius. Adding at least two more satellites' information can help the UAV estimate its location in 2-D by finding the points where the three satellites' spheres intersect. Further, adding more satellites' information to the equation can pinpoint the UAV's location and reduce the uncertainty (error) to a few meters.

**2.3. Related Work.** Most prior works in UAV location estimation use GPS. UAVs can be used for many applications such as delivering products and acting as a flying ad-hoc network for broadband wireless access during emergencies [30–32]. Most of these applications need to know the location of the UAV, and they use GPS coordination for that. However, GPS is not always available and not usable for identification. Thus, investigating other alternative localization solutions with an identification feature is desirable for UAV localization in all applications.

Wang et al. investigate a UAV rescue system, named GuideLoc, that helps to rescue people during a natural disaster using UAVs [33]. GuideLoc captures the average RSSI value of a wireless device signal such as a mobile phone carried by a trapped person. The system uses the antennas attached to the UAV to capture the average RSSI value. If the average RSSI value is less than a threshold, the angle of

arrival of the signal gets updated to find the location of that person and to record the GPS coordinates of the trapped person. The angle of arrival is determined by the strength of the average RSSI value. Lee et al. utilize the same technique to localize the sensor nodes in the wireless sensor networks [34]. Our system differs from GuideLoc by relying only on the RSSI values to estimate the UAV location and not the GPS.

Raimundo et al. examine the possibility of using the LoRaWAN communication protocol for a UAV location system [35]. The system consists of a UAV that uses a global navigation satellite system (GNSS) receiver to gather the GNSS data and then sends them by a LoRaWAN module attached to the UAV. GNSS receivers can connect to different satellite-based systems such as GPS and other navigation systems [36]. The LoRaWAN module sends the GNSS positions to a base station on the ground. In our system, the UAV is located and identified using the RSSI values and a message that is broadcasted using the LoRaWAN technology.

UAVs have been used by Ferreira et al. to find the network distribution and coverage in remote areas or hazard locations [37]. The proposed system uses the UAV's center-modem to detect the network access points (APs) using the RSSI values broadcasted by the APs in the network. The system uses these RSSI values to estimate the AP locations based on known UAV locations in different reference points, during the UAV flying path, and the estimates distance to these APs. The free-space propagation model is utilized in the system for distance estimation, and three different location methods are tested [38]. They conclude that Bound Box method has the lowest estimation error with a low variance when increasing the number of reference points. Another system by Greco et al. is similar to that by Ferreira et al., but they rely on radio-frequency identification (RFID) tags instead of APs to be located by the UAVs [39].

One of the issues facing location-based systems is to locate objects or UAVs in indoor environments. Tian et al. introduce the HiQuadLoc system that uses Wi-Fi access points to locate a UAV in an indoor environment [40]. Twenty APs are utilized in the system in an area of 1100 m<sup>2</sup>. The system uses two phases: an offline phase and an online phase. The offline phase divides the indoor area into cubes with known RSSI values to correctly help detect the UAV location in the online phase. The system achieves an average error of 1.64 m. The UAV speed is varied up to three meters per second. They conclude that the location error increases as the UAV speed increases.

Cheng et al. propose a system that can locate a nonline of sight (NLOS) UAV in an indoor environment [41]. The system uses RSSI values in the NLOS identification algorithm to identify the propagation conditions. Also, they use particle swarm optimization-based maximum joint probability algorithm to find the UAV's 2-D coordinates. The system achieves an average error of 0.85 m.

Our system also uses RSSI values for distance estimation; however, we target outdoor environments rather than indoors, and we use LoRaWAN to allow location estimation over much longer distances.

### 3. System Architecture

In this section, the system components, distance estimation modeling, and location estimation for the RSSI method are discussed. The discussion also includes the modeling methods used to estimate the distance from the RSSI values, along with graphs that illustrate that method.

*3.1. Prototype Components.* As shown in Figure 1, our prototype system consists of five main components: LoRaWAN modules, GSs, antennas, a battery, and a UAV. In the following, we briefly discuss these components:

- (i) *LoRaWAN Modules.* Two different modules are used—Moteino LoRa and Seeeduno LoRaWAN—for our prototype, as shown in Figure 1. Seeeduno module uses 433/868 MHz frequency bands while the Moteino module uses the 915 MHz band. Both modules can report the RSSI values while the Moteino module has an external antenna for longer ranges. The details of these modules can be found in [42, 43]. Alternatively, we could have used Libelium LoRaWAN module [44]. However, we have used Seeeduno and Moteino as shown in the distance estimation modeling since they meet our requirements such as reporting RSSI values where Libelium module lacks this feature.
- (ii) *GS.* For each GS, we use a regular computer connected to a LoRaWAN module. The computer is used to program the LoRaWAN module and record the data.
- (iii) *Antenna.* Moteino LoRa module requires a separate directional antenna to work, while the Seeeduno LoRaWAN module has a built-in wire antenna on the module.
- (iv) *Battery.* Any power bank is sufficient to power the LoRaWAN module connected to the UAV.
- (v) *UAVs.* We use two different UAVs for the prototype: DJI Phantom 2 and DJI Phantom 4 Pro. As discussed earlier, a LoRaWAN module and a battery have been attached to each UAV.

*3.2. Modeling for Distance Estimation.* Using the configuration shown in Figure 1, we estimate the distance between one of the GSs and the UAV using the RSSI values, and the log-distance path loss model as will be discussed. For each LoRaWAN module, two modules are used: one is attached to the UAV and powered by a battery and the other is connected to a computer to control and record the data and serves as the GS.

For distance estimation, the UAV continuously broadcasts a message that has its ID. The interval time of successive messages is two seconds, which is the minimum interval time for the LoRaWAN modules to avoid losing messages [45]. The message length and its effect are explained later in Section 4.

The log-distance path loss model states that [46]

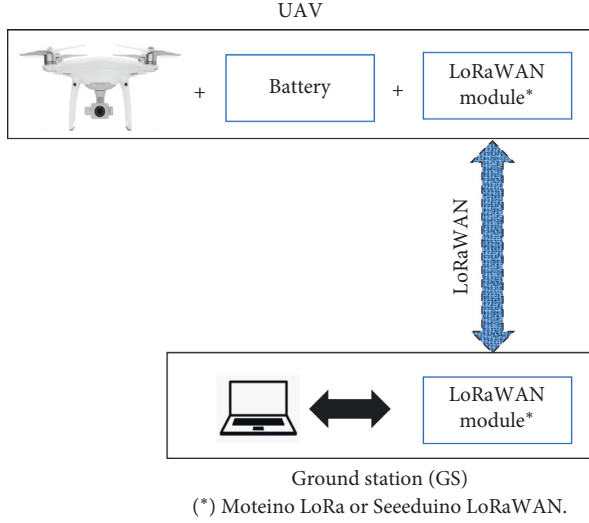


FIGURE 1: System architecture for distance estimation. Two LoRaWAN modules, Moteino and Seeeduino LoRaWAN, are used for distance estimation.

$$\text{RSSI} = -10 * L * \log_{10}(d) - C, \quad (1)$$

where RSSI is the RSSI value measured at the destination,  $d$  is the distance,  $L$  is the path loss exponent, and  $C$  is a constant. Given (1), the distance between the UAV and the GS can be measured as follows:

$$d = 10^{-((\text{RSSI}-C)/10L)}. \quad (2)$$

However, the measured RSSI values can fluctuate, and thus, using one value is not sufficient to estimate the distance. Typically, multiple values need to be used. In our experiments, we used an average of five RSSI values to measure the distance. Five is chosen arbitrarily as a tradeoff between the time and the fluctuation in the RSSI values.

That is, the distance between a GS and the UAV can be estimated as follows:

$$d = 10^{-((\text{meanRSSI}-C)/10L)}. \quad (3)$$

Here, meanRSSI is the average RSSI value of five RSSI values.

Even though  $C$  and  $L$  are constants in (1), their values are initially unknown and depend on the environment, as discussed by Sherazi et al. [47]. To estimate these parameters, we need meanRSSI values and their corresponding distances for a few known positions. Therefore, a model is needed to estimate these values using (1). To do so, we fit a linear model to the meanRSSI values. In the resulting linear model, the slope is  $-10 * L$  (thus,  $L = -\text{slope}/10$ ), and it can be calculated as follows:

$$\text{slope} = \left( \frac{\sum xy - n\bar{x}\bar{y}}{\sum x^2 - n\bar{x}^2} \right), \quad (4)$$

where  $x$  is the meanRSSI value at a known position or a known distance,  $y$  is the  $\log_{10}(d)$  value corresponding to the meanRSSI value,  $n$  is the number of RSSI values included in

that mean, and  $\bar{x}$  and  $\bar{y}$  are the mean over all meanRSSI values and the mean over all  $\log_{10}(d)$  values, respectively.

In the resulting linear model, the intersection point is  $-C$  (thus,  $C = -\text{intersection}$ ) which can be calculated from the linear model as follows:

$$\text{intersection} = \bar{y} - \text{slope} \times \bar{x}. \quad (5)$$

To get the distances between the UAV and the GS, we tried to use a laser meter to measure the distance between the two ends. However, it becomes difficult to do such measurements when the actual distance gets above 200 m. In such a case, the UAV gets smaller and harder to detect by the laser meter. Hence, as shown in Figure 2, we measure the ground distance (GD) between a ground point (GP) and the GS to compute the slant distance (SD) between the GS and the UAV, which equals  $d$  in (3). The measurement is relatively accurate, as will be shown in Section 4. The slant distance can be estimated as follows [48]:

$$\text{SD} = \sqrt{\text{GD}^2 + H^2 - (2 * \text{GD} * H * \cos(\beta))}, \quad (6)$$

where  $H$  is the height of the UAV, which is set to 50 m, GD is the ground distance between the GP under the UAV and the GS, and  $\beta$  is the angle between the GS and the UAV. The height is fixed to take the distance as the only variable parameter to simplify the measurements. The GD and its corresponding angle are measured using the laser meter. The GP is selected to be directly below the UAV. Thus, the angle between the UAV and the GP is 90 degrees, and it is measured using the laser meter, which is attached to a tripod. The angle  $\alpha$  between the GP and the GS is measured with the laser meter. Note that,  $\beta$  can be calculated by subtracting  $\alpha$  from 90 degrees:

$$\beta = (90 - \alpha). \quad (7)$$

Using the above technique, one can estimate the values for the parameters  $C$  and  $L$ . These parameters can then be used with the measured meanRSSI value to estimate distances at other UAV positions.

**3.3. Location Estimation.** In the first stage of our experiments, the Seeeduino LoRaWAN module is used to estimate the location of the UAV using the RSSI method. The location system consists of four GSs and one UAV, as illustrated in Figure 3.

Seeeduino LoRaWAN module is attached to each of the GSs and the UAV. In addition, a battery to power the LoRaWAN module is also attached to the UAV. In each GS, there is a computer that records the meanRSSI values received from the module connected to it. In this stage, the data are manually collected from all the four GS computers and transferred to a fifth computer called the central computer, which is not shown in Figure 3. The transferred data are processed based on three elements: the GSs' 3-D locations, the distances between each of the four GSs, which is 200 m, and the meanRSSI values received from the four GSs.

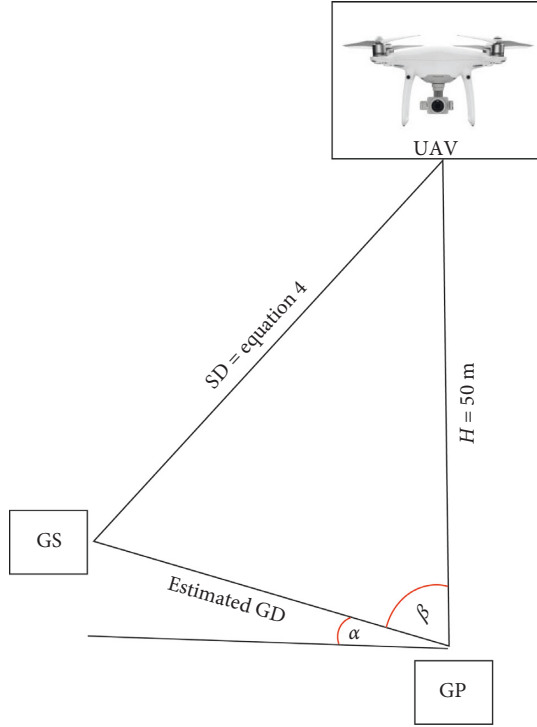


FIGURE 2: Slant-distance estimation technique. This technique is used if the distance between the two nodes is larger than 200 m.

The location estimation uses the SD between the UAV and four GSs. As explained earlier, the Seeeduino module requires an interval time of two seconds between successive messages. To satisfy this requirement and that we need to use the mean of 5 RSSI values, the UAV must stay in one spot for at least 10 seconds. Trilateration technique is used to determine the location of the UAV [49, 50]. This technique has been used to estimate the location in [51–53]. It allows us to determine the exact 3-D location of any object using its distance from at least four points with their known 3-D locations. In our case, the UAV is the object whose location and height need to be determined, while the four GSs are the points with known locations, as shown in Figure 4.

The UAV is on the surface of a sphere with radius ( $r_i$ ) centered at  $GS_i$ . The  $r_i$  is equal to  $SD_i$  for each GS. The location of the UAV is a 3-element vector  $\mathbf{w} = \{x, y, z\}$ . It can be computed as the intersection of the four spheres. Each sphere consists of the 3-D location of each GS and the radius value between itself and the UAV. The radius value represents the estimated distance, SD, from the previous subsection. Therefore,

$$\begin{aligned} r_1^2 &= (x - x_1)^2 + (y - y_1)^2 + (z - z_1)^2, \\ r_2^2 &= (x - x_2)^2 + (y - y_2)^2 + (z - z_2)^2, \\ r_3^2 &= (x - x_3)^2 + (y - y_3)^2 + (z - z_3)^2, \\ r_4^2 &= (x - x_4)^2 + (y - y_4)^2 + (z - z_4)^2. \end{aligned} \quad (8)$$

We can expand out the squares in each one, as shown in the following equation:

$$\begin{aligned} r_1^2 &= x^2 - 2x_1x + x_1^2 + y^2 - 2y_1y + y_1^2 + z^2 - 2z_1z + z_1^2, \\ r_2^2 &= x^2 - 2x_2x + x_2^2 + y^2 - 2y_2y + y_2^2 + z^2 - 2z_2z + z_2^2, \\ r_3^2 &= x^2 - 2x_3x + x_3^2 + y^2 - 2y_3y + y_3^2 + z^2 - 2z_3z + z_3^2, \\ r_4^2 &= x^2 - 2x_4x + x_4^2 + y^2 - 2y_4y + y_4^2 + z^2 - 2z_4z + z_4^2. \end{aligned} \quad (9)$$

By subtracting the 4<sup>th</sup> equation ( $r_4$ ) from the first three equations in (9), we get the following:

$$\begin{aligned} 2(x_4 - x_1)x + 2(y_4 - y_1)y + 2(z_4 - z_1)z \\ &= r_1^2 - r_4^2 - x_1^2 - y_1^2 - z_1^2 + x_4^2 + y_4^2 + z_4^2, \\ 2(x_4 - x_2)x + 2(y_4 - y_2)y + 2(z_4 - z_2)z \\ &= r_2^2 - r_4^2 - x_2^2 - y_2^2 - z_2^2 + x_4^2 + y_4^2 + z_4^2, \\ 2(x_4 - x_3)x + 2(y_4 - y_3)y + 2(z_4 - z_3)z \\ &= r_3^2 - r_4^2 - x_3^2 - y_3^2 - z_3^2 + x_4^2 + y_4^2 + z_4^2. \end{aligned} \quad (10)$$

Putting (10) in a matrix form, we get (11) where  $\mathbf{A}$  is the coefficient matrix,  $\mathbf{w}$  is a vector of variables to be estimated, i.e.,  $(x, y, z)$  in (10), and  $\mathbf{b}$  is the right-side vector.

$$\begin{bmatrix} 2(x_4 - x_1) & 2(y_4 - y_1) & 2(z_4 - z_1) \\ 2(x_4 - x_2) & 2(y_4 - y_2) & 2(z_4 - z_2) \\ 2(x_4 - x_3) & 2(y_4 - y_3) & 2(z_4 - z_3) \end{bmatrix} \begin{bmatrix} x \\ y \\ z \end{bmatrix} = \begin{bmatrix} r_1^2 - r_4^2 - x_1^2 - y_1^2 - z_1^2 + x_4^2 + y_4^2 + z_4^2 \\ r_2^2 - r_4^2 - x_2^2 - y_2^2 - z_2^2 + x_4^2 + y_4^2 + z_4^2 \\ r_3^2 - r_4^2 - x_3^2 - y_3^2 - z_3^2 + x_4^2 + y_4^2 + z_4^2 \end{bmatrix}. \quad (11)$$

$\mathbf{A} \qquad \mathbf{w} = \qquad \mathbf{b}$

Note that  $\mathbf{w}$  is the UAV 3-D location that we need to determine given other values in (11). To find  $\mathbf{w}$ , the closed-form of the least squares method can be used to solve the equation in one step, as shown in the following equation:

$$\mathbf{w} = (\mathbf{A}^T \mathbf{A})^{-1} \mathbf{A}^T \mathbf{b}. \quad (12)$$

If the height for all the GSs is the same, the last column of matrix  $\mathbf{A}$  will be all zeros, and the matrix becomes non-invertible. This step can be taken care of by removing the last column of matrix  $\mathbf{A}$ , computing only  $x$  and  $y$  values from the above equations, and separately determining  $z$  as in (13) by substituting  $z_4$  value in (8) with zero and solving for  $z$ . Here,  $z$  represents the height of the UAV, while  $x$  and  $y$  represent the 2-D location of the UAV.

$$z = \sqrt{r_4^2 - (x - x_4)^2 - (y - y_4)^2}. \quad (13)$$

## 4. Experimental Implementation and Results

In this section, the experimental implementation and results are discussed. We present the steps to prepare the software and hardware for the experiments. Also, we show some statistical results for the location estimation method.

**4.1. Distance Estimation Using RSSI Method.** Two different outdoor environments were used to model and validate our experiments. All the nodes in the experiment used the Seeeduino LoRaWAN module, which is based on Arduino Zero bootloader with LoRaWAN protocol embedded in it;

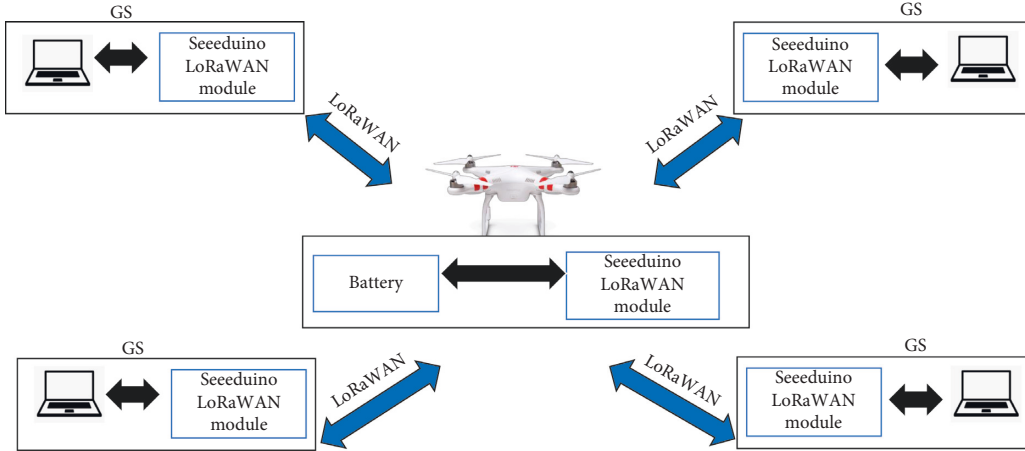


FIGURE 3: System architecture for the location estimation.

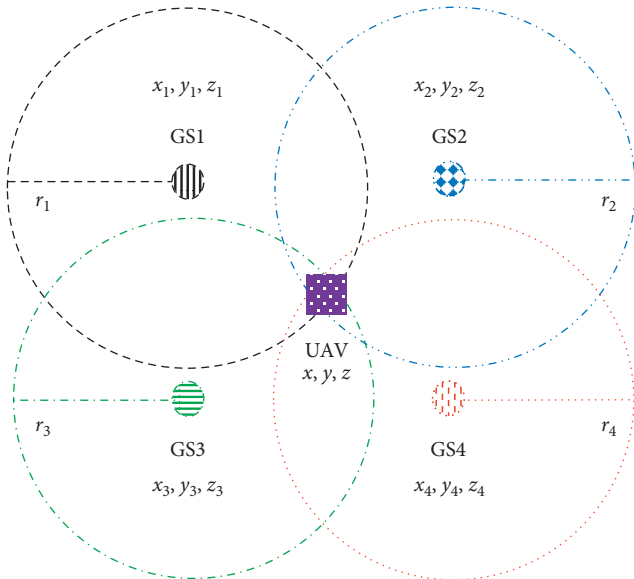


FIGURE 4: Trilateration system architecture. A minimum of four GSs 3-D locations are required to find the UAV 3-D location.

thus, no additional module was needed [43]. Seeeduino provides a library and examples to use their module. Using these examples, we found that it is possible to vary the contents and formats of the transmitted messages. Hence, three messages with different lengths and formats were tested, as shown in Table 1.

Initially, our test was based on using two nodes mounted on two tripods and not attached to the UAV with distances ranging from 100 to 500 m. As shown in Figure 5, we fitted a linear model to show the relationship between a set of meanRSSI values and their corresponding distances using different message lengths. Also, we calculated the confidence interval for each distance and message length to see if different meanRSSI values for different distances use one message overlap or not. From Figure 5, we can see that as the message length gets larger, the meanRSSI value increases. This finding is essential since with lower meanRSSI values, different distances

using different meanRSSI values overlap, causing a significant error in distance estimation. For example, by using message 2 (M2), we may get a meanRSSI value that could be 100 to 300 m away, resulting in an error of 200 m. Based on this realization, the most extended message among the three messages, M3, was used with the Seeeduino LoRaWAN module to complete the rest of this experiment.

For the second stage, we calculated the SDs for six different positions with nominal distance ranging from 100 to 600 m, as shown in Table 2. The SD values were those computed using (6). Notice that the calculated SDs were close to the nominal distances.

After getting the SDs, we performed a statistical analysis on the collected data, as shown in Table 3 using the methods described in [54]. The measurements consist of six meanRSSI values, each of which consists of 125 samples in each of the six distance ranges. Initially, the height for the UAV was fixed to 50 m to keep the analysis simple. Then, we conducted another experiment to check if the meanRSSI values were the same for different heights up to 100 m. Then, we decreased the GD and correspondingly we increased the UAV height to keep the same SD. Results showed that the meanRSSI values were the same as long the SDs were the same; that is, the meanRSSI values were not affected by the height.

As shown in Table 3, the sample variance decreased as the distance increased. To find the two unknown parameters,  $L$  and  $C$ , we used the linear regression model discussed earlier in Section 3.2. The results are shown in Figure 6. Note the decreasing variance (and hence narrower confidence interval) as the distance between the UAV and the GS increases. Overall, the model resulted in an  $R^2$  value of 97%, which showed that the linear regression model was a good fit.

The confidence interval is essential to see if any meanRSSI value for any distance was overlapping with another meanRSSI value. After calculating these confidence intervals, we found that their values for 300/400 m values overlap. This overlap showed that the meanRSSI values for these two distances were not statistically different. In other words, given a meanRSSI value and the calculated  $L$  and  $C$ , we may estimate the distance with an error of 100 m, which



TABLE 1: Different message lengths and formats list.

#	Message	No. of bytes	Format
M1	FF 31	2	Hexadecimal
M2	FF1	3	String
M3	FF1 is the UAV ID number that is being used to identify this UAV	66	String

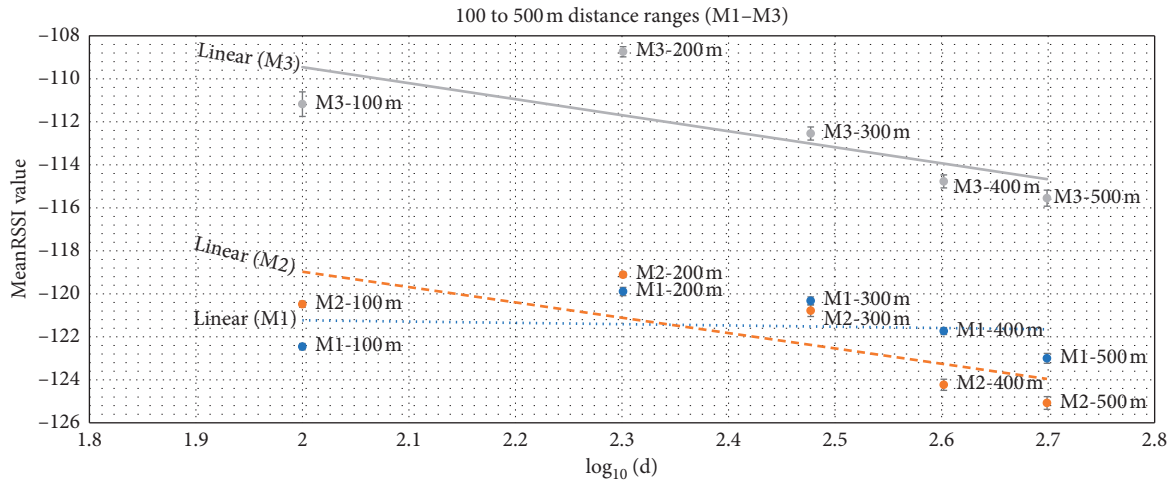


FIGURE 5: MeanRSSI values for different message lengths at different distances.

TABLE 2: Calculated SDs.

Nominal distance	Ground distance (GD)	Height ( $H$ )	UAV-GS angle ( $\beta$ )	GP-GS angle ( $\alpha$ )	Slant distance (SD)
100 m	100.0 m	50 m	79.1°	10.9°	102.97 m
200 m	200.2 m	50 m	81.7°	8.3°	199.19 m
300 m	299.8 m	50 m	83.3°	6.7°	298.19 m
400 m	400.3 m	50 m	84.0°	6.0°	398.15 m
500 m	500.5 m	50 m	84.7°	5.3°	498.34 m
600 m	600.7 m	50 m	84.9°	5.1°	598.29 m

TABLE 3: Statistical characteristics of meanRSSI values using the Seeduino LoRaWAN module.

Nominal distance	100 m	200 m	300 m	400 m	500 m	600 m
Sample variance	4.78	2.34	2.62	1.46	1.30	1.22
Sample standard deviation	2.19	1.53	1.62	1.21	1.14	1.10
Sample standard error	0.20	0.14	0.14	0.11	0.10	0.10
Sample mean ( $\bar{x}$ )	-79.41	-82.94	-85.81	-85.58	-87.93	-88.32
95% confidence interval	(-79.79, -79.03)	(-83.21, -82.68)	(-86.09, -85.52)	(-85.79, -85.37)	(-88.13, -87.73)	(-88.52, -88.13)
$L$				1.165		
$C$				-56.134		
$R^2$				0.97		

is a drawback. At this point, we decided to check the meanRSSI value with the other LoRaWAN modules (i.e., Moteino LoRaWAN).

As shown in Table 4, the Moteino module produced meanRSSI values for different distances that overlap with other distance ranges from 100 to 800 m; hence, it is not a perfect candidate for the linear regression model to find  $L$  and  $C$  parameters. We found that the perfect length of the message for the Moteino module was M2 (shown earlier in Table 1).

Longer messages, e.g., M3, were transmitted in several fragments. Hence, we ended up using M2 instead of M3.

**4.2. Location Estimation Using RSSI Method.** Location estimation stage consisted of four GSs and one UAV. The UAV used in this stage was DJI Phantom 4. The GSs were 200 m away from each other where all antennas' directions were pointing up since that impacts the meanRSSI values,

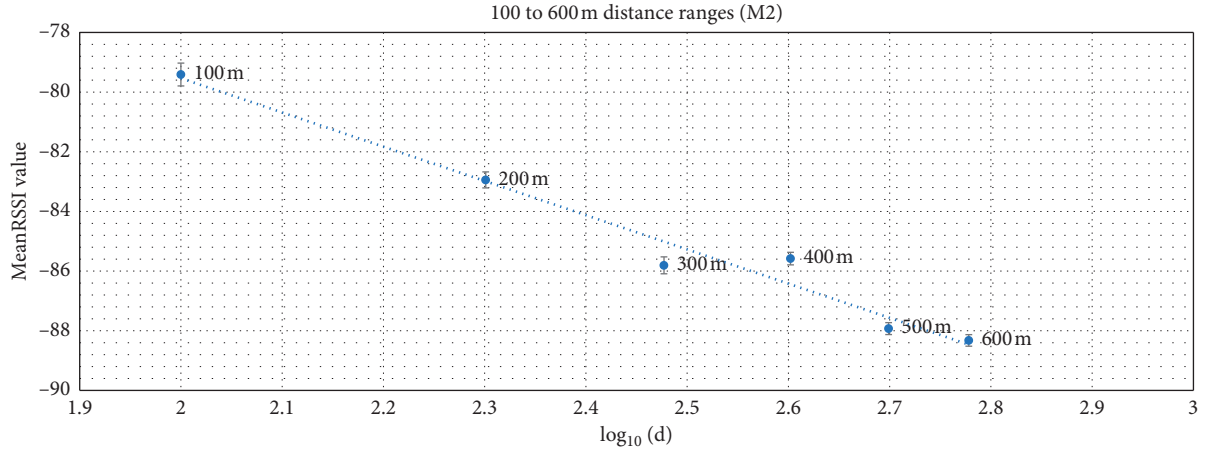


FIGURE 6: Linear regression model. These measurements are based on the use of the Seeeduno LoRaWAN module.

TABLE 4: Statistical characteristics of meanRSSI values using the Moteino LoRaWAN module.

Distance	100 m	200 m	300 m	400 m	500 m	600 m	700 m	800 m
Sample mean	-104.48	-103.68	-103.51	-104.97	-105.06	-104.86	-104.62	-104.65
Confidence interval	(-104.61, -104.36)	(-103.81, -103.55)	(-103.61, -103.40)	(-105.03, -104.90)	(-105.11, -105.00)	(-104.93, -104.80)	(-104.72, -104.52)	(-104.75, -104.56)

according to Wadhwa et al. [55]. The UAV antenna had a spring shape facing down, as shown in Figure 7. The battery that was used to power-up the LoRaWAN module attached on the UAV was under the module itself as shown in the figure.

The measured and estimated SD with UAV at the height of 50 m are shown in Table 5. The real SDs were measured using the GPS, while the estimated SDs were based on the meanRSSI values.

After we calculated the distance error based on the difference between the estimated SDs and real SDs, we found that GS2 showed a distance error of 127%. This error is discussed further in the next section.

## 5. Issues and Challenges

Although LoRaWAN can be used for distance estimation using RSSI method, we run into several issues that are important and are the main results of this paper. These are

- (1) *LoRaWAN Module*. LoRaWAN is designed for low cost and; therefore, there is significant variability in the results using different modules. Each module has its peculiarities. Further work is required to make either a standard module for consistent results or a standard that when implemented by different manufactures results in similar results.
- (2) *RSSI Model Accuracy*. MeanRSSI values fluctuate and depend upon the LoRaWAN module. As shown in Figure 6, our distance estimation model could be considered accurate except at distances between 300 and 400 m. Designing a better method or using a better module can resolve this problem.

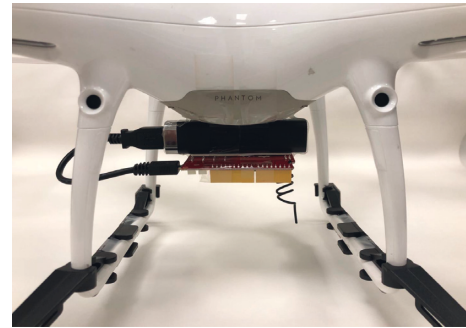


FIGURE 7: Seeeduno LoRaWAN module with the battery attached to the UAV. The shape of the antenna and the battery location is essential since the meanRSSI values are affected by them.

TABLE 5: Statistical characteristics of location determination using the Seeeduno LoRaWAN module.

	GS1	GS2	GS3	GS4
MeanRSSI (dB)	-80	-86	-79	-81
Estimated SD (m)	112	366	92	136
Real SD <sup>1</sup> (m)	146	161	140	155
Distance error <sup>2</sup> (%)	23	127	34	12

<sup>1</sup>Using Google Maps “measure distance” feature. <sup>2</sup>The error is calculated based on the difference between the estimated SDs and real SDs.

- (3) *Battery Capacity*. Different battery capacities to run the UAV’s LoRaWAN module cause different meanRSSI values for short distances (below 300 m); hence, we recommend using the same battery capacity throughout the whole set of measurements.
- (4) *Antenna Direction*. The module antenna direction and position affect the meanRSSI values captured by

the GSs. Thus, when building the distance model, the position and direction of the antenna need to be fixed for all UAVs during the distance estimation modeling and location estimation stage. Otherwise,  $C$  and  $L$  factors will change, resulting in inaccurate estimation of the distances, and thus, wrong locations.

- (5) *Seeeduino LoRaWAN Module Power Cable*. We found that the cable used to provide the power to the module attached to the UAV should be in the opposite direction of the antenna to balance the power in all directions. This issue is due to the fact that the cable can act as a second antenna for the Seeeduino LoRaWAN module, which affects the meanRSSI values for the modules in that direction of the UAV.
- (6) *Battery Location*. The battery used with the LoRaWAN module attached to the UAV needs to be under the module; otherwise, the meanRSSI values will be higher from the battery side, resulting in inaccurate distance estimation models.
- (7) *Environments*. Different environments affect the meanRSSI values because the model is based on a specific environment. This factor also results in different  $L$  and  $C$  values and thus different distance estimation models. As a result, the values of  $L$  and  $C$  need to be calibrated to fix the difference in the meanRSSI value between the two environments.
- (8) *Modeling Range*. The meanRSSI values for shorter distances (less than 100 m) are not useable because of their high variability. If there are GSs located throughout a city, some GSs will be more than 100 m distance from a UAV; hence, it may not be a problem.
- (9) *Movement*. We had to keep the UAV stationary for at least ten seconds to get the meanRSSI value to be used for distance estimation. This factor is because our LoRaWAN module required at least two seconds interval between successive messages and we need five such messages to compute the meanRSSI value. A better module design may allow to overcome this and continuously measure the location.
- (10) *Underestimation*. In our experiments, we had the minimum number of GSs required for the 3-D location. In such cases, it is possible that the estimated distances are lower than actual, and the four spheres do not intersect. Mathematically, this shows up as a negative value under the square root resulting in “imaginary” height for the UAV.

## 6. Conclusions and Future Work

Remote IDs on UAVs will allow law-enforcement authorities to determine the ownership of the UAVs. Making the UAVs simply broadcasting their GPS-determined location may not be sufficient in all environments. In some situations, determining the location using the reception on ground

stations is appropriate. In this paper, we proposed LoRaWAN as one possible wireless technology to use for Remote ID transmission and showed how ground stations could use meanRSSI values to determine the 3-D location of UAVs. We developed a prototype using commercially available low-cost LoRaWAN modules to identify and locate the UAVs, and we uncovered several issues that were documented in Section 5. These are the main contributions of this paper. We plan to do further work to address these issues in the near future.

## Data Availability

The LoRaWAN module configurations, Arduino IDE setups, and codes used to support the findings of this study are documented in [56].

## Conflicts of Interest

The authors declare that there are no conflicts of interest regarding the publication of this paper.

## Acknowledgments

I would like to thank my master thesis committee, Professor Roger Chamberlain and Ben Moseley, for their excellent comments and help to improve the overall write-up. In addition, I would like to thank my colleagues Guillaume Valentis, Xipeng Wang, Arghya Datta, Marcio Teixeira, Maede Zolanvari, Ria Das, and Yousef AlShehri for their help in this paper. Ali Ghubaish was financially supported by Prince Sattam bin Abdulaziz University, AlKharj 11942, Saudi Arabia.

## References

- [1] Federal Aviation Administration, *FAA Releases 2016 to 2036 Aerospace Forecast*, 2016, <https://www.faa.gov/news/updates/?newsId=85227>.
- [2] W. Bellamy III, *Drones Came Too Close to Airplanes 1,800 Times in 2016*, 2017, <http://www.aviationtoday.com/2017/03/17/drones-came-close-airplanes-1800-times-2016/>.
- [3] M. Zanona, “Drone sightings near airplanes on the rise,” 2017, <http://thehill.com/policy/transportation/362556-drone-sightings-near-airplanes-on-the-rise>.
- [4] C. Shine, “FAA playing high-tech hide and seek at DFW to stop drones from colliding with flights,” 2017, <https://www.dallasnews.com/business/dfw-airport/2017/04/28/1800-drone-sightings-last-year-faa-testing-systems-prevent-airport-collisions>.
- [5] Federal Aviation Administration, “Drone registration,” 2019, [http://federaldroneregistration.com/?gclid=CjwKCAiAxarQBRAmEiwA6YcGKHV8CMGVsGIsDn0cSsvl4lX-n7Z4lMB3aFl9iIXuRf8Bx2p6Co7QyRoCYBcQAvD\\_BwE](http://federaldroneregistration.com/?gclid=CjwKCAiAxarQBRAmEiwA6YcGKHV8CMGVsGIsDn0cSsvl4lX-n7Z4lMB3aFl9iIXuRf8Bx2p6Co7QyRoCYBcQAvD_BwE).
- [6] Wikipedia, “Regulation of UAVs in the United States,” 2019, [https://en.wikipedia.org/wiki/Regulation\\_of\\_UAVs\\_in\\_the\\_United\\_States](https://en.wikipedia.org/wiki/Regulation_of_UAVs_in_the_United_States).
- [7] DJI, “DJI introduces new geofencing system for its drones,” 2015, <https://www.dji.com/newsroom/news/dji-fly-safe-system>.
- [8] Wikipedia, *Global Positioning System*, 2019, [https://en.wikipedia.org/wiki/Global\\_Positioning\\_System](https://en.wikipedia.org/wiki/Global_Positioning_System).

- [9] K. D. Atherton, "This device turns any gun into an anti-drone ray," 2015, <https://www.popsoci.com/dronedefender-is-anti-drone-rifle-attachment>.
- [10] K. D. Atherton, "This drone gun knocks drones out of the sky gently, with radio waves," 2016, <https://www.popsoci.com/drone-gun-downs-drones-with-radio-waves>.
- [11] L. Shi, I. Ahmad, Y. He, and K. Chang, "Hidden Markov model based drone sound recognition using MFCC technique in practical noisy environments," *Journal of Communications and Networks*, vol. 20, no. 5, pp. 509–518, 2018.
- [12] M. Z. Anwar, Z. Kaleem, and A. Jamalipour, "Machine learning inspired sound-based amateur drone detection for public safety applications," *IEEE Transactions on Vehicular Technology*, vol. 68, no. 3, pp. 2526–2534, 2019.
- [13] Federal Aviation Administration, "UAS remote identification," 2019, [https://www.faa.gov/uas/research\\_development/remote\\_id/](https://www.faa.gov/uas/research_development/remote_id/).
- [14] J. Plaza, "FAA issues an RFI for a remote ID system for drones," 2019, <https://www.expouav.com/news/latest/faa-rfi-remote-id-drones/>.
- [15] L. Alliance, "A technical overview of LoRa® and LoRaWAN™," p. 20, 2015, [https://docs.wixstatic.com/ugd/eccc1a\\_ed71ea1cd969417493c74e4a13c55685.pdf](https://docs.wixstatic.com/ugd/eccc1a_ed71ea1cd969417493c74e4a13c55685.pdf).
- [16] J. Rafferty, J. Synnott, A. Ennis, I. Cleland, C. Nugent, and M. Little, "A secure, out of band, mechanism to manage IoT devices," in *Proceedings of the 11th International Conference on Ubiquitous Computing and Ambient Intelligence*, vol. 10586, pp. 77–90, Philadelphia, PA, USA, November 2017.
- [17] Wikipedia, "Unmanned aerial vehicle," 2019, [https://en.wikipedia.org/wiki/Unmanned\\_aerial\\_vehicle#Flight\\_controls](https://en.wikipedia.org/wiki/Unmanned_aerial_vehicle#Flight_controls).
- [18] M. Saari, A. M. b. Baharudin, P. Sillberg, S. Hyrynsalmi, and W. Yan, "LoRa—a survey of recent research trends," in *Proceedings of the 2018 41st International Convention on Information and Communication Technology, Electronics and Microelectronics (MIPRO)*, pp. 872–877, Opatija, Croatia, May 2018.
- [19] P. Kinney, "Zigbee technology: wireless control that simply works," in *Proceedings of the Communications Design Conference*, pp. 1–7, San Jose, CA, USA, September–October 2003.
- [20] W. Wang, G. He, and J. Wan, "Research on Zigbee wireless communication technology," in *Proceedings of the 2011 International Conference on Electrical and Control Engineering*, pp. 1245–1249, Yichang, China, September 2011.
- [21] Z. Yang and C. H. Chang, "6LoWPAN overview and implementations," in *Proceedings of the 2019 International Conference on Embedded Wireless Systems and Networks*, pp. 357–361, Beijing, China, February 2019.
- [22] A. Lavric and A. I. Petrariu, "LoRaWAN communication protocol: the new era of IoT," in *Proceedings of the 2018 International Conference on Development and Application Systems (DAS)*, pp. 74–77, Suceava, Romania, May 2018.
- [23] S. Schwarzer, M. Vossiek, M. Pichler, and A. Stelzer, "Precise distance measurement with IEEE 802.15.4 (Zigbee) devices," in *Proceedings of the 2008 IEEE Radio and Wireless Symposium*, pp. 779–782, Orlando, FL, USA, January 2008.
- [24] A. Savvides, C.-C. Han, and M. B. Strivastava, "Dynamic fine-grained localization in Ad-Hoc networks of sensors," in *Proceedings of the 7th Annual International Conference on Mobile Computing and Networking*, pp. 166–179, Rome, Italy, 2001.
- [25] S. Lanzisera, D. Zats, and K. S. J. Pister, "Radio frequency time-of-flight distance measurement for low-cost wireless sensor localization," *IEEE Sensors Journal*, vol. 11, no. 3, pp. 837–845, 2011.
- [26] Y. Miao, H. Wu, and L. Zhang, "The accurate location estimation of sensor node using received signal strength measurements in large-scale farmland," *Journal of Sensors*, vol. 2018, Article ID 2325863, 10 pages, 2018.
- [27] Wikipedia, "Distance measuring equipment," 2019, [https://en.wikipedia.org/wiki/Distance\\_measuring\\_equipment](https://en.wikipedia.org/wiki/Distance_measuring_equipment).
- [28] Wikipedia, "Received signal strength indication," 2019, [https://en.wikipedia.org/wiki/Received\\_signal\\_strength\\_indication](https://en.wikipedia.org/wiki/Received_signal_strength_indication).
- [29] Wikipedia, "Indoor positioning system," 2019, [https://en.wikipedia.org/wiki/Indoor\\_positioning\\_system](https://en.wikipedia.org/wiki/Indoor_positioning_system).
- [30] Amazon, "Amazon Prime Air," 2017, <https://www.amazon.com/Amazon-Prime-Air/b?node=8037720011>.
- [31] A. Jamalipour, Z. Kaleem, P. Lorenz, and W. Choi, "Special issue on amateur drone and UAV communications and networks," *Journal of Communications and Networks*, vol. 20, no. 5, pp. 429–433, 2018.
- [32] Z. Kaleem, M. Yousaf, A. Qamar et al., "UAV-empowered disaster-resilient edge architecture for delay-sensitive communication," *IEEE Network*, pp. 1–9, 2019.
- [33] A. Wang, X. Ji, D. Wu et al., "GuideLoc: UAV-assisted multitarget localization system for disaster rescue," *Mobile Information Systems*, vol. 2017, Article ID 1267608, 13 pages, 2017.
- [34] Y. S. Lee, J. W. Park, and L. Barolli, "A localization algorithm based on AOA for ad-hoc sensor networks," *Mobile Information Systems*, vol. 8, no. 1, pp. 61–72, 2012.
- [35] A. Raimundo, D. Fernandes, D. Gomes, O. Postolache, P. Sebastiao, and F. Cercas, "UAV GNSS position corrections based on IoT™ communication protocol," in *Proceedings of the 2018 International Symposium in Sensing and Instrumentation in IoT Era (ISSI)*, pp. 1–5, Shanghai, China, September 2018.
- [36] Wikipedia, "GNSS applications," 2019, [https://en.wikipedia.org/wiki/GNSS\\_applications](https://en.wikipedia.org/wiki/GNSS_applications).
- [37] S. Ferreira, G. Carvalho, F. Ferreira, and J. Sousa, "Assessing the capacity of man-portable UAVs for network access point localization, using RSSI link data," in *Proceedings of the 2014 International Conference on Unmanned Aircraft Systems (ICUAS)*, pp. 355–364, Orlando, FL, USA, May 2014.
- [38] Wikipedia, "Free-space path loss," 2019, [https://en.wikipedia.org/wiki/Free-space\\_path\\_loss](https://en.wikipedia.org/wiki/Free-space_path_loss).
- [39] G. Greco, C. Lucianaz, S. Bertoldo, and M. Allegretti, "Localization of RFID tags for environmental monitoring using UAV," in *Proceedings of the 2015 IEEE 1st International Forum on Research and Technologies for Society and Industry Leveraging a better tomorrow (RTSI)*, pp. 480–483, Turin, Italy, September 2015.
- [40] X. Tian, Z. Song, B. Jiang, Y. Zhang, T. Yu, and X. Wang, "HiQuadLoc: a RSS fingerprinting based indoor localization system for quadrotors," *IEEE Transactions on Mobile Computing*, vol. 16, no. 9, pp. 2545–2559, 2017.
- [41] L. Cheng, C. Wu, Y. Zhang, and a. Y. Wang, "An indoor localization strategy for a mini-UAV in the presence of obstacles," *International Journal of Advanced Robotic Systems*, vol. 9, no. 4, 2017.
- [42] Lowpowerlab, "Moteino Mega," 2019, <https://lowpowerlab.com/shop/product/119>.
- [43] Seeedstudio, "Seeedstudio LoRaWAN," 2016, <https://www.seeedstudio.com/Seeedstudio-LoRaWAN-p-2780.html>.
- [44] Cooking Hacks, "LoRaWAN technology for Arduino, Waspote and raspberry pi," 2019, <https://www.cooking-hacks.com/documentation/tutorials/lorawan-for-arduino-raspberry-pi-waspote-868-900-915-433-mhz>.
- [45] A. Rahmadhani, Richard, R. Isswandhana, A. Giovani, and R. A. Syah, "LoRaWAN as secondary telemetry communication system for drone delivery," in *Proceedings of the 2018*

- IEEE International Conference on Internet of Things and Intelligence System (IOTAIS)*, pp. 116–122, Bali, Indonesia, November 2018.
- [46] T. Salman, “Parameters estimation to achieve distance-based security breaching,” Master thesis, Computer Science and Engineering, Qatar University, Spring, Doha, Qatar, 2015.
- [47] H. H. R. Sherazi, R. Iqbal, S. U. Hassan, M. H. Chaudary, and S. A. Gilani, “ZigBee’s received signal strength and latency evaluation under varying environments,” *Journal of Computer Networks and Communications*, vol. 2016, Article ID 9409402, 8 pages, 2016.
- [48] MathsisFun, “The law of cosines,” 2019, <https://www.mathsisfun.com/algebra/trig-cosine-law.html>.
- [49] Wikipedia, “True range multilateration,” 2019, [https://en.wikipedia.org/wiki/True\\_range\\_multilateration](https://en.wikipedia.org/wiki/True_range_multilateration).
- [50] W. Dargie and C. Poellabauer, *Fundamentals of Wireless Sensor Networks*, John Wiley & Sons, Hoboken, NJ, USA, 2010.
- [51] R. Jin, H. Wang, B. Peng, and N. Ge, “Research on RSSI-based localization in wireless sensor networks,” in *Proceedings of the 2008 4th International Conference on Wireless Communications, Networking and Mobile Computing*, pp. 1–4, Dalian, China, October 2008.
- [52] O. S. Oguejiofor, A. N. Aniedu, H. C. Ejiofor, and A. U. Okolibe, “Trilateration based localization algorithm for wireless sensor network,” *International Journal of Science and Modern Engineering (IJISME)*, vol. 1, no. 10, 2013.
- [53] R. Javaid, R. Qureshi, and R. N. Enam, “RSSI based node localization using trilateration in wireless sensor network,” *Bahria University Journal of Information & Communication Technologies*, vol. 8, no. 2, 2015.
- [54] R. Jain, *The Art of Computer Systems Performance Analysis: Techniques for Experimental Design, Measurement, Simulation, and Modeling*, Wiley Interscience, New York, NY, USA, 1991.
- [55] M. Wadhwa, M. Song, V. Rali, and S. Shetty, “The impact of antenna orientation on wireless sensor network performance,” in *Proceedings of the 2009 2nd IEEE International Conference on Computer Science and Information Technology*, pp. 143–147, Beijing, China, August 2009.
- [56] A. Ghubaish, “Locating unmanned aerial vehicles (UAVs),” M.S. thesis, Department of Computer Science and Engineering, Washington University in Saint Louis, Saint Louis, MO, USA, 2017, <https://www.cse.wustl.edu/~jain/theses/agms.htm>.

## Research Article

# UAV-Enabled Data Collection: Multiple Access, Trajectory Optimization, and Energy Trade-Off

Lin Xiao , Yipeng Liang , Chenfan Weng, Dingcheng Yang , and Qingmin Zhao 

Information Engineering School, Nanchang University, Nanchang 330031, China

Correspondence should be addressed to Dingcheng Yang; ydcxuan@msn.com and Qingmin Zhao; zhaoqm@ncu.edu.cn

Received 17 May 2019; Accepted 21 July 2019; Published 25 August 2019

Guest Editor: Zeeshan Kaleem

Copyright © 2019 Lin Xiao et al. This is an open access article distributed under the Creative Commons Attribution License, which permits unrestricted use, distribution, and reproduction in any medium, provided the original work is properly cited.

In this paper, we consider a ground terminal (GT) to an unmanned aerial vehicle (UAV) wireless communication system where data from GTs are collected by an unmanned aerial vehicle. We propose to use the ground terminal-UAV (G-U) region for the energy consumption model. In particular, to fulfill the data collection task with a minimum energy both of the GTs and UAV, an algorithm that combines optimal trajectory design and resource allocation scheme is proposed which is supposed to solve the optimization problem approximately. We initialize the UAV's trajectory firstly. Then, the optimal UAV trajectory and GT's resource allocation are obtained by using the successive convex optimization and Lagrange duality. Moreover, we come up with an efficient algorithm aimed to find an approximate solution by jointly optimizing trajectory and resource allocation. Numerical results show that the proposed solution is efficient. Compared with the benchmark scheme which did not adopt optimizing trajectory, the solution we propose engenders significant performance in energy efficiency.

## 1. Introduction

With series of features such as low cost, long duration, high flexibility, and high adaptability, extensive research endeavour has been rendered to exploring the application of UAV. In [1], the authors made a survey on autonomous cargo pickup with an UAV helicopter by designing systems including self-tracking, payload pickup, and deployment of cargo. In [2], the UAVs are employed to airborne maritime surveillance, which commits to monitoring of the marine environment, safeguarding national security, sovereignty, and as sea rescue. Anwar et al. [3] studied the framework of detecting and classifying sounds of amateur aircraft out in noisy environment by leveraging machine learning to maintain public safety. They also [4] proposed a disaster-resilient architecture including centralized control and edge computing for disaster areas, which can reduce delay effectively. Moreover, UAV networks are developing rapidly embracing the wireless technologies such as IEEE 802.11n, IEEE 802.15.4, and 3G/LTE [5–9]. However, UAVs will also face many challenges in its application. Researchers are also trying to solve these problems. In particular, it can not only

be hired for delivery of goods, but also serve as low-altitude aircraft to improve the coverage and rate of wireless networks in different scenarios. First, placement/deployment optimization is a major challenge for quasistatic drones [10–14]. In [10], coverage was optimized by adjusting the height of the platform. In [11], the authors characterize the performance and trade-offs of UAV with underlaid device-to-device communication. Compared with terrestrial base stations, UAV has more advantages as airborne static base stations, for its excellent capability to have line-of-sight communication links (LOSs) to the ground terminal, which will achieve the maximum communication coverage of the ground terminal. Thus, in [12], the authors propose an efficient deployment method based on circle packing theory, using minimum transmit power and maximizing the total coverage area. Bor-Yaliniz et al. [13] emphasized the performances of drone-cell placement problem by designing it as a 3D placement that leads to maximum revenue of the network. Second, UAV's energy efficiency and resource management are crucial factors in its communication systems. There are many differences between traditional wireless communication system and UAV communication.

Energy efficiency maximization of traditional wireless communication systems is to save energy of communication, but in the UAV communication system, the energy for communication is much lower than that of the UAV itself. So, the UAV's energy consumption is the main factor that needs to be considered toward high efficiency and energy saving [14–16]. Inspired by this, trajectory optimization of energy-efficient UAV communication has been studied, in which sequential convex optimization techniques are applied to deal with the nonconvex trajectory optimization problems [17], despite its research object being single UAV and a ground user, but the frame can extend to a joint trajectory and communication design in multi-UAVs wireless network. Motivated by this, the joint optimization problem of user scheduling, transmit power, and UAV trajectories was studied in the multi-UAV system [18]. In IoT networks, an efficient mobile scheme of uplink data collection was studied [19]. Wu and Zhang [20] consider the user communication delay requirements, maximizing the system total throughput via joint resource allocation and UAV trajectory. Furthermore, energy saving has been recognized as a vital target in designing future wireless communication system [21]. In particular, UAV communication systems are considered. In [22], the author proposed a throughput-delay trade-off in a new cyclical multiple access scheme in UAV communications. In the previous work, we have investigated an energy trade-off between a UAV and single ground user [23], with results being extendable to UAV-enabled multiuser communication networks.

As we discussed previously, energy efficiency is a factor that cannot be ignored for UAV due to the limited on-board power. He et al. [24] investigated the throughput by jointly optimizing the UAV's flying altitude and antenna beamwidth in case of downlink multicasting, downlink broadcasting, and uplink multiple access models without considering energy consumption. Lyu et al. [25] optimize the deployment of the UAV to provide wireless coverage for ground terminal which does not study the issue of energy efficiency. Zeng et al. [26] aim to design trajectories to minimize the mission completion time and also hardly consider energy consumption. Zeng and Zhang [17] study energy efficiency by trajectory optimization, but only a UAV and a user included. For a UAV communication system, besides coverage, UAV's energy efficiency and resource management is necessary to investigate, especially in multiuser UAV communication.

In this paper, a flexible UAV is deployed to collect data from a group of ground terminals at known location in ground terminals to a UAV (G2U) system. Intuitively, the study needs to jointly consider the uplink transmission energy of GTs and the UAV's propulsion energy consumption. To obtain the most fundamental insights, we focus on a G2U wireless communication system, where a group of ground terminals are collected data by a UAV, as shown in Figure 1. Specially, an efficient algorithm that combines optimal trajectory design and resource allocation scheme is proposed to approximately solve the optimization problem. For optimal trajectory design and resource allocation, we gain the optimal GTs transmit power and UAV trajectory, respectively. Numerical results evaluate the trade-

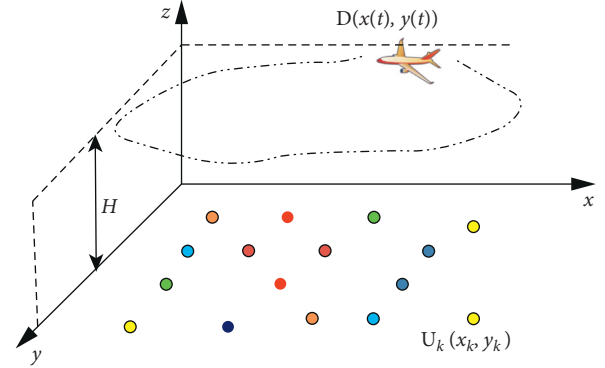


FIGURE 1: A UAV-enabled data collection system.

off involved in the proposed designs. A special case where a G2U communication scheme considering two ordinary UAV trajectories with circular and straight trajectories has been studied in [23].

The rest of this paper is organized as follows. Section 2 introduces the system model, and problem formulation for a high-mobile UAV is deployed regularly to total ground nodes for data collection. In Section 3, we first formulate the optimization problem to describe the Pareto boundary of the energy region. An efficient iterative algorithm is proposed by combining optimal trajectory design and resource allocation scheme; then the numerical results are solved in Section 4. Finally, we conclude the paper in Section 5.

## 2. System Model and Problem Formulation

**2.1. System Model.** We consider a wireless system consisting of  $K$  ground nodes, denoted as  $U_1, \dots, U_k$ , where the coordinate of  $U_k$  is denoted as  $\mathbf{q}_k = [x_k, y_k]^T$ . We assume that each of the ground node  $U_k$  periodically generates data of size  $\hat{R}_k$  for each period of duration  $T_s$ , which need to be regularly uploaded to the fusion center for data processing. This could correspond to the practical periodic sensing applications. We assume that there is no established communication link between the ground nodes and fusion center due to their long separation distance as well as the high cost in deploying fixed communication infrastructure such as relays. Instead, we assume that a high-mobile UAV is despatched regularly to fly over the ground nodes for data collection and then brings it back to the fusion center for off-line processing.

We assume that the UAV flying at a fixed altitude  $H$  around the ground terminals for data collection for a finite time horizon  $T$ . Note that  $T$  is the time required for the UAV to complete the data collection task  $\{\hat{R}_k\}$  for each period  $T_s$ . In practice, we usually have  $T \ll T_s$  (e.g., dozens of minutes versus several days) since the data are only generated intermittently. We denote the time-varying coordinate of the UAV's horizontal location as  $\mathbf{w}(t) = [x(t), y(t)]^T$ ,  $0 \leq t \leq T$ . Thus,  $\mathbf{w}(t)$  represents the UAV trajectory, which is to be optimized. We assume that the initial and final locations of the UAV are predetermined, which are denoted as  $\mathbf{w}_0$  and  $\mathbf{w}_f \in \mathbb{R}^{2 \times 1}$ , respectively. Furthermore, we assume that the maximum UAV speed and acceleration is  $V_{\max}$  and  $a_{\max}$ , respectively. Thus, the UAV trajectory must satisfy

$\|\mathbf{v}(t)\| \leq V_{\max}$  and  $\|\mathbf{a}(t)\| \leq a_{\max}$ , where  $\mathbf{v}(t) = \dot{\mathbf{w}}(t)$  and  $\mathbf{a}(t) = \ddot{\mathbf{w}}(t)$  denotes the instantaneous velocity and acceleration, respectively.

We assume that the channels between the UAV and the ground nodes are dominated by LoS links. Furthermore, we assume that the Doppler effect due to the UAV mobility can be perfectly compensated. Thus, the channel coefficient from the ground terminal  $U_k$  to the UAV at time  $t$  can then be expressed as

$$h_k(t) = \beta_0 d_k^{-2}(t) = \frac{\beta_0}{H^2 + \|\mathbf{q}_k - \mathbf{w}(t)\|^2}, \quad k = 1, \dots, K, \quad (1)$$

where  $\beta_0$  denotes the channel gain at the reference distance  $d_0 = 1$  meter, and  $d_k(t) = \sqrt{H^2 + \|\mathbf{q}_k - \mathbf{w}(t)\|^2}$  represents the distance between ground node  $U_k$  and the UAV. Denote by  $B$  the total bandwidth assigned for the uplink data collection system, which is assumed to be dynamically allocated to the  $K$  ground terminals for orthogonal multiple access. Specifically, denote by  $0 \leq \alpha_k(t) \leq 1$  the fractional of the spectrum bandwidth that is assigned to  $U_k$  at time  $t$ . Note that, in practical implementation,  $\alpha_k(t)$  is determined by the number of subbands allocated for  $U_k$  normalized by the total number of frequency subbands, which has discrete values in general. However, we assume that the number of subbands is sufficiently large so that  $\alpha_k(t)$  can be approximated to have continuous values between 0 and 1 for simplicity. Denote by  $P_k(t)$  the transmit power of  $U_k$  at time  $t$ . Then, the maximum transmission rate for the uplink from  $U_k$  to the UAV can be expressed as

$$\begin{aligned} R_k(t) &= \alpha_k(t) B \log_2 \left( 1 + \frac{P_k(t) h_k(t)}{\alpha_k(t) B N_0} \right) \\ &= \alpha_k(t) B \log_2 \left( 1 + \frac{P_k(t) \gamma_0}{\alpha_k(t) (H^2 + \|\mathbf{q}_k - \mathbf{w}(t)\|^2)} \right), \end{aligned} \quad (2)$$

where  $N_0$  is the noise power spectrum density in Watts/Hz, and  $\gamma_0 \triangleq (\beta_0 / B N_0)$  represents the reference SNR. It is observed from (2) that the data collection rate for  $U_k$  is a function of  $\alpha_k(t)$ ,  $P_k(t)$ , as well as the UAV trajectory  $\mathbf{w}(t)$ . The aggregated transmission throughput over the time horizon  $T$  for  $U_k$  can be presented as

$$\begin{aligned} Q_k(\{T, \alpha_k(t), P_k(t), \mathbf{w}(t)\}) &= \int_0^T R_k(t) dt \\ &= \int_0^T \alpha_k(t) B \log_2 \left( 1 + \frac{P_k(t) \gamma_0}{\alpha_k(t) (H^2 + \|\mathbf{q}_k - \mathbf{w}(t)\|^2)} \right) dt, \end{aligned} \quad (3)$$

where the total rate  $Q_k$  of each ground terminal  $U_k$  should be larger than the data collection task  $\hat{Q}_k$ :  $Q_k \geq \hat{Q}_k$ .

There are two parts of energy consumption in the UAV-enabled data collection system:

- (1) *Ground Terminal Energy Consumption.* The total energy consumption  $E_{GT}$  for ground terminals can be written as

$$E_{GT}(T, P_k(t)) = \sum_{k=1}^K \int_0^T P_k(t) dt. \quad (4)$$

- (2) *UAV Energy Consumption.* The UAV energy consumption of the considered data collection system consists of two main components. The first one is the energy consumption related to the communication functions, such as circuitry and signal processing. The other component is the propulsion energy consumption, which is required for the UAV to remain aloft as well as for supporting its mobility. In practice, the communication-related energy is much smaller than the propulsion energy and hence is neglected in this paper.

For fixed-wing UAVs, the total propulsion energy  $\bar{E}(\{\mathbf{w}(t)\})$  as a function of the trajectory  $\mathbf{w}(t)$  can be modelled as [21]

$$\begin{aligned} \bar{E}(\{T, \mathbf{w}(t)\}) &= \int_0^T \left[ c_1 \|\mathbf{v}(t)\|^3 \right. \\ &\quad \left. + \frac{c_2}{\|\mathbf{v}(t)\|} \left( 1 + \frac{\|\mathbf{a}(t)\|^2 - (\mathbf{a}^T(t) \mathbf{v}(t))^2 / \|\mathbf{v}(t)\|^2}{g^2} \right) \right] dt \\ &\quad + \frac{1}{2} m (\|\mathbf{v}(T)\|^2 - \|\mathbf{v}(0)\|^2), \end{aligned} \quad (5)$$

where  $c_1$  and  $c_2$  are the parameters depending on the aircraft's weight, wing area, air density, etc,  $m$  is the mass of the aircraft including all its payload, and  $g$  denotes the gravitational acceleration with nominal value 9.8 m/s<sup>2</sup>, and  $\mathbf{v}(t)$  and  $\mathbf{a}(t)$  are the instantaneous UAV velocity and acceleration vectors, respectively, which are related to its trajectory  $\{\mathbf{w}(t)\}$  as

$$\begin{aligned} \mathbf{v}(t) &\triangleq \dot{\mathbf{w}}(t), \\ \mathbf{a}(t) &\triangleq \dot{\mathbf{v}}(t). \end{aligned} \quad (6)$$

The energy consumption  $E_{UAV}$  for UAV can be expressed as

$$E_{UAV} = \bar{E}(T, \mathbf{w}(t)). \quad (7)$$

Note that the achievable data rate for each ground terminal is a function of total operating time  $T$ , spectrum, and power allocation  $\{\alpha(t), P_k(t)\}$ , as well as UAV trajectory  $\mathbf{w}(t)$ . Denote by  $\mathcal{S}$  the set of strategies in terms of the resource allocations and UAV trajectories such that the data collection requirement  $\hat{R}_k$  can be fulfilled. The set can be expressed as



$$\mathcal{S} \triangleq \{(T, P_k(t), \alpha_k(t), \mathbf{w}(t)) \mid Q_k(\{T, P_k(t), \alpha_k(t), \mathbf{w}(t)\}) \geq \widehat{Q}_k, \\ k = 1, \dots, K\}. \quad (8)$$

Consider the data collection system which both ground terminals and UAV would consume energy to support the data transmission and UAV flying. There are two parts of energy consumption: (1) ground terminal energy  $E_{GT}$  and (2) UAV energy  $E_{UAV}$ . It is seen that the optimal strategies for minimizing the transmitting power of ground terminals and UAV energy consumption for flying are in general different. For data transmission, UAV would be slowly flying when it is near to the ground terminals. On the other hand, for UAV flying, the steady level flight would be a better choice for energy decreasing. It thus motivates our investigation of the following question: what are the optimal UAV flying trajectory strategies for data transmission and UAV flight energy consumption? To answer this question, we propose to use *ground terminal-UAV* (G-U) region for the energy consumption model to characterize all the ground terminal transmit power and UAV energy consumption pairs under a given data collection rate constraint. We define the *feasible energy region* to be the set of all energy pairs of ground terminal and UAV that can be achieved using the wireless resource and trajectory vector  $\mathbf{s} \in \mathcal{S}$  that satisfy the rate constraint. It can be presented as

$$\varepsilon \triangleq \bigcup_{\mathbf{s} \in \mathcal{S}} \{E_{GT}(\mathbf{s}), E_{UAV}(\mathbf{s})\}. \quad (9)$$

The outer boundary of this region is called the *Pareto boundary*, because it consists of operating points  $(E_{GT}, E_{UAV})$  for which it is impossible to decrease one of the energies, without simultaneously increasing one of the other energies. More precisely, we define the *Pareto optimality* of an operating point as follows:

*Definition 1.* An energy pair  $(E_{GT}, E_{UAV})$  is Pareto optimal if there is no other energy pair  $(U_{GT}, U_{UAV})$  with  $(Q_{GT}, Q_{UAV}) \leq (E_{GT}, E_{UAV})$  and  $(U_{GT}, U_{UAV}) \neq (E_{GT}, E_{UAV})$  (the inequality is component-wise) can meet the rate constraints for the data collection system.

The Pareto boundary of the energy region characterizes that the minimum energy consumption for UAV and ground terminal for data collection task. It can be adopted to evaluate the trade-off of the energy consumption in the data collection system. It is an interesting topic to investigate the UAV trajectory strategy and resource allocation scheme for UAV and ground terminals to finish the data collection task cooperatively.

### 3. Multiple Ground Terminals with UAV Arbitrary Flight

In this section, we address the data collection system in a general scenario where there are multiple ground terminals which is served by a flexible flying UAV. We first formulate the optimization problem to describe the Pareto boundary of

the energy region. Then, we investigate the optimal solution of the optimization problem for this scenario, from which we obtain an upper bound for the achievable energy consumption pairs in the G-U region. Then, we propose an alternating iterative method to derive the optimal resource allocation scheme and optimal trajectory design strategy.

*3.1. Problem Formulation for Optimal Resource Allocation and Trajectory Design.* In order to characterize the trade-off of the energy region effectively, we adopt the strategy to minimize the ground terminal energy consumption with fixed UAV energy consumption. By traversing  $E_{UAV}$ , the Pareto boundary of G-U region can be obtained. In this case, the design objective for data collection system is to minimize the energy consumption for ground terminals with the fixed UAV energy consumption. The optimization problem can be formulated as

$$\begin{aligned} (\text{P2}) \quad & \text{Minimize}_{T, \{\mathbf{w}(t)\}, \{P_k(t)\}, \{\alpha_k(t)\}} & E_{GT} &= \sum_{k=1}^K \int_0^T P_k(t) dt, \\ & \text{subject to} & \mathbf{C}_{a1} &: \bar{R}_k(\{\alpha_k(t), P_k(t), \mathbf{w}(t)\}) \geq \widehat{R}_k, \quad \forall k, \\ & & \mathbf{C}_{a2} &: \bar{E}(\mathbf{w}(t)) \leq E_{UAV}, \\ & & \mathbf{C}_{a3} &: \mathbf{w}(0) = \mathbf{w}_0, \mathbf{w}(T) = \mathbf{w}_F, \\ & & \mathbf{C}_{a4} &: \mathbf{v}(0) = \mathbf{v}_0, \mathbf{v}(T) = \mathbf{v}_F, \\ & & \mathbf{C}_{a5} &: \|\mathbf{v}(t)\| \leq V_{\max}, \quad \forall t, \\ & & \mathbf{C}_{a6} &: \|\mathbf{a}(t)\| \leq a_{\max}, \quad \forall t, \\ & & \mathbf{C}_{a7} &: \int_0^T \alpha_k(t) dt = 1, \quad 0 \leq \alpha_k(t) \leq 1, \quad \forall k, t. \end{aligned} \quad (10)$$

The constraint  $\mathbf{C}_{a1}$  is the data collection requirement for each ground node, which  $\widehat{R}_k$  denotes the total amount of data to be collected for  $U_k$ .  $\mathbf{C}_{a2}$  is the energy consumption constraint for UAV, with  $E_{UAV}$  denoting the total available energy consumption for UAV.  $\mathbf{C}_{a3} - \mathbf{C}_{a6}$  represent the UAV's initial/final location and velocity constraints, respectively. It is noted that the amount of available energy for UAV is larger than the minimum energy consumption for UAV flying from the initial location to final location. Without considering the UAV's energy consumption, the minimum transmit power for ground terminal is the situation that the UAV would be sequentially located above each ground terminal during the data collection time  $T$ . However, the optimal solution to the above problem is difficult to be directly solved.

*3.2. Linear Discrete State-Space Approximation.* Note that the problem (P2) is difficult to be directly solved since the trajectory  $\mathbf{w}[n]$  is a continuous variable respect to the optimization problem and its first- and second-order derivatives. To tackle the problem more tractable, we utilize the linear discrete state-space approximation to reformulate the optimization problem (P2).

For ease of exposition, the time horizon  $T$  is discreteized into  $N + 2$  equally spaced time slots with step  $\delta_t$ , where  $\delta_t$  is chosen to be sufficiently small so that the UAV location can be assumed to be approximately constant. Therefore, the UAV trajectory can be represented by the sequence  $\{\mathbf{w}[n]\}$ .

Moreover,  $\mathbf{v}[n]$  and  $\mathbf{a}[n]$  are the instantaneous UAV velocity and acceleration vectors, respectively. Considering the relationship between  $\mathbf{w}[n]$  and  $\mathbf{v}[n]$ ,  $\mathbf{w}[n]$  and  $\mathbf{a}[n]$  are first- and second-order derivatives, respectively. Then, applying Taylor approximation, the velocity  $\mathbf{v}[n]$  and acceleration  $\mathbf{a}[n]$  are related to its trajectory  $\{\mathbf{w}[n]\}$  as

$$\begin{aligned}\mathbf{v}[n+1] &= \mathbf{v}[n] + \mathbf{a}[n]\delta_t, \\ \mathbf{w}[n+1] &= \mathbf{w}[n] + \mathbf{v}[n]\delta_t + \frac{1}{2}\mathbf{a}[n]\delta_t^2.\end{aligned}\quad (11)$$

Correspondingly, the spectrum and power allocation  $\alpha_k(t), p_k(t)$  can be expressed as  $\alpha_k[n], p_k[n]$  for the discretization.

For the problem (P2), the objective is to minimize the total ground node transmit power while satisfying the data collection requirements of all the ground terminals, subject to a fixed UAV energy consumption. It should jointly optimize the operation period  $N$  with fixed step size  $\delta_t$ , the UAV trajectory  $\{\mathbf{w}[n]\}$ , and spectrum and power allocation  $\{\alpha_k[n], p_k[n]\}$ . The problem (P2) can be reformulated as

$$\begin{aligned}(\text{P3}) \quad & \underset{N, \{\mathbf{w}[n]\}, \{P_k[n]\}, \{\alpha_k[n]\}}{\text{Minimize}} & E_{\text{GT}} &= \sum_{k=1}^K \sum_{n=1}^N P_k[n], \\ & \text{subject to} & \mathbf{C}_{\text{b1}} &: \bar{R}_k(\{\alpha_k[n], P_k[n], \mathbf{w}[n]\}) \geq \hat{R}_k, \quad \forall k, \\ & & \mathbf{C}_{\text{b2}} &: \bar{E}(\mathbf{w}[n]) \leq P_{\text{UAV}}, \\ & & \mathbf{C}_{\text{b3}} &: \mathbf{w}[0] = \mathbf{w}_0, \mathbf{w}[N+1] = \mathbf{w}_F, \\ & & \mathbf{C}_{\text{b4}} &: \mathbf{w}[n+1] = \mathbf{w}[n] + \mathbf{v}[n]\delta_t + \frac{1}{2}\mathbf{a}[n]\delta_t^2, \quad n = 0, \dots, N, \\ & & \mathbf{C}_{\text{b5}} &: \mathbf{v}[0] = \mathbf{v}_0, \mathbf{v}[N+1] = \mathbf{v}_F, \\ & & \mathbf{C}_{\text{b6}} &: \mathbf{v}[n+1] = \mathbf{v}[n] + \mathbf{a}[n]\delta_t, \quad n = 0, \dots, N, \\ & & \mathbf{C}_{\text{b7}} &: \|\mathbf{v}[n]\| \leq V_{\text{max}}, \quad n = 1, \dots, N, \\ & & \mathbf{C}_{\text{b8}} &: \|\mathbf{a}[n]\| \leq a_{\text{max}}, \quad n = 0, \dots, N, \\ & & \mathbf{C}_{\text{b9}} &: \sum_{k=1}^K \alpha_k[n] = 1, \quad 0 \leq \alpha_k[n] \leq 1, \quad \forall k, n.\end{aligned}\quad (12)$$

The constraint  $\mathbf{C}_{\text{b1}}, \mathbf{C}_{\text{b2}}, \mathbf{C}_{\text{b9}}$  are the discrete mode for the data collection requirement for each ground node, energy consumption constraint for UAV, and spectrum allocation constraint for ground terminals, respectively.  $\mathbf{C}_{\text{b3}}$  to  $\mathbf{C}_{\text{b8}}$  represent the UAV's initial/final location and velocity constraints, respectively. It is noted that the amount of available energy for UAV is larger than the minimum energy consumption for UAV flying from the initial location to final location.

Problem (13) is nonconvex; hence, it cannot be directly solved by standard convex optimization techniques. In the following sections, we propose an efficient algorithm to find an approximate solution to (13) via iteratively optimizing trajectory and resource optimizations.

**3.3. Combining Optimal Trajectory Design and Resource Allocation Scheme for Multiuser UAV Network.** In this section, an efficient algorithm that combines optimal trajectory design and resource allocation scheme is proposed to approximately solve the original optimization problem. The sequential convex optimization method is applied to meet

the optimized goal by iteratively obtaining the optimal trajectory and allocating the wireless resource to the ground terminals.

The original optimization problem can be classified into two subproblems: (1) wireless resource allocation issue for the multiple ground nodes and (2) the UAV trajectory optimization problem. To make the optimization problem more trackable, we propose to adopt the iteratively optimization method which assumes that one issue is determined when the other issue is considered to be optimized, and vice versa.

**3.3.1. Minimizing Energy Consumption for Constrained UAV Flight.** Firstly, we should find a feasible solution for the UAV flight trajectory from the initial point to the final location by the predefined available energy  $P_{\text{UAV}}$ . In other words, we should examine whether the UAV can finish the flight under the initial/final location, velocity constraints within the  $N+2$  operation time slots without considering any rate constraints of ground terminals. The optimization problem can be formulated as

$$\begin{aligned}
\text{(P3.1) Minimize}_{\{\mathbf{w}[n]\}} \quad & E_{\text{UAV}} = \overline{E}\{w(n)\}, \\
\text{subject to} \quad & \mathbf{C}_{c1} : \mathbf{w}[0] = \mathbf{w}_0, \quad \mathbf{w}[N+1] = \mathbf{w}_F, \\
& \mathbf{C}_{c2} : \mathbf{w}[n+1] = \mathbf{w}[n] + \mathbf{v}[n]\delta_t + \frac{1}{2}\mathbf{a}[n]\delta_t^2, \quad n = 0, \dots, N, \\
& \mathbf{C}_{c3} : \mathbf{v}[0] = \mathbf{v}_0, \quad \mathbf{v}[N+1] = \mathbf{v}_F, \\
& \mathbf{C}_{c4} : \mathbf{v}[n+1] = \mathbf{v}[n] + \mathbf{a}[n]\delta_t, \quad n = 0, \dots, N, \\
& \mathbf{C}_{c5} : \|\mathbf{v}[n]\| \leq V_{\max}, \quad n = 1, \dots, N, \\
& \mathbf{C}_{c6} : \|\mathbf{a}[n]\| \leq a_{\max}, \quad n = 0, \dots, N.
\end{aligned} \tag{13}$$

It is noted that the constraints  $\mathbf{C}_{c1} - \mathbf{C}_{c6}$  are convex sets. However, the objective function is nonconvex. The problem cannot be directly solved with the standard convex optimization techniques. We should adopt some relaxation method to construct the standard convex form and solve the problem (P3.1) efficiently.

The UAV energy consumption of the objective function can be upper-bounded by the following equation:

$$\begin{aligned}
\overline{E}(\{\mathbf{w}[n]\}) \leq & \sum_{n=1}^N \left[ c_1 \|\mathbf{v}[n]\|^3 + \frac{c_2}{\mathbf{v}[n]} \left( 1 + \frac{\|\mathbf{a}\|^2}{g^2} \right) \right] \delta_t \\
& + \Delta_K \triangleq \overline{E}_{\text{ub}}(\{\mathbf{w}[n]\}),
\end{aligned} \tag{14}$$

where  $\Delta_K \triangleq (1/2)m(\|\mathbf{v}[N+1]\|^2 - \|\mathbf{v}[0]\|^2)$  denotes the amount of the UAV's kinetic energy variation, which would be determined as a constant value by the initial and final velocity constraints  $\mathbf{C}_{c3}$ . It is noted that the energy consumption upper bound is tight for the circular flight mode, in which case  $\mathbf{a}[n]\mathbf{v}[n] = 0$ . Therefore, the objective function can be approximately formulated as

$$\text{(P3.1.1) Minimize} \quad \overline{E}_{\text{ub}}(\{\mathbf{w}[n]\}). \tag{15}$$

Considering the function is still a nonconvex set for the variable  $\mathbf{v}[n]$ , we propose to introduce a slack variable  $\xi_n$  to reformulate the objective function as

$$\begin{aligned}
\text{P3.1.2 Minimize} \quad & \overline{E}_{\text{ub}}(\{\mathbf{v}[n]\}, \xi_n) = \left( \sum_{n=1}^N \left[ c_1 \|\mathbf{v}[n]\|^3 + \frac{c_2}{\xi_n} \left( 1 + \frac{\|\mathbf{a}\|^2}{g^2} \right) \right] \delta_t + \Delta_K \right), \\
\text{subject to} \quad & \mathbf{C}_{c1} - \mathbf{C}_{c6}, \\
& (\mathbf{C}_{c7}) : \|\mathbf{v}[n]\|^2 \geq \xi_n^2.
\end{aligned} \tag{16}$$

It can be shown that we must have  $\xi_n = \|\mathbf{v}[n]\|$ ,  $\forall n$ , for all  $n$  at the optimal solution for (P3.1.2), since otherwise one can always increase  $\xi_n$  and decrease  $\mathbf{v}[n]$  when the UAV near the ground terminal to decrease the objective function value and obtain a strictly lower energy consumption. Until now, the objective is a convex with respect to  $[\{\mathbf{v}[n]\}, \{\mathbf{a}[n]\}, \{\xi_n\}]$ , but with a new nonconvex constraint  $\mathbf{C}_{c7}$ . Similarly, to tackle the nonconvexity of the constraint, a local convex approximation is adopted to tackle this issue. For any given local point  $\mathbf{v}_j[n]$ , we have the following expression by applying the first-order Taylor expansion:

$$\left\{ \mathbf{v}[n] \geq \|\mathbf{v}_j[n]\| + 2\mathbf{v}_j^T[n](\mathbf{v}[n] - \mathbf{v}_j[n]) \triangleq \varphi_{\text{lb}}(\mathbf{v}[n]), \right. \tag{17}$$

where the equality holds at the point  $\mathbf{v}[n] = \mathbf{v}_j[n]$ . The function  $\varphi_{\text{lb}}(\mathbf{v}[n])$  is a linear function. Then, the new constraint is a convex set, which can be expressed as

$$\mathbf{C}_{c7}^{\text{lb}} : \varphi_{\text{lb}}(\mathbf{v}[n]) \geq \xi_n^2, \quad \forall n. \tag{18}$$

Then, the inequality in first-order Taylor expansion shows that the new constructed convex constraint  $\mathbf{C}_{c7}^{\text{lb}}$  always implies the nonconvex constraint  $\mathbf{C}_{c7}$ , but the reverse is not true in general.

Then, the optimization problem (P3.1) can be reformulated as

$$\begin{aligned}
\text{P3.1.3 Minimize} \quad & \bar{E}_{\text{ub}}(\{\mathbf{v}[n]\}, \xi_n) = \left( \sum_{n=1}^N \left[ c_1 \|\mathbf{v}[n]\|^3 + \frac{c_2}{\xi_n} \left( 1 + \frac{\|\mathbf{a}\|^2}{g^2} \right) \right] \right) \delta_t + \Delta_K \\
\text{subject to} \quad & \mathbf{C}_{c1} - \mathbf{C}_{c6}, \\
& (\mathbf{C}_{c7}^{\text{lb}}) : \varphi_{\text{lb}}(\mathbf{v}[n]) \geq \xi_n^2, \quad \forall n.
\end{aligned} \tag{19}$$

Based on the previous discussions, the optimal solution of (P3.1.3) is the upper bound to that of problem (P3.1). Fortunately, the optimization problem (P3.1.3) is a standard convex optimization problem with the convex objective function with all convex constraints. It can be solved efficiently via the bisection method or the standard Dinkelbach's algorithm.

**3.3.2. Optimal Resource Allocation with Fixed Trajectory.** For the wireless resource allocation issue, it is proposed to minimize the ground nodes transmit power under the fixed UAV trajectory  $\mathbf{w}^*[n]$  assumption. Then, the optimization problem for wireless resource allocation can be formulated as

$$\begin{aligned}
\text{(P3.2) Minimize} \quad & \sum_{k=1}^K \sum_{n=1}^N P_k[n], \\
& \text{subject to} \quad \mathbf{C}_{d1} : \bar{R}_k(\{\alpha_k[n], P_k[n], \mathbf{w}^*[n]\}) \geq \hat{R}_k, \quad \forall k, \\
& \quad \quad \quad \mathbf{C}_{d2} : \sum_{k=1}^K \alpha_k[n] \leq 1, \quad 0 \leq \alpha_k[n] \leq 1, \quad \forall k, n.
\end{aligned} \tag{20}$$

This subproblem may correspond to the practical scenario when the UAV's trajectory is predetermined due to

other tasks (e.g., surveillance) rather than data collection. In this case, the optimal solution of the subproblem (P3.2) can minimize the transmit power of the ground nodes and extend the life time of the node.

Since the trajectory  $\mathbf{w}^*[n]$  is fixed, the constraint  $\mathbf{C}_{d1}$  is a convex set combined with respect to  $\{P_k[n], \alpha_k[n]\}$ . It can be verified that the subproblem (P3.2) satisfied the Slater's condition. Using the dual Lagrangian method, the optimal power allocation  $P_k^*[n]$  can be expressed as

$$P_k^*[n] = \left[ \frac{\lambda_k B \delta_t}{\ln 2} - \frac{1}{\gamma_k^*[n]} \right]^+ \alpha_k^*[n], \tag{21}$$

where  $\gamma_k^*[n] = \gamma_0 / (H^2 + \|\mathbf{q}_k - \mathbf{w}^*[n]\|^2)$ ,  $\lambda_k$  is the Lagrange multiplier (or dual variable) associated with the constraint.

$\sum_{n=1}^N R_k\{P_k[n], \alpha_k[n], \mathbf{w}^*[n]\} \geq \hat{R}_k$ ;  $\alpha_k^*[n]$  is the optimal frequency band allocation factor. This is one instance of the water-filling solution to the optimal power allocation.

Substitute the optimal  $P_k^*[n]$  in the equation, the optimal frequency band allocation factor  $\alpha_k^*[n]$  can be obtained as equation (22):

$$\alpha_k^*[n] = \begin{cases} 1, & \text{if } \left( \left[ \frac{\lambda_k B \delta_t}{\ln 2} - \frac{1}{\gamma_k^*[n]} \right]^+ - B \delta_t \lambda_k \log_2 \left( 1 + \left[ \frac{\lambda_k B \delta_t \gamma_k^*[n]}{\ln 2} - 1 \right]^+ \right) + \mu_n \right) < 0, \\ a_k^*, & \text{if } \left( \left[ \frac{\lambda_k B \delta_t}{\ln 2} - \frac{1}{\gamma_k^*[n]} \right]^+ - B \delta_t \lambda_k \log_2 \left( 1 + \left[ \frac{\lambda_k B \delta_t \gamma_k^*[n]}{\ln 2} - 1 \right]^+ \right) + \mu_n \right) = 0, \\ 0, & \text{otherwise,} \end{cases} \tag{22}$$

where  $\mu_n$  is the Lagrange multiplier (or dual variable) associated with the constraint  $\sum_{k=1}^K \alpha_k[n] \leq 1$ ;  $a_k^*$  can be any real number between 0 and 1, which can be calculated by satisfying the constraints  $\mathbf{C}_{a1}$  and  $\mathbf{C}_{a2}$ . Generally, the

optimal solution for  $\alpha_k[n]$  is binary solution if the amount of time slot  $n$  is large enough. Otherwise,  $a_k^*$  is adopted to fine-tune the resource allocation solution to meet the constraint.

It is proposed to adopt an iterative subgradient method (Algorithm 1) to optimize the dual variable  $\lambda_k, \mu_n$ : the subgradient for  $\lambda_k$  of ground node  $k$  is given by  $g_k = \widehat{R}_k - \sum_{n=1}^N R_k^*[n]$  and for  $\mu_n$  of each time slot is given by  $t_n = \sum_{k=1}^K \alpha_k^*[n] - 1$ . The update procedure of Lagrangian dual variables are performed as

$$\begin{aligned} \lambda_k^{(l)} &= \max\{\lambda_k^{(l-1)} + \beta^{(l)} g_k, 0\}, \\ \mu_n^{(l)} &= \max\{\mu_n^{(l-1)} + \theta^{(l)} t_n, 0\}, \end{aligned} \quad (23)$$

where  $\beta^{(l)}, \theta^{(l)}$  are the step size for the iterative search process. Several step size rules have been proven to guarantee convergence under some general conditions.

The optimal solution includes two steps: (1) each of subproblem in slot  $n$  can be solved with fixed Lagrangian multipliers using the combinatorial method, (2) the convergency updates of Lagrangian multipliers are performed to meet the constraints. For the optimal dual variables optimization, it can also adopt the ellipsoid method to find the optimal solution. Our proposed procedure above is convenient for the transceiver processing for both UAV and ground nodes.

**3.3.3. UAV Trajectory Optimization with Fixed Resource Allocation.** Since the ground node has been allocated with fixed frequency band and power resource, we should adopt a dual problem to achieve the optimization goal by optimizing the UAV trajectory. In this section, we consider the issue to maximize the total rate of ground nodes by optimizing the UAV's trajectory with fixed frequency band and power allocation. It is noted that maximizing the total rate of ground nodes can minimize the total energy consumption of ground nodes with the rate constraints. They are dual problems with

each other. The optimization subproblem (P3.3) can be formulated as

$$\begin{aligned} \text{(P3.3) Maximize}_{\{\mathbf{w}[n]\}} & \sum_{k=1}^K \overline{R}_k(\{\alpha_k^*[n], P_k^*[n], \mathbf{w}[n]\}), \\ \text{subject to} & \mathbf{C}_{e1} : \overline{R}_k(\{\alpha_k^*[n], P_k^*[n], \mathbf{w}[n]\}) \geq \widehat{R}_k, \quad \forall k, \\ & \mathbf{C}_{e2} : \mathbf{w}[0] = \mathbf{w}_0, \quad \mathbf{w}[N+1] = \mathbf{w}_F, \\ & \mathbf{C}_{e3} : \mathbf{w}[n+1] = \mathbf{w}[n] + \mathbf{v}[n]\delta_t + \frac{1}{2}\mathbf{a}[n]\delta_t^2, \\ & \quad \quad \quad n = 0, \dots, N, \\ & \mathbf{C}_{e4} : \mathbf{v}[0] = \mathbf{v}_0, \mathbf{v}[N+1] = \mathbf{v}_F, \\ & \mathbf{C}_{e5} : \mathbf{v}[n+1] = \mathbf{v}[n] + \mathbf{a}[n]\delta_t, \quad n = 0, \dots, N, \\ & \mathbf{C}_{e6} : \|\mathbf{v}[n]\| \leq V_{\max}, \quad n = 1, \dots, N, \\ & \mathbf{C}_{e7} : \|\mathbf{a}[n]\| \leq a_{\max}, \quad n = 0, \dots, N, \\ & \mathbf{C}_{e8} : \overline{E}(\mathbf{w}[n]) \leq P_{\text{UAV}}. \end{aligned} \quad (24)$$

It is noted that the constraints  $\mathbf{C}_{e2} - \mathbf{C}_{e7}$  are convex sets. However, the constraint  $\mathbf{C}_{e1}$  and  $\mathbf{C}_{e8}$  are nonconvex, and the objective function is nonconvex neither. The problem cannot be directly solved with the standard convex optimization techniques. We should adopt some relaxation method to construct the standard convex form and solve the problem (P3.3) efficiently.

Firstly, to tackle the nonconvexity of the objective function, for any local point  $\mathbf{w}_j[n]$ , define function  $\overline{R}_{k,\text{lb}}(\{\mathbf{w}[n]\})$  for each ground node as

$$\begin{aligned} \overline{R}_{k,\text{lb}}(\{\mathbf{w}[n]\}) &= B\delta_t \sum_{n=1}^{N-1} [\eta_{j,k}[n] - \psi_{j,k}[n]] \\ &\quad \cdot (\|\mathbf{q}_k - \mathbf{w}[n]\|^2 - \|\mathbf{q}_k - \mathbf{w}_j[n]\|^2), \end{aligned} \quad (25)$$

where

$$\begin{aligned} \eta_{j,k}[n] &= \alpha_k^*[n] \log_2 \left( 1 + \frac{P_k^*[n]\gamma_0}{\alpha_k^*[n](H^2 + \|\mathbf{q}_k - \mathbf{w}[n]\|^2)} \right), \\ \psi_{j,k}[n] &= \frac{(\log_2 e)P_k^*[n]\gamma_0}{\left(\alpha_k^*[n](H^2 + \|\mathbf{q}_k - \mathbf{w}_j[n]\|^2) + P_k^*[n]\gamma_0\right)(H^2 + \|\mathbf{q}_k - \mathbf{w}_j[n]\|^2)}. \end{aligned} \quad (26)$$

Note that  $\overline{R}_{k,\text{lb}}(\{\mathbf{w}[n]\})$  is a concave function with respect to  $\mathbf{w}[n]$ . Then the upper contour set  $\overline{R}_{k,\text{lb}}(\{\mathbf{w}[n]\}) \geq \widehat{R}_k$  is convex set. Moreover, as mentioned in [21],  $\overline{R}_k(\{\mathbf{w}[n]\}) \geq \overline{R}_{k,\text{lb}}(\{\mathbf{w}[n]\})$  holds true for any given  $\mathbf{w}_j[n]$ . The lower bound equation is the first order Taylor expansion

of a convex differential function which is its global underestimator. Both  $\overline{R}_k(\{\mathbf{w}[n]\})$  and  $\overline{R}_{k,\text{lb}}(\{\mathbf{w}[n]\})$  have an identical gradient.

Therefore, the optimization problem (P3.3) can be approximately solved by maximizing the lower bound as

- (1) Initialize  $\{\lambda_k^{(l)}, \mu_n^{(l)}\}$ . Let  $l = 0$
- (2) **repeat**
- (3) Obtain the optimal power  $P_k^*[n]$  and  $\alpha_k^*[n]$  from the equations (21) and (22).
- (4) Get the subgradient  $g_k$  and  $t_n$  for all  $n$
- (5) Update the dual variable according the equation (23) for all  $n$ .
- (6) Update  $l = l + 1$ .
- (7) **Until** Converges to a prescribed accuracy.

ALGORITHM 1: Iterative subgradient method for (P3.2).

- (1) Initialize  $\{\mathbf{w}_0[n], \mathbf{v}_0[n]\}$ . Let  $j = 0$
- (2) **repeat**
- (3) Solve problem (P3.3.2) under the given local point  $\{\mathbf{w}_j[n], \mathbf{v}_j[n]\}$ , and obtain the optimal solution as  $\{\mathbf{w}_j^*[n], \mathbf{v}_j^*[n]\}$ .
- (4) Update the local point  $\{\mathbf{w}_{j+1}[n] = \mathbf{w}_j^*[n], \mathbf{v}_{j+1}[n] = \mathbf{v}_j^*[n]\}$ ,  $\forall n$ .
- (5) Update  $j = j + 1$ .
- (6) **Until** Converges to a prescribed accuracy

ALGORITHM 2: Sequential convex optimization for (P3.3).

$$\begin{aligned}
\text{(P3.3.1) Maximize}_{\{\mathbf{w}[n]\}} & \sum_{k=1}^K \bar{R}_{k,\text{lb}}(\{\alpha_k^*[n], P_k^*[n], \mathbf{w}[n]\}), \\
\text{subject to} & \mathbf{C}_{e1}^{\text{lb}} : \bar{R}_{k,\text{lb}}(\{\alpha_k^*[n], P_k^*[n], \mathbf{w}[n]\}) \geq \bar{R}_k, \quad \forall k, \\
& \mathbf{C}_{e2} - \mathbf{C}_{e7} : \\
& \mathbf{C}_{e8} : \bar{E}(\mathbf{w}[n]) \leq P_{\text{UAV}}, \\
& \mathbf{C}_{e8}^{\text{ub}} : \bar{E}_{\text{ub}}(\{\mathbf{v}[n]\}, \xi_n) \\
& \mathbf{C}_{e9} : \varphi_{\text{lb}}(\mathbf{v}[n]) \geq \xi_n^2, \quad \forall n.
\end{aligned} \tag{27}$$

where the constraint of  $\mathbf{C}_{e1}$  is reformulated as a convex set  $\mathbf{C}_{e1}^{\text{lb}}$ .

Secondly, considering the constraint set is still a non-convex set for the variable  $\mathbf{v}[n]$ . Just like the approximation method as in minimizing energy consumption for constrained UAV flight, we propose to introduce a slack variable  $\xi_n$  to reformulate the constraint  $\mathbf{C}_{e8}$  as

Then, all the constraints are convex set. Until now, we reformulate the optimization problem for any given local point  $\{\mathbf{w}_j[n], \mathbf{v}_j[n]\}$ , and it can be written as:

$$\begin{aligned}
\text{(P3.3.2) Maximize}_{\{\mathbf{w}[n]\}} & \sum_{k=1}^K \bar{R}_{k,\text{lb}}(\{\alpha_k^*[n], P_k^*[n], \mathbf{w}[n]\}), \\
\text{subject to} & \mathbf{C}_{e1}^{\text{lb}} : \bar{R}_{k,\text{lb}}(\{\alpha_k^*[n], P_k^*[n], \mathbf{w}[n]\}) \geq \bar{R}_k, \quad \forall k, \\
& \mathbf{C}_{e2} - \mathbf{C}_{e7} : \\
& \mathbf{C}_{e8}^{\text{ub}} : \bar{E}_{\text{ub}}(\mathbf{w}[n]) \leq P_{\text{UAV}}, \\
& \mathbf{C}_{e8}^{\text{ub}} : \bar{E}_{\text{ub}}(\mathbf{w}[n]) \leq P_{\text{UAV}}, \\
& \mathbf{C}_{e9}^{\text{lb}} : \varphi_{\text{lb}}(\mathbf{v}[n]) \geq \xi_n^2, \quad \forall n, \\
& \mathbf{C}_{e10} : \xi_n \geq 0, \quad \forall n.
\end{aligned} \tag{29}$$

Based on the previous discussions, the optimal solution of (P3.3.2) is the lower bound to that of problem (P3.3). Fortunately, the optimization problem (P3.3.2) is a standard convex optimization problem with the convex objective function with all convex constraints. It can be solved efficiently via the bisection method or the standard

Dinkelbach's algorithm. Then, the nonconvex problem (P3.3) can be solved by iteratively optimization (P3.3.2) with local point updated in each iteration. It can be summarized as the following table (Algorithm 2).

In summary, through adopting the relaxation method and sequential convex optimization technique, an efficient

- (1) **Feasible solution check:** Solve the problem (P3.1) to calculate the minimum energy consumption  $P_{\text{UAV}}^{\min}$  for UAV flight from initial point to final location.  
**If**  $P_{\text{UAV}}^{\min} \leq P_{\text{UAV}}$ ;  
**Set:** The initial UAV trajectory with minimum energy consumption as  $\{\mathbf{w}_0^{\text{Fix}}[n], \mathbf{v}_0^{\text{Fix}}[n]\}$ .  
Let  $l = 0$ ;  
Go to **Step 2**;  
**Otherwise,** There is no feasible solution, **End**
- (2) **repeat**
- (3) Solve problem (P3.2) under the fixed trajectory  $\{\mathbf{w}_l^{\text{Fix}}[n], \mathbf{v}_l^{\text{Fix}}[n]\}$  by Algorithm 1, and obtain the optimal resource allocation solution as  $\{\alpha_{k,l}^*[n], P_{k,l}^*[n]\}, \forall n$ .
- (4) Update the fixed resource allocation solution  $\{\alpha_{k,l}^{\text{Fix}}[n] = \alpha_{k,l}^*[n], P_{k,l}^{\text{Fix}}[n] = P_{k,l}^*[n]\}$ ;
- (5) Solve problem (P3.3) under the fixed resource allocation  $\{\alpha_{k,l}^{\text{Fix}}[n], P_{k,l}^{\text{Fix}}[n]\}$  by Algorithm 2, and obtain the optimal UAV trajectory as  $\{\mathbf{w}_{g,l}^*[n], \mathbf{v}_{g,l}^*[n]\}, \forall n$
- (6) Update the fixed UAV trajectory  $\{\mathbf{w}_{l+1}^{\text{Fix}}[n] = \mathbf{w}_{g,l}^*[n], \mathbf{v}_{l+1}^{\text{Fix}}[n] = \mathbf{v}_{g,l}^*[n]\}, \forall n$
- (7) **Update**  $l = l + 1$ .
- (8) **Until** Converges to a prescribed accuracy

ALGORITHM 3: Alternate iterative solution for original optimization problem (P3).

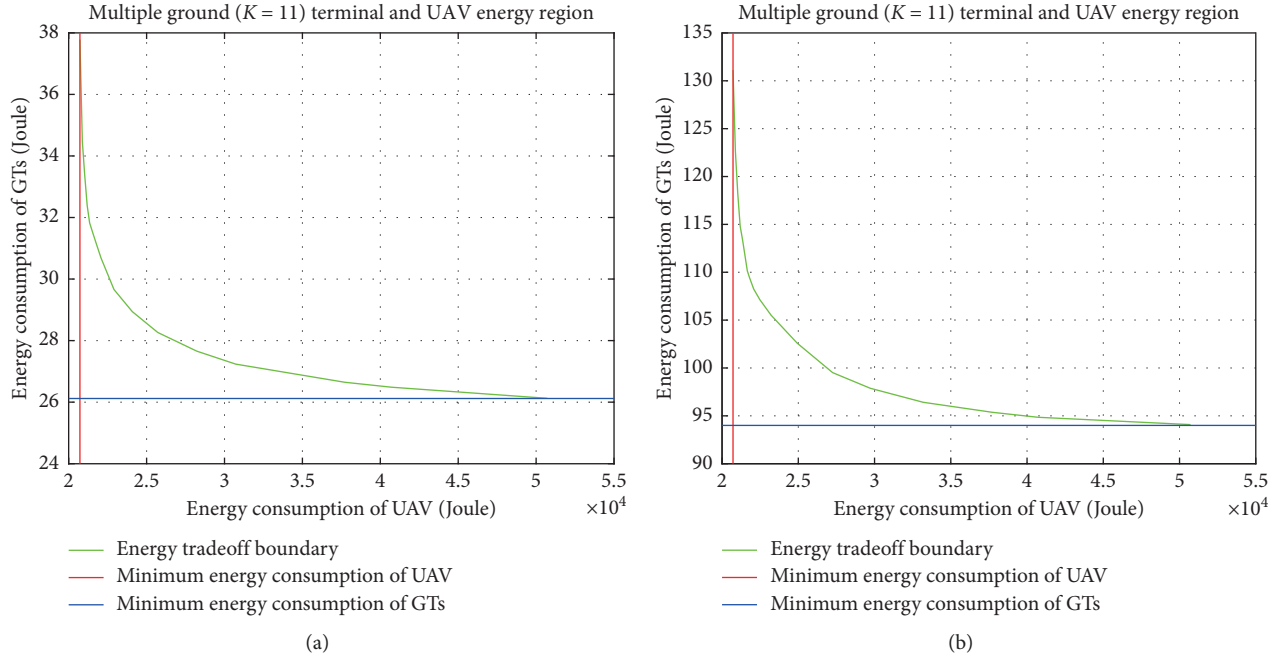


FIGURE 2: Multiple GTs and UAV energy region. (a)  $\widehat{Q}_k = 80$  Mbits (Mb). (b)  $\widehat{Q}_k = 100$  Mbits (Mb).

solution is proposed to solve the UAV trajectory optimization problem which is guaranteed that the optimal point is fulfill the Karush–Kuhn–Tucker conditions of the original nonconvex problem (P3.3).

**3.3.4. Iterative Method for Optimal Resource Allocation and UAV Trajectory Design.** Until now, we have solved the issues of UAV trajectory optimal design and resource allocation for ground terminals when one of them is fixed. In order to obtain the optimal solution for the original optimization problem (P3), we propose an alternate iterative solution to optimize the UAV trajectory and resource

allocation, based on the methods mentioned in Sections 3.3.1.–3.3.3.

The proposed optimal solution can be summarized as follows (Algorithm 3).

Note that the solution for problem (P3.2) adopts an iterative subgradient method in Algorithm 1 whose complexity is  $\mathcal{O}(\text{IN})$  where  $l$  is the iteration time. As Algorithm 2 requires to solve convex optimization problems, it has a polynomial complexity in the worst case each iteration [27]. Thus, the complexity of Algorithm 3 combining Algorithms 1 and 2 is the polynomial complexity because polynomial complexity multiplied by iterations is still polynomial complexity which is affordable.

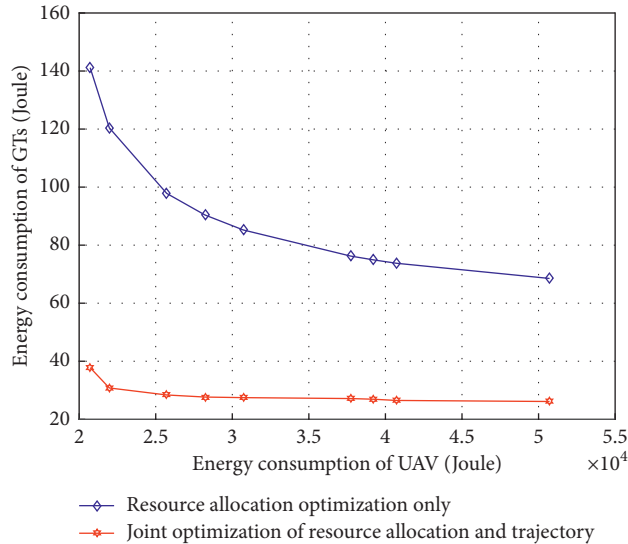


FIGURE 3: Energy consumption for GTs of different  $\hat{Q}_k$ .

### 4. Simulation Results and Analysis

In this part, we provide numerical results to prove the reliability of the proposed algorithm. We assume that  $K = 10$  ground users are randomly distributed in this system with an area of  $1 \times 1 \text{ km}^2$ . Other reference values are as follows: UAV’s altitude is  $H = 100 \text{ m}$ . The communication bandwidth is  $B = 1 \text{ MHz}$  and noise power is assumed to be  $\sigma^2 = -150 \text{ dBm}$ . Besides, we set that  $c_1 = 9.264 \times 10^{-4}$  and  $c_2 = 2250$ , the maximum speed of UAVs are assumed as  $V_{\max} = 100 \text{ m/s}$ , and the maximum acceleration of UAVs are assumed as  $a_{\max} = 30 \text{ m/s}^2$  and  $\hat{Q}_k = 100 \text{ Mbits (Mb)}$ .

Firstly, we evaluate the energy trade-off between the consumption of ground terminals and UAV.

We consider a certain trajectory. Multiple ground terminal and UAV energy region are shown in Figure 2. We can see clearly from the figure that the energy consumption of the ground user decreases as the drone energy consumption increases with different data collect requirement of  $\hat{Q}_k$ . More concretely, when increasing the UAV’s energy from  $22 \text{ kJoule}$  to  $31 \text{ kJoule}$  under the requirement of  $\hat{Q}_k = 80 \text{ Mbits (Mb)}$ , the GTs energy consumption would be significantly reduced from  $32 \text{ Joule}$  to  $27 \text{ Joule}$ .

By comparing with the resource allocation optimization shown in Figure 3, the solution we propose that optimizes the resource allocation and trajectory jointly delivers significant performance in energy efficiency. Specifically, the GTs’ energy consumption of combined resource allocation optimization is  $27 \text{ Joule}$  when the UAV’s energy consumption is  $35 \text{ kJoule}$ , while that of resource allocation optimization only is  $86 \text{ Joule}$ . It can be observed that the total energy consumption for ground terminals achieved by the proposed algorithm dramatically decreases with the number of iterations and the algorithm converges in about 4–6 iterations from Figure 4. Thus, the solution we propose is able to converge

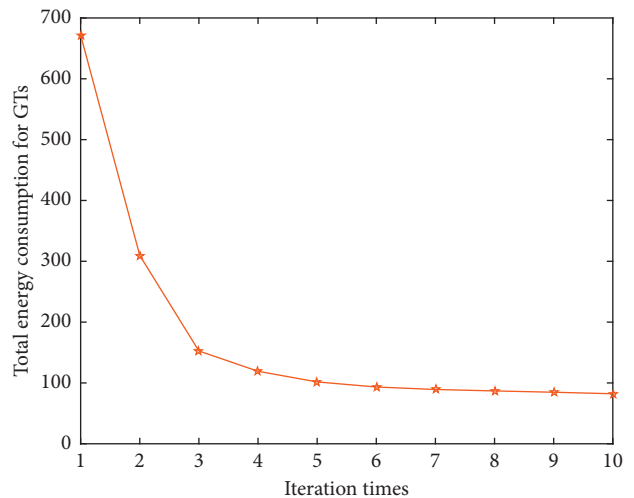


FIGURE 4: Total energy consumption for ground terminals with  $\hat{Q}_k = 100 \text{ Mbits (Mb)}$ .

fast and the computational complexity is suitable for practical implementation.

Next, we study the UAV trajectory optimization.

As shown in Figure 5, the UAV flies to the top of each GT eventually to fulfill the communication task. It is observed that the obtained trajectories tend to be converged for comparing the trajectory of fifth iteration and that of seventh iteration proposed by the algorithm. We also show the scheduling of every GT in Figure 6 where the UAV maintains communicating with GT all the time in order to save the energy.

We also collect the UAV trajectory optimization results. In multiuser scenario, we obtained the UAV trajectory under the constraints of limited flight energy and data collection rate, minimizing the energy consumption problem of user communication. The UAV trajectories under different UAV energy consumption are shown in



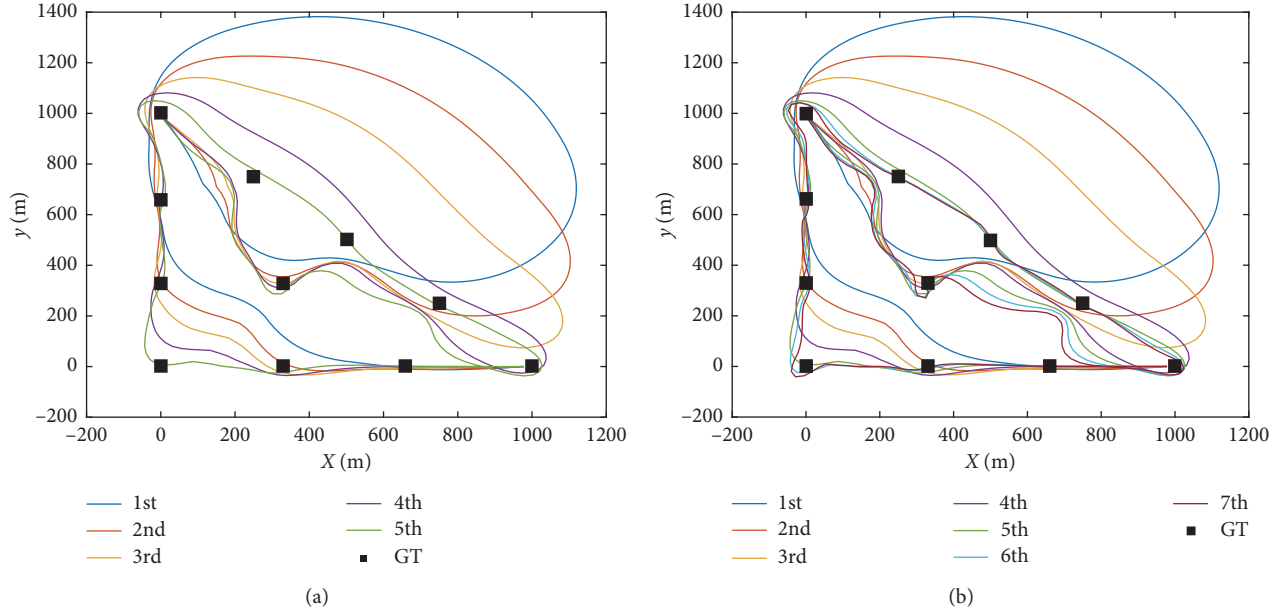


FIGURE 5: Trajectories in different iterations. (a) Five iterations. (b) Seven iterations.

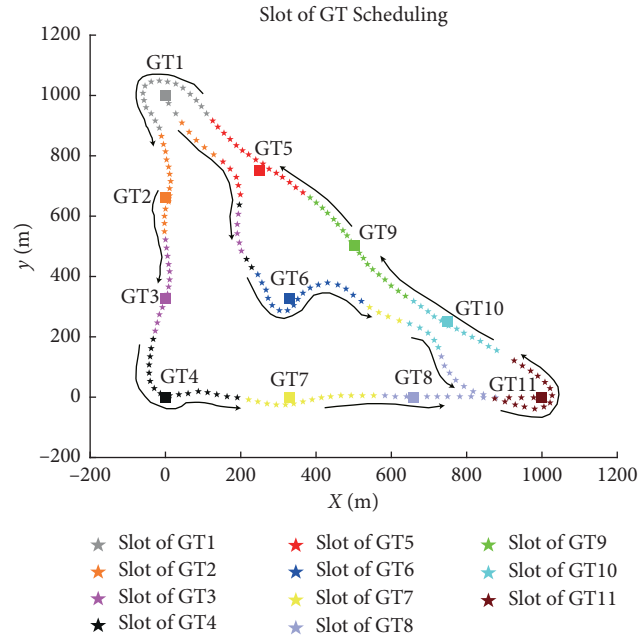


FIGURE 6: Schedule for each GT.

Figure 7. With the increase of  $\Delta_K$ , the UAV hovers around more on the top of GTs so as to save that of the GTs but consume energy of the UAV. It is beneficial for energy-limited GTs.

## 5. Conclusions

In this paper, we have studied the optimal resource allocation scheme and optimal trajectory design strategy for multiple ground terminals with UAV arbitrary flight. First, UAV's energy consumption and GT's energy

consumption are derived, and we describe their Pareto optimal trade-offs and adopt the strategy to minimize the ground terminal energy consumption with fixed UAV energy consumption and consider rate constraints of ground terminals. Second, through calculating minimum energy consumption for constrained UAV flight, we gain the initial UAV flight in the G-U system. Next, we propose to get the optimal resource allocation under the fixed flight. Then, through maximizing the total rate of ground nodes by optimizing the UAVs trajectory with fixed frequency band and power allocation. Finally, we use

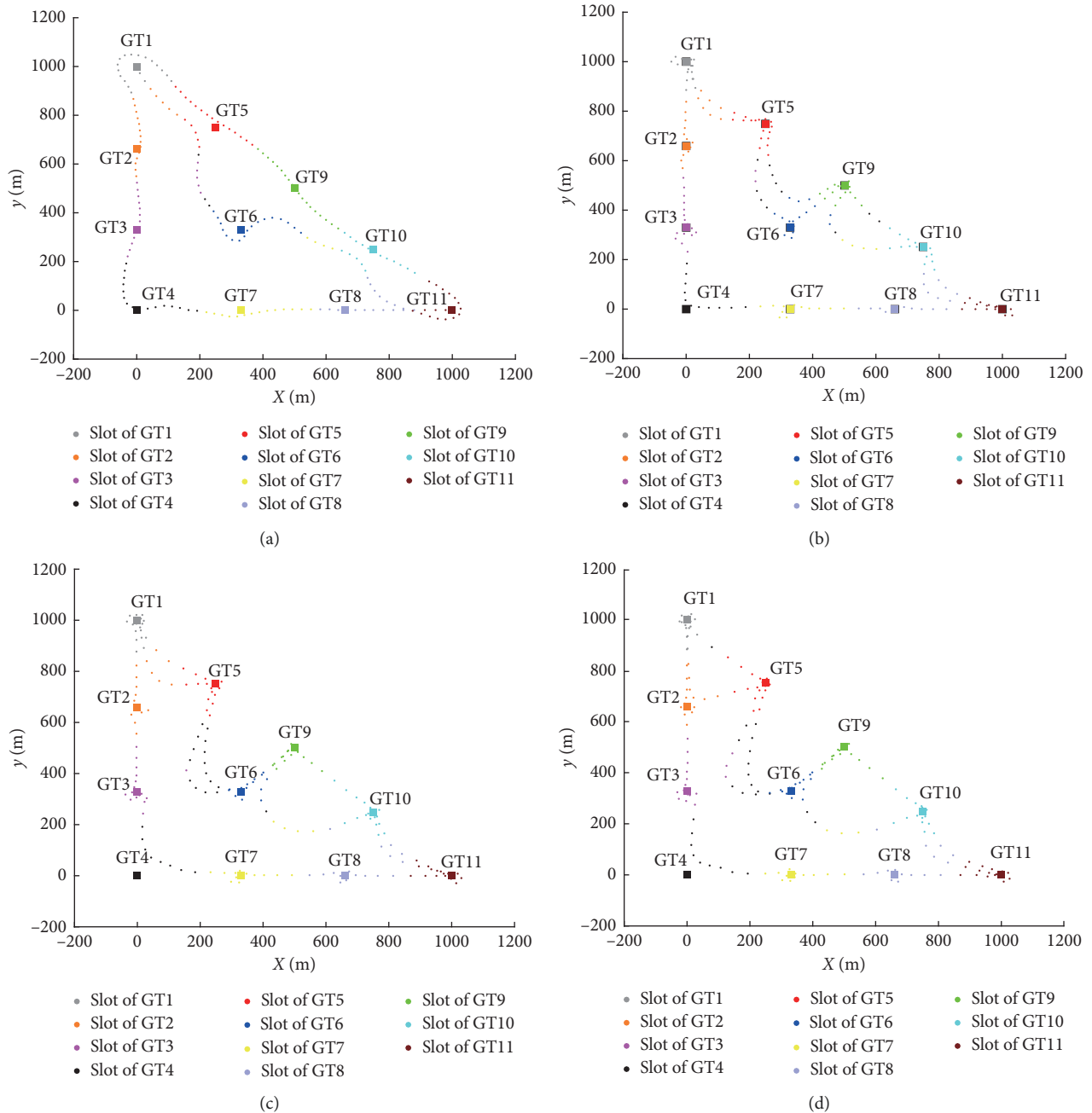


FIGURE 7: Trajectories under different UAV energy consumption. (a)  $\Delta k = 0$  J. (b)  $\Delta k = 3300$  J. (c)  $\Delta k = 6600$  J. (d)  $\Delta k = 10000$  J.

an alternate iterative solution to optimize the UAV trajectory and resource allocation. Simulation results show the alternate solution we proposed can significantly improve the performance in energy efficiency compared with the scheme without optimizing trajectory. Through this paper, we consider a point-to-point G2U communication scheme formerly [23], extending to a UAV to multiusers on designing energy-saving UAV communication. We hope that there will be more development in the future wireless communication.

### Data Availability

The data used to support the findings of this study are available from the corresponding author upon request.

### Conflicts of Interest

The authors declare that there are no conflicts of interest regarding the publication of this paper.

## Authors' Contributions

Dingcheng Yang and Qingmin Zhao are contributed equally to this work.

## Acknowledgments

This work was supported in part by the National Natural Science Foundation of China (grant nos. 61703197, 61561032, and 61461029), Graduate Student Innovation Special Funds of Nanchang University (grant no. CX2019077), and Key Research and Development Program of Jiangxi Province (grant no. 20182ABC28008).

## References

- [1] N. R. Kuntz and P. Y. Oh, "Development of autonomous cargo transport for an unmanned aerial vehicle using visual servoing," in *Proceedings of the ASME Dynamic Systems and Control Conference*, pp. 731–738, Ann Arbor, MI, USA, October 2008.
- [2] S. O'Young and P. Hubbard, "Raven: A maritime surveillance project using small UAV," in *Proceedings of the IEEE Conference on Emerging Technologies & Factory Automation*, Piscataway, NJ, USA, September 2007.
- [3] M. Z. Anwar, Z. Kaleem, and A. Jamalipour, "Machine learning inspired sound-based amateur drone detection for public safety applications," *IEEE Transactions on Vehicular Technology*, vol. 68, no. 3, pp. 2526–2534, 2019.
- [4] M. Z. Anwar, Z. Kaleem, and A. Jamalipour, "UAV-empowered disaster-resilient edge architecture for delay-sensitive communication," *IEEE Network*, pp. 1–9, 2019.
- [5] S. Morgenthaler, T. Braun, Z. Zhao, T. Staub, and M. Anwander, "UAVNet: a mobile wireless mesh network using unmanned aerial vehicles," in *Proceedings of the IEEE Globecom Workshops*, pp. 1603–1608, Anaheim, CA, USA, December 2012.
- [6] E. Yanmaz, R. Kuschnig, and C. Bettstetter, "Achieving air-ground communications in 802.11 networks with three-dimensional aerial mobility," in *Proceedings of the IEEE International Conference. Computer Communications (INFOCOM)*, pp. 120–124, Ser, Turin, Italy, April 2013.
- [7] M. Asadpour, D. Giustiniano, K. A. Hummel, S. Heimlicher, and S. Egli, "Now or later?: delaying data transfer in time-critical aerial communication," in *Proceedings of the Ninth ACM Conference on Emerging Networking Experiments and Technologies (CoNEXT)*, pp. 127–132, Santa Barbara, CA, USA, December 2013.
- [8] Y. Xu, L. Xiao, D. Yang, Q. Wu, and L. Cuthbert, "Throughput maximization in multi-UAV enabled communication systems with difference consideration," *IEEE Access*, vol. 6, pp. 55291–55301, 2018.
- [9] S. Hayat, E. Yanmaz, and C. Bettstetter, "Experimental analysis of multipoint-to-point UAV communications with IEEE 802.11n and 802," in *Proceedings of the IEEE 26th Annual International Symposium on Personal, Indoor, and Mobile Radio Communications (PIMRC)*, pp. 1991–1996, Hong Kong, China, August 2015.
- [10] A. Al-Hourani, S. S. Kandeepan, and S. Lardner, "Optimal LAP altitude for maximum coverage," *IEEE Wireless Communications Letters*, vol. 3, no. 6, pp. 569–572, 2014.
- [11] M. Mozaffari, M. W. Saad, M. Debbah, and D. Mérouane, "Unmanned aerial vehicle with underlaid device-to-device communications: performance and tradeoffs," *IEEE Transactions on Wireless Communications*, vol. 15, no. 6, pp. 3949–3963, 2016.
- [12] M. Mozaffari, M. W. Saad, M. Debbah, and M. Debbah, "Efficient deployment of multiple unmanned aerial vehicles for optimal wireless coverage," *IEEE Communications Letters*, vol. 20, no. 8, pp. 1647–1650, 2016.
- [13] R. I. Bor-Yaliniz, A. El-Keyi, and H. Yanikomeroglu, "Efficient 3-D placement of an aerial base station in next generation cellular networks," in *Proceedings of the IEEE International Conference on Communications*, pp. 985–989, Kuala Lumpur, Malaysia, May 2016.
- [14] Y. Chen, S. Zhang, S. Xu, and G. Y. Li, "Fundamental trade-offs on green wireless networks," *IEEE Communications Magazine*, vol. 49, no. 6, pp. 30–37, 2011.
- [15] F. Wu, D. Yang, L. Xiao, and L. Cuthbert, "Energy consumption and completion time tradeoff in rotary-wing UAV enabled WPCN," *IEEE Access*, vol. 7, pp. 79617–79635, 2019.
- [16] F. Wu, D. Yang, L. Xiao, and L. Cuthbert, "Minimum-throughput maximization for multi-UAV-enabled wireless-powered communication networks," *Sensors*, vol. 19, no. 7, p. 1491, 2019.
- [17] Y. Zeng and R. Zhang, "Energy-efficient UAV communication with trajectory optimization," *IEEE Transactions on Wireless Communications*, vol. 16, no. 6, pp. 3747–3760, 2017.
- [18] Q. Wu, Y. Zeng, and R. Zhang, "Joint trajectory and communication design for multi-UAV enabled wireless networks," *IEEE Transactions on Wireless Communications*, vol. 17, no. 3, pp. 2109–2121, 2018.
- [19] M. Mozaffari, W. Saad, M. Bennis, and M. Debbah, "Mobile unmanned aerial vehicles UAVs for energy-efficient internet of things communications," *IEEE Transactions on Wireless Communications*, vol. 16, no. 11, pp. 7574–7589, 2016.
- [20] Q. Wu and R. Zhang, "Common throughput maximization in UAV-enabled multiuser OFDMA systems with delay consideration," *IEEE Transactions on Wireless Communications*, vol. 66, no. 12, pp. 6614–6627, 2018.
- [21] Q. Wu, W. Li, D. W. K. Chen, D. W. K. Ng, and R. Schober, "An overview of sustainable green 5G networks," *IEEE Wireless Communications*, vol. 24, no. 4, pp. 72–80, 2017.
- [22] J. Lyu, R. Y. Zeng, and R. Zhang, "Cyclical multiple access in UAV-aided communications: a throughput-delay tradeoff," *IEEE Wireless Communications Letters*, vol. 5, no. 6, pp. 600–603, 2016.
- [23] D. Yang, Q. Wu, and Y. Zeng, "Energy trade-off in ground-to-UAV communication via trajectory design," *IEEE Transactions on Vehicular Technology*, vol. 67, no. 7, pp. 6721–6726, 2018.
- [24] H. He, S. Zhang, Y. Zeng, and R. Zhang, "Joint altitude and beamwidth optimization for UAV-enabled multiuser communications," *IEEE Communications Letters*, vol. 22, no. 2, pp. 344–347, 2018.
- [25] J. Lyu, Y. Zeng, R. Zhang, and T. J. Lim, "Placement optimization of UAV-mounted mobile base stations," *IEEE Communications Letters*, vol. 21, no. 3, pp. 604–607, 2017.
- [26] Y. Zeng, X. Xu, and R. Zhang, "Trajectory design for completion time minimization in UAV-enabled multicasting," *IEEE Transactions on Wireless Communications*, vol. 17, no. 4, pp. 2233–2246, 2018.
- [27] S. Boyd and L. Vandenberghe, *Convex Optimization*, Cambridge University Press, Cambridge, UK, 2004.

## Research Article

# An Efficient Contention-Window Based Reporting for Internet of Things Features in Cognitive Radio Networks

Muhammad Sajjad Khan <sup>1,2</sup>, Junsu Kim <sup>2</sup>, Eung Hyuk Lee,<sup>2</sup> and Su Min Kim <sup>2</sup>

<sup>1</sup>Department of Electrical Engineering, International Islamic University Islamabad, Islamabad, Pakistan

<sup>2</sup>Department of Electronics Engineering, Korea Polytechnic University, 237 Sangidaehak-ro, Siheung-si, Gyeonggi-do 15073, Republic of Korea

Correspondence should be addressed to Su Min Kim; [suminkim@kpu.ac.kr](mailto:suminkim@kpu.ac.kr)

Received 24 May 2019; Revised 19 July 2019; Accepted 25 July 2019; Published 18 August 2019

Guest Editor: Fadi Al-Turjman

Copyright © 2019 Muhammad Sajjad Khan et al. This is an open access article distributed under the Creative Commons Attribution License, which permits unrestricted use, distribution, and reproduction in any medium, provided the original work is properly cited.

Internet of things (IoT) is a new challenging paradigm for connecting heterogeneous networks. However, an explosive increase in the number of IoT cognitive users requires a mass of sensing reporting; thus, it increases complexity of the system. Moreover, bandwidth utilization, reporting time, and communication overhead arise. To realize spectrum sensing, how to collect sensing results by reducing the communication overhead and the reporting time is a problem of major concern in future wireless networks. On the other hand, cognitive radio is a promising technology to access the spectrum opportunistically. In this paper, we propose a contention-window based reporting approach with a sequential fusion mechanism. The proposed reporting scheme reduces the reporting time and the communication overhead by collecting sensing results from the secondary users with the highest reliability at a fusion center by utilizing Dempster-Shafer evidence theory. The fusion center broadcasts the sensing results once a global decision requirement is satisfied. Through simulations, we evaluate the proposed scheme in terms of percentage of the number of reporting secondary users, error probability, percentage of reporting, and spectral efficiency. As a result, it is shown that the proposed scheme is more effective than a conventional order-less sequential reporting scheme.

## 1. Introduction

Wireless communication networks have tremendous progress in the last 30 years to support the growth of the application devices from 1G to 4G LTE-Advanced wireless network [1]. Each generation has played its role to enhance data rate, reliability, latency, etc. During the past years, connecting each device with another device at anytime and anywhere is a big challenge in wireless communication networks. In a line of evolution, 5G will provide an unexpected contribution and a big step forward toward the spectrum management, public safety, energy efficiency, high data rate, low latency, and so on [2–5].

On the other hands, unmanned aerial vehicle (UAV) is expected to be an important component of the upcoming wireless network, i.e., 5G, because of its countless applications such as public safety, health, management, and remotely services [6, 7]. In [8], the authors deployed a UAV-

based cognitive system to maximize energy efficiency by optimizing the transmit power. Similarly, in [9], the authors studied resource allocation and trajectory design for an energy-efficient secure UAV communication system, where a UAV base station serves multiple secondary users in the presence of the potential eavesdroppers. One of the potential UAV applications is to remotely deploy and monitor sensor devices for future Internet of things (IoT) networks.

IoT was first mentioned by Ashton, who introduces a technological revolution to bring heterogeneous networks under a single umbrella of the IoT [10]. IoT is a promising subject of technical, social, and economic implications; it can be presumed that IoT has a strong and meaningful impact on daily life in the near future, such as automation, improvised learning, logistic, intelligent transportation, e-health care, and so on [11, 12]. Technically, the most focused area of paradigm is computing, communication, and connectivity in IoT. Among them, the connectivity and management

spectrum are more challenging and of great concern. Additionally, it is noteworthy to mention that with the rapid increase in connecting devices, a lot of spectrum are required for coverage and capacity of these connecting devices in IoT. Femtocell can be a promising candidate to meet the demand for capacity and coverage of the growing IoT devices [13, 14]. As over 50 billion wireless devices will be connected by 2020, all of which will demand a lot of spectrum resources [15]; the authors in [16] argued the importance of the cognitive capability, that is, without comprehensive cognitive capability, IoT is just like an awkward stegosaurus: all brawn and no brains. The static management and allocation of spectrum resources are not efficient to meet requirements of wireless devices and applications. With static allocation of spectrum resources, some of them are heavily overloaded, whereas another part of the spectrum is rarely used. According to the report revealed by Federal Communication Commission (FCC), the spectrum usage varies from 15% to 85% in some cases [17].

One of tempting solutions against the spectrum shortage is cognitive radio technology (CRT), which has yielded extensive studies on spectrum allocation and management for decades [18]. CRT can be integrated with IoT to provide a more intelligent and efficient networking and resource utilization [19]. CRT allows wireless devices to sense the spectrum bands, search for suitable frequency channels, and reconfigure their parameters to meet channel requirements while minimizing energy consumption [20]. In CRT, spectrum sensing plays a vital role to find a spectrum hole and efficiently utilize the spectrum while avoiding interference to primary users (PUs) [21]. In [22, 23], the authors have presented a detailed survey for the key enabling techniques, such as detection, localization, tracking, and controlling. A number of various detection techniques such as energy detection, matched filtering, and cyclostationary have been utilized to detect the existence of the PU in the network [24, 25]. Among these techniques, the energy detection is one of the most engaging techniques, thanks to its ease of implementation and no requirement on prior information of the PU. However, a major drawback of the energy detection is weakness of the received signal strength induced by fading, shadowing, and hidden terminal problem.

The fading and hidden terminal problems can be overcome by cooperative spectrum sensing (CSS) [26]. CSS mainly consists of three steps: sensing, reporting, and global decision. In [27], the authors considered a centralized CSS mechanism to make a firm decision for the status of the channel and broadcast it to the others in the network; the authors also optimized the number of secondary users (SUs) and threshold to get the best result with minimum resources. In [28], the authors proposed a novel CoMAC-based CSS scheme that allow cooperative SUs to encode their local statistics in transmit power and to transmit sequence information of the modulated symbols to a fusion center (FC) for making a final decision on the existence of the PU. The authors in [29] have improved the sensing performance by adjusting parameters such as decision threshold, sensing frequency, and the number of sensing operations.

In this paper, we propose an ordered-sequential reporting mechanism based on contention window and D-S evidence

theory IoTs in order to reduce the reporting time and communication overheads, which ultimately reduce costs such as control channel bandwidth and energy consumption. Once sensing is performed by utilizing energy detection techniques, SUs determine its basic probability assignment and reliability. Then, SUs wait for listening to the medium (control channel) and contents for the channel access. The SU with the highest reliability wins the contention and reserve time slots for transmitting sensing reports to the FC. Then, the FC broadcasts a burst of report messages in the whole medium (control channels) if the global requirement is satisfied. Through simulations, we demonstrate that the proposed scheme achieves better performance than a conventional order-less sequential reporting scheme. The main contributions of this paper are summarized as follows:

- (i) We propose a contention-window based mechanism, in which SUs contend for the channel access. The SU with the highest reliability wins and access the channel for reporting sensing information to the FC.
- (ii) We propose an ordered-sequential reporting scheme instead of conventional order-less sequential reporting scheme, which ultimately enhances the performance of the system including reduced reporting time.
- (iii) To this end, we utilize Dempster-Shafer evidence theory in combining reports at the FC to decide the existence of PU in the network.
- (iv) We evaluate the proposed scheme in terms of percentage of number of sensing reports, error probability, percentage of reporting, and spectral efficiency. Through simulations, we demonstrate that the proposed scheme outperforms the order-less sequential reporting scheme.

The remainder of this paper is organized as follows. In Section 2, we present related work. In Section 3, we discuss the cooperative spectrum sensing and sequential fusion. In Section 4, we provide a detailed description of the proposed contention-window based reporting scheme. In Section 5, the numerical results are shown. Finally, the paper is concluded in Section 6.

## 2. Related Work

In recent years, reporting in CSS has drawn much more attention. In [30], the author proposed a random-access mechanism, in which the author discussed how to collect local sensing reports in CSS. A backward induction approach is applied to decide the optimal stopping time of the collection period. Similarly, in [31], the authors designed a reporting channel scheme based on random-access protocols including slotted ALOHA and reservation ALOHA to measure the performance of the probability of detection and probability of false alarm. In [32], the author proposed a CSS scheme for cognitive radio networks (CRN) with limited reporting. Two kinds of CSS approach with limited reporting in a centralized CRN have been proposed: a soft combination approach with

threshold-based reporting and a soft combination approach with contention-based reporting. In [33], the authors designed a reporting channel structure based on a random-access protocol, which is introduced for SUs and FC; in addition, k-out-of-N rules are implemented at FC to determine the global detection.

A data fusion scheme for CSS based on Dempster-Shafer (D-S) theory was first proposed in [34]. This scheme has significantly improved the probability of detection and the probability of false alarm. The performance of D-S evidence theory can be enhanced to obtain a larger gain of combination by utilizing the signal-to-noise-ratio (SNR) of the PU [35]. However, the advantages of performance enhancement cost overhead in traffic control signaling; which results in consuming more communication resources such as reporting time delay, control channel bandwidth and transmission energy. The resource demands drastically increase with the increasing of the number of SUs. However, only few researchers have addressed these problems. In [36], the authors proposed a sequential test to control the number of reporting bits and average detection time. Similarly, in [37], the authors proposed a cooperative sequential detection scheme to reduce the sensing time. However, these schemes do not utilize an ordered-sequential approach for fast detection with a limited number of reports. Our proposed approach is ordered-sequential contention-window based reporting by the SU with the highest reliability, which significantly reduces reporting time and the error probability, and after all, it is more efficient than a conventional order-less sequential reporting scheme.

### 3. Cooperative Sensing and Sequential Fusion

We consider a cooperative sensing scenario in a CRN, in which each SU conducts local sensing by utilizing energy detection technique and collects basic information about the PU status in the network. After local sensing, each SU measures its basic probability assignment (BPA) and reliability and reports this information to FC. Figure 1 shows the cooperative sensing scenario and a frame structure consisting of sensing period, reporting period, and transmission.

At the beginning, each SU performs local spectrum sensing in a distributed manner. The local spectrum sensing can be represented as a binary hypothesis testing of the presence or absence of PU in the network and is measured as

$$y_i(n) = \begin{cases} z(n), & H_0, \\ h_i(n)s(n) + z(n), & H_1, \end{cases} \quad (1)$$

where  $H_0$  is the absence,  $H_1$  is the presence of the PU,  $h_i(n)$  is the fading coefficient,  $z(n)$  is the additive white Gaussian noise (AWGN),  $s(n)$  is the PU signal, and  $y_i(n)$  is the signal received at the  $i$ -th SU, respectively.

Each SU measures test statistics of the received signal by utilizing an energy detection technique, given as

$$X_{Ei}(n) = \sum_{k=1}^{N_T} |y_k(n)|^2, \quad (2)$$

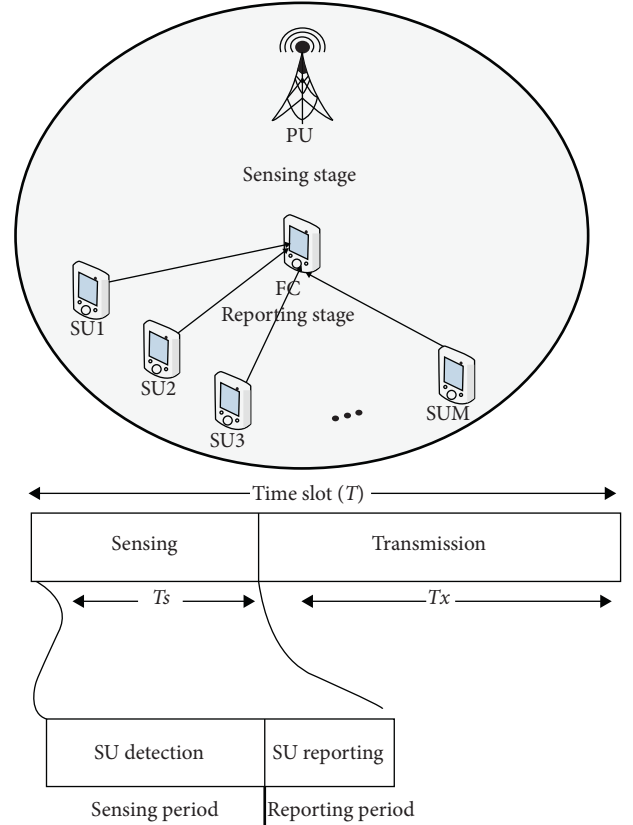


FIGURE 1: System model.

where  $N_T = 2TW$ , in which  $T$  is the sensing time and  $W$  is the bandwidth, and  $y_k$  is the  $j$ -th sample of the received signal. When  $N_T$  is large enough, by central limit theorem (CLT),  $X_{Ei}$  can be well approximated as a Gaussian distribution [26].

After performing local sensing, each SU measures its self-assessed credibility, which is equivalent to BPA for  $H_0$  and  $H_1$  hypotheses. BPA is defined as a form of cumulative distribution function, given as [35]

$$\begin{cases} H_0: m_i(H_0) = \int_{X_{Ei}} \frac{1}{2\pi\sigma_{0i}} e^{-(X_{Ei}-\mu_{0i})^2/\sigma_{0i}^2} dx, \\ H_1: m_i(H_1) = \int_{X_{Ei}} \frac{1}{2\pi\sigma_{1i}} e^{-(X_{Ei}-\mu_{1i})^2/\sigma_{1i}^2} dx, \end{cases} \quad (3)$$

where  $m_i(H_0)$  and  $m_i(H_1)$  are the BPAs of hypothesis  $H_0$ , the absence of PU, and hypothesis  $H_1$ , the presence of PU.

According to D-S evidence theory, the BPAs of each SU at the FC are combined as

$$\begin{cases} m(H_0) = \frac{\sum_{A_1 \cap A_1 \cap \dots \cap A_N = H_0} \prod_{i=1}^N mH_i(A_i)}{1 - K}, \\ m(H_1) = \frac{\sum_{A_1 \cap A_1 \cap \dots \cap A_N = H_1} \prod_{i=1}^N mH_i(A_i)}{1 - K}, \\ \text{where } K = \sum_{A_1 \cap A_1 \cap \dots \cap A_N = \emptyset} \prod_{i=1}^N mH_i(A_i), \end{cases} \quad (4)$$

where  $(A_i)$  is one of the elements of a set  $\{H_0, H_1, \Omega\}$ , in which  $\Omega$  is the ignorance hypothesis that either hypothesis  $\{H_0, H_1\}$  can be true.

The main problem of D-S evidence theory as well as other schemes is that it requires a large amount of resources for reporting sensing results.

In order to reduce the overhead, processing time and reporting time, and energy consumption, we consider an ordered-sequential fusion CSS. After local sensing, each SU measures its BPA. At FC, the BPAs are combined sequentially according to their reliability.

It is noteworthy that the combined results of the proposed ordered-sequential fusion are equal to nonsequential one when all SUs send reports to FC. Therefore, instead of keeping threshold 0, we adopt a threshold ( $\eta$ ). The threshold is set to a large enough value so that the cooperation gain is equivalently maintained even if the number of combined sensing results is lower.

The final sequential decision is based on the following strategy.

The following two strategies are applied to FC to make a global decision. When the number of reports  $k$  at the FC is less than the total number of SUs, the global decision can be determined as

$$F_d = \begin{cases} H_0: & r_{k,\text{global}} < -\eta, \\ H_1: & r_{k,\text{global}} > \eta, \\ \text{no decision:} & -\eta < r_{k,\text{global}} < \eta, \end{cases} \quad (5)$$

where the condition  $-\eta < r_{k,\text{global}} < \eta$  denotes that the reports at the FC are not enough to declare a global decision and wait for more sensing reports.  $r_{k,\text{global}}$  represents the global decision reliability at the  $k$ -th report expressed as

$$r_{k,\text{global}} = \left( \frac{m_{k,\text{global}}(H_1)}{m_{k,\text{global}}(H_0)} \right), \quad (6)$$

where  $m_{k,\text{global}}(H_j) = m_{k-1,\text{global}}(H_j) \oplus m_{k,\text{global}}(H_j)$  is the order of sequential combination of the BPAs  $j = [0, 1]$ , and  $m_{k,\text{global}}(H_j)$  and  $m_{k-1,\text{global}}(H_j)$  are the  $k$ -th and  $(k-1)$ -th global BPA hypotheses  $H_j$ , respectively.

When the number of reports  $k$  is equal to the total number of SU at the FC, the global decision can be determined as

$$F_d = \begin{cases} H_0: & r_{k,\text{global}} < 0, \\ H_1: & r_{k,\text{global}} > 0. \end{cases} \quad (7)$$

#### 4. Proposed Contention-Window Based Reporting Scheme

In this section, we first describe the conventional order-less sequential fusion reporting scheme and then discuss the proposed contention-window based reporting scheme.

At the beginning, each SU performs spectrum sensing, measures its BPA information, and waits for the FC request to send their information to the FC.

In the conventional order-less sequential fusion reporting scheme, the FC sends a request to SUs in a predefined order.

Then, the requested SU responds its own sensing report to the FC. The FC accumulates the sensing reports of the current SU with the previous SU and verifies whether the decision requirement is satisfied or not. If the required decision is satisfied, the FC sends the stop reporting message to all SUs, and further reporting is stopped. If the decision is not satisfied, FC sends a request to next SU in the predefined order, and the process is repeated until the decision requirement is satisfied. The overall process for the conventional order-less sequential reporting scheme is shown in Figure 2.

In the proposed reporting scheme, instead of reporting in a predefined manner, we consider a contention-window based reporting scheme, in which the SUs report to the FC according to their sensing data reliability given in (6). The sensing data reliability of each SU depends on the offset time for accessing the medium (control channel) for reporting to the FC for its turn. As in this mechanism, SUs content to access medium (control channel) for a specific time to report its sensing information to the FC; thus, it is named as the contention-window based reporting scheme.

In the reporting period, from the beginning of the contention slot, each SU listens to the medium (control channel). If there is no signal till  $t_{\text{offset}}$  for SUs, then it is assumed that SU wins the contention slot  $t_{\text{con}}$ . The winner SU generates a burst signal to the medium (control channel) for reservation of the channel and reports in the next reporting slot. It is worth noting that the offset is in the range of  $t_{\text{slot}} < t_{\text{offset}} < t_{\text{con}} - t_{\text{slot}}$ . The first  $t_{\text{slot}}$  is reserved for the SU with higher priority for the transmission to the FC. Whenever the global decision requirement is satisfied, the FC sends a burst message signal in the whole medium (control channel). The overall proposed contention-based reporting scheme is shown in Figure 3.

In the  $k$ -th contention slot, the value of the offset time  $t_{\text{offset}}$  is calculated as follows:

$$t_{\text{offset}} = \frac{t_{\text{con}} - 2t_{\text{slot}}}{(r_{k,\text{max}} - r_{k,\text{min}})} (r_{k,\text{max}} - r_i) + t_{\text{slot}}, \quad (8)$$

where  $t_{\text{slot}}$  is the slot time corresponding to the time required by the radio layer carrier sensing to function and  $t_{\text{con}}$  is the length of the contention slot.  $r_{k,\text{max}}$  and  $r_{k,\text{min}}$  are the maximum and minimum values of the data sensing reliability at the  $k$ -th contention slot, respectively. The values of  $r_{k,\text{max}}$  and  $r_{k,\text{min}}$  are first time defined by the FC and then updated automatically after every reporting slot.

The average reporting time  $T_{\text{avg\_rep}}$  for the order-less sequential reporting scheme can be determined as

$$T_{\text{avg\_rep}} = M \cdot P_{\text{poll}} \cdot (t_{\text{report}} + t_{\text{poll}}), \quad (9)$$

where  $M$  is the number of SUs and  $P_{\text{poll}}$  is the percentage of the number of reporting SUs.

The average reporting time for the proposed contention-window based reporting scheme,  $T_{\text{avg\_rep\_prop}}$ , is determined as

$$T_{\text{avg\_rep\_prop}} = M \cdot P_{\text{con}} \cdot (t_{\text{report}} + t_{\text{con}}), \quad (10)$$

where  $P_{\text{con}}$  is the percentage of the number of reporting SUs for the proposed contention-window based reporting scheme.

The overall flowchart of the proposed contention-window based reporting scheme is shown in Figure 4.

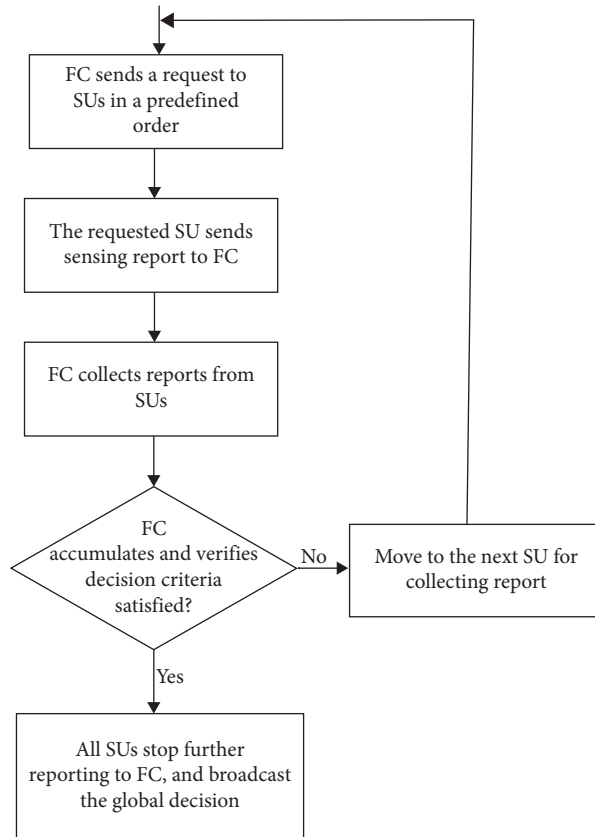


FIGURE 2: Conventional order-less sequential fusion reporting scheme.

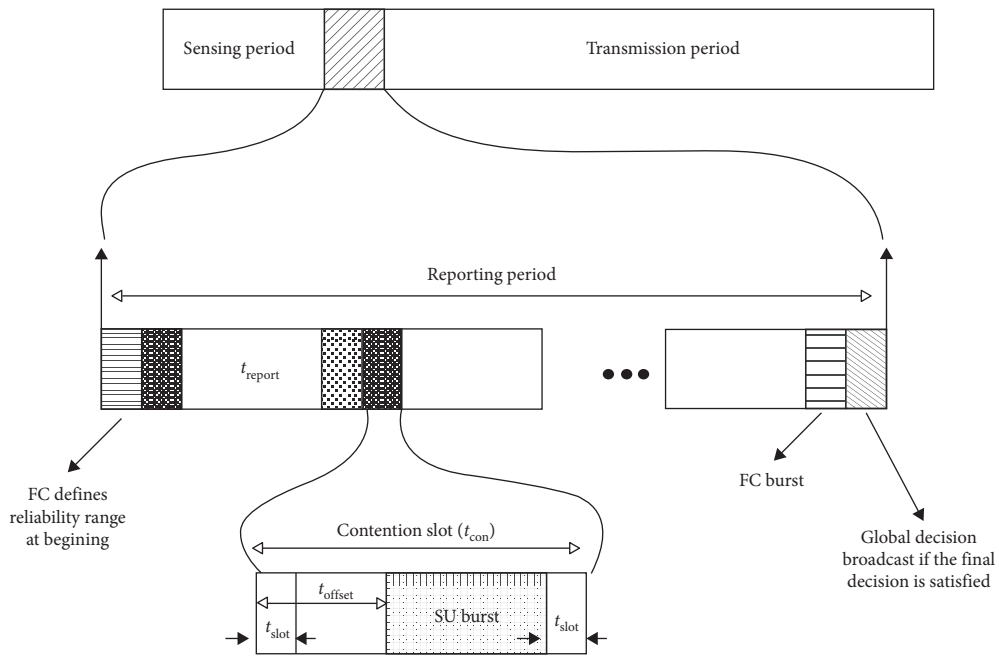


FIGURE 3: Proposed contention-window based reporting.

## 5. Numerical Evaluation

In this section, we present simulation results for the proposed contention-window based reporting scheme in

consideration with the ordered-sequential fusion and compare its performance with the conventional order-less sequential reporting scheme. We consider IEEE 802.22 standards; it is assumed that the existence of the PU is 0.5



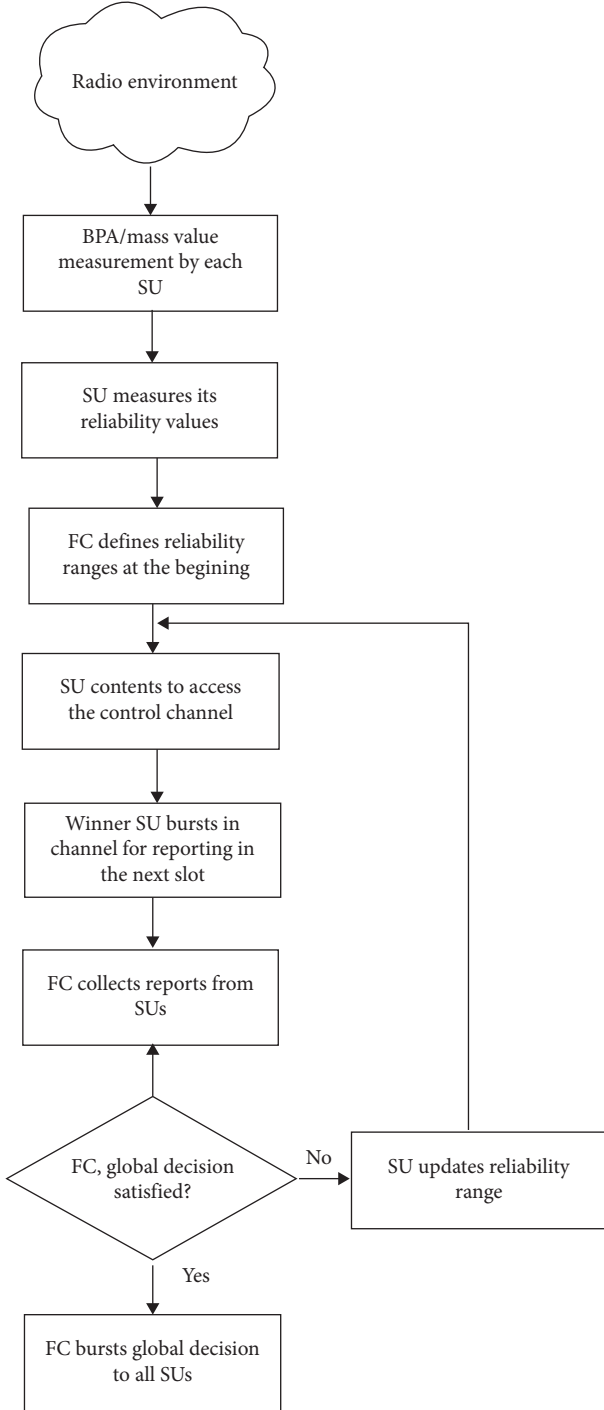


FIGURE 4: Flow chart for the proposed contention-window based reporting scheme.

and the used bandwidth is 6 MHz. The simulation environment is developed by utilizing MATLAB as an implementation tool. The parameters for the numerical evaluation are summarized in Table 1.

Figure 5 shows the percentage of the number of reporting SUs against the different value of SNRs ( $-20$  to  $-10$  dB). It can be observed from Figure 5 that as the number of SUs in the network increases, the percentage of the number of reporting SUs decreases for the proposed contention-based ordered-

TABLE 1: Simulation parameters.

Parameter	Value
Number of SUs	100, 150, 200
Probability of PU appearance	0.5
Bandwidth	6 MHz
Slot time $t_{\text{slot}}$	20 $\mu\text{sec}$
Poll time $t_{\text{poll}}$	200 $\mu\text{sec}$
Contention slot $t_{\text{con}}$	200 $\mu\text{sec}$
Reporting slot interval $t_{\text{report}}$	1 msec

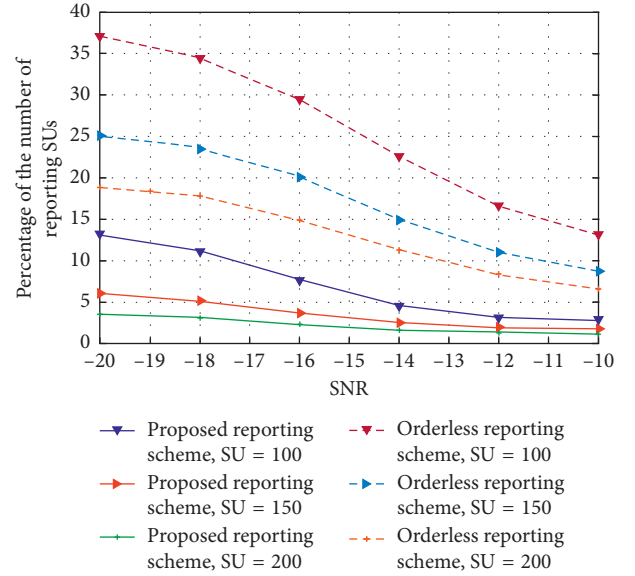


FIGURE 5: Percentage of the number of reporting SUs vs. SNR.

sequential fusion for a specific threshold value (threshold  $\eta = 15$ ). Specifically, it is shown in Figure 5 that with the orderless sequential reporting scheme, approximately 37% of the number of reporting SUs is required to satisfy the global decision requirement, whereas the proposed scheme requires approximately 14% of the number of reporting SUs, when 100 SUs are considered in the network. The reason is obvious that instead of the SU reporting in an order-less manner, only SU with the highest reliability reports to FC to satisfy the global decision requirement, which ultimately reduces the number of reports. The proposed contention-window based reporting scheme requires less percentage of the number of reports compared with the order-less sequential reporting scheme. It is noted that as the SNR value increases, the reports for the proposed scheme decrease. Also, it is worth noting that as the value of the threshold increases, the percentage of the number of reporting SUs increases.

Figure 6 shows the performance comparison of the proposed scheme in terms of error probability for varying average number of reporting SUs. It can be observed from Figure 6 that error probability of the proposed contention-window based reporting scheme is smaller than the order-less sequential reporting scheme, and it becomes identical to that of the order-less scheme as the average number of reporting SUs increases. It is obvious that in the beginning of the proposed contention-window based reporting, the highly reliable SUs report to FC; thus, its global requirements converge and the error probability

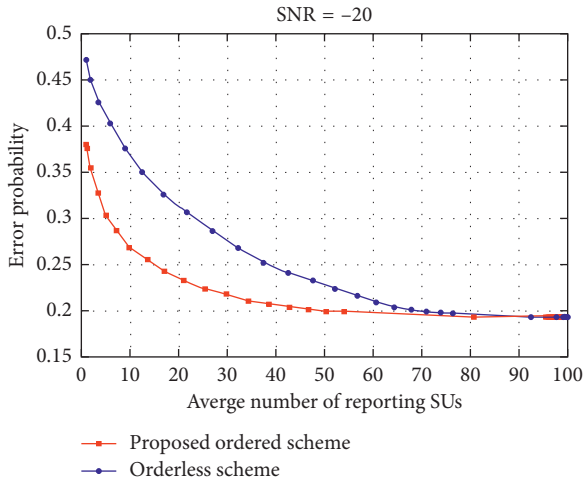


FIGURE 6: Error probability vs. average number of reporting SUs.

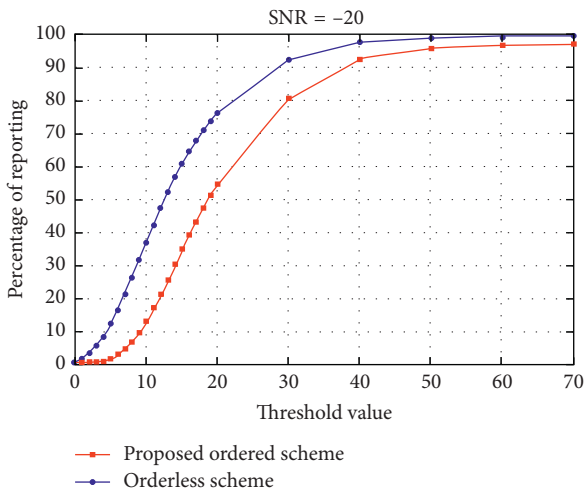


FIGURE 7: Percentage of reporting vs. threshold value.

is smaller than the order-less sequential fusion scheme. However, as the average number of reporting SUs increases, more SUs will report to FC to meet the required global decision and converges, and thus the error probability decreases. As a result, at a large average number of reporting SUs, the error probability is low and almost the identical for both schemes.

Figure 7 shows the percentage of reporting for varying threshold value. It is worth noting that the proposed contention-window based reporting scheme requires a smaller number of SUs for reporting than the conventional order-less reporting scheme. Also, it is important to mention that as the number of threshold value increases, the percentage of reporting increases. It is well justified because more SUs report to FC in order to satisfy the global decision requirement. After all, it is shown that the proposed contention-window based reporting scheme is more effective than the conventional order-less sequential fusion reporting scheme.

Figure 8 shows the spectral efficiency for varying detection probability. As the detection probability increases, spectrum availability for the SUs decreases; thus, the spectral

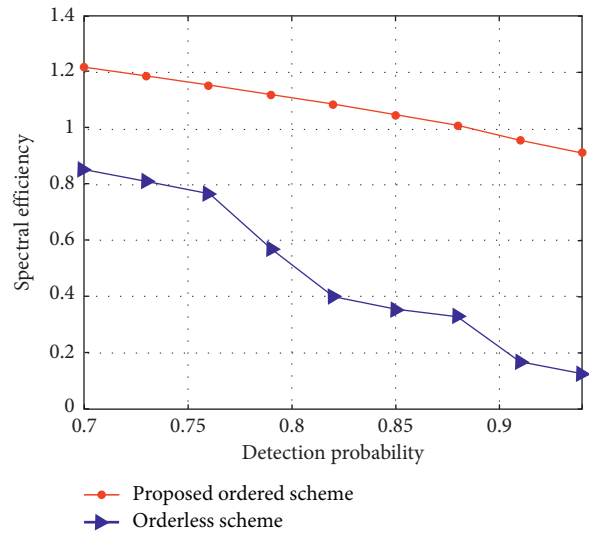


FIGURE 8: Spectral efficiency vs. detection probability.

efficiency of the system decreases. However, the proposed scheme achieves better performance than the conventional order-less scheme. As a result, the proposed scheme is also more effective in the perspective of spectral efficiency.

## 6. Conclusion

The integration of cognitive radio technology and the Internet of things seems to shift future wireless networks (5G). Cognitive radio technology has the potential to efficiently utilize the spectrum via cooperative sensing. However, the rise in cooperative sensing users increases the average reporting time, bandwidth utilization, and communication overhead. In this paper, we proposed an ordered-sequential fusion scheme with contention-window based reporting for Internet of things to reduce the reporting time and the communication overhead, which ultimately reduces cost and bandwidth utilization. Secondary users content to access the shared control channel and report their information to FC based on reliability to reduce the reporting time duration by satisfying the global decision requirement. The effectiveness of the proposed contention-window based reporting scheme is shown through simulations by considering percentage of the number of reporting SUs, error probability, percentage of reporting, and spectral efficiency. The results showed that the proposed ordered-sequential contention-window based reporting scheme outperforms the conventional order-less sequential reporting scheme in various aspects.

## Data Availability

The data used to support the findings of this study are included within the article.

## Conflicts of Interest

The authors declare no conflicts of interest.

## Acknowledgments

This work was supported in part by the MSIT (Ministry of Science and ICT), Korea, under the ITRC (Information Technology Research Center) support program (IITP-2019-2018-0-01426) supervised by the IITP (Institute for Information and Communication Technology Planning & Evaluation) and in part by the National Research Foundation (NRF) funded by the Korean government (MSIT) (No. 2019R1F1A1059125).

## References

- [1] A. Agarwal, G. Misra, and K. Agarwal, "The 5th generation mobile networks-key concepts, network architecture and challenges," *American Journal of Electrical and Electronic Engineering*, vol. 3, no. 2, pp. 22–28, 2015.
- [2] H. Shakhatareh, A. Sawalmeh, A. Al-Fuqaha et al., *Unmanned Aerial Vehicles: A Survey on Civil Applications and Key Research Challenges*, IEEE Access, Piscataway, NJ, USA, 2019.
- [3] Z. Kaleem and M. H. Rehmani, "Amateur drone monitoring: state-of-the-art architectures, key enabling technologies, and future Research directions," *IEEE Wireless Communications*, vol. 25, no. 2, pp. 150–159, 2018.
- [4] M. A. Khan, I. M. Qureshi, and F. Khanzada, "A hybrid communication scheme for efficient and low-cost deployment of future flying ad-hoc network (FANET)," *Drones*, vol. 3, no. 1, p. 16, 2019.
- [5] Z. Kaleem, Y. Li, and K. Chang, "Public safety users' priority-based energy and time-efficient device discovery scheme with contention resolution for ProSe in third generation partnership project long-term evolution-advanced systems," *IET Communications*, vol. 10, no. 15, pp. 1873–1883, 2016.
- [6] Z. Kaleem, M. H. Rehmani, E. Ahmed et al., "Amateur drone surveillance: applications, architectures, enabling technologies, and public safety issues: part 1," *IEEE Communications Magazine*, vol. 56, no. 1, pp. 14–15, 2018.
- [7] Z. Kaleem, M. Yousaf, A. Qamar et al., "UAV-empowered disaster-resilient edge architecture for delay-sensitive communication," 2019, <https://arxiv.org/abs/1809.09617v2>.
- [8] L. Sboui, H. Ghazzai, Z. Rezki, and M. Alouini, "Energy-Efficient power allocation for UAV cognitive radio systems," in *Proceedings of the IEEE 86th Vehicular Technology Conference (VTC-Fall)*, IEEE, Toronto, ON, Canada, September 2017.
- [9] Y. Cai, Z. Wei, R. Li, D. W. K. Ng, and J. Yuan, "Energy-efficient resource allocation for secure UAV communication systems," 2019, <http://arxiv.org/abs/1901.09308>.
- [10] K. Ashton, "That "internet of things": in the real world, things matter more than ideas," *RFID Journal*, vol. 22, 2009.
- [11] S. Chatterjee, R. Mukherjee, S. Ghosh, D. Gosh, S. Gosh, and A. Mukherjee, "Internet of things and cognitive radio-issues and challenges," in *Proceedings of the IEEE International Conference on Opto-Electronics and Applied Optics (Optronix)*, IEEE, Kolkata, India, November 2017.
- [12] A. A. Khan, M. H. Rehmani, and A. Rachedi, "When cognitive radio meets the internet of things?," in *Proceedings of the IEEE International Wireless Communications and Computing Conference (IWCMC)*, IEEE, Paphos, Cyprus, September 2016.
- [13] F. Al-Turjman, E. Ever, and H. Zahmatkesh, "Green femto-cells in the IoT era: traffic modeling and challenges—an overview," *IEEE Network*, vol. 31, no. 6, pp. 48–55, 2017.
- [14] F. Al-Turjman, E. Ever, and H. Zahmatkesh, "Small cells in the forthcoming 5G/IoT: traffic modeling and deployment overview," *IEEE Communications Surveys and Tutorials*, vol. 21, no. 1, pp. 28–65, 2018.
- [15] A. Al-Fuqaha, M. Guizani, M. Mohammadi, M. Aledhari, and M. Ayyash, "Internet of things: a survey on enabling technologies, protocols, and applications," *IEEE Communications Surveys and Tutorials*, vol. 17, no. 4, pp. 2347–2376, 2015.
- [16] Q. Wu, G. Ding, Y. Xu et al., "Cognitive internet of things: a new paradigm beyond connection," *IEEE Internet of Things Journal*, vol. 1, no. 2, pp. 129–143, 2014.
- [17] FCC, "Notice of proposed rule-making and order," ET Docket No. 03-222, FCC, Washington, DC, USA, 2003.
- [18] P. Rawat, K. D. Singh, and J. M. Bonnin, "Cognitive radio for M2M and internet of things: a survey," *Computer Communications*, vol. 94, pp. 1–29, 2016.
- [19] S. Aslam, W. Ejaz, and M. Ibnkahla, "Energy and spectral efficient cognitive radio sensor networks for internet of things," *IEEE Internet of Things Journal*, vol. 5, no. 4, pp. 3220–3233, 2018.
- [20] J. Mitola and G. Q. Maguire, "Cognitive radio: making software radio more personal," *IEEE Personal Communication*, vol. 6, no. 4, pp. 13–18, 1999.
- [21] Y. Arjoun and N. Kaabouch, "A comprehensive survey on spectrum sensing in cognitive radio networks: recent advances, new challenges, and future research direction," *Sensors*, vol. 19, no. 1, p. 126, 2019.
- [22] G. Ding, Q. Wu, L. Zhang, Y. Lin, T. A. Tsiftsis, and Y. Yao, "An amateur drone surveillance system based on cognitive internet of things," *IEEE Communications Magazine*, vol. 56, no. 1, pp. 29–35, 2018.
- [23] Y. Saleem, M. H. Rehmani, and S. Zeadally, "Integration of cognitive radio technology with unmanned aerial vehicles: issues, opportunities, and future research challenges," *Journal of Network and Computer Applications*, vol. 50, pp. 15–31, 2015.
- [24] A. Ranjan, Anurag, and B. Singh, "Design and analysis of spectrum sensing in cognitive radio based on energy detection," in *Proceedings of the IEEE International Conference on Signal and Information Processing (IconSIP)*, IEEE, Nanded, India, October 2016.
- [25] I. Ilyas, S. Paul, A. Rahman, and R. K. Kundu, "Comparative evaluation of cyclo-stationary detection based cognitive spectrum sensing," in *Proceedings of the IEEE 7th Annual Ubiquitous Computing, Electronics and Mobile Communication Conference (UEMCON)*, IEEE, New York, NY, USA, October 2016.
- [26] I. F. Akilidz, B. F. Lo, and R. Balakrishnan, "Cooperative spectrum sensing in cognitive radio networks: a survey," *Physical Communication*, vol. 4, no. 1, pp. 40–62, 2011.
- [27] S. C. Shinde and A. N. Jadhav, "Centralized cooperative spectrum sensing with energy detection in cognitive radio and optimization," in *Proceedings of the IEEE International Conference on Recent Trends in Electronics, Information and Communication Technology (RTEICT)*, IEEE, Bangalore, India, May 2016.
- [28] M. Zheng, C. Xu, W. Liang, H. Yu, and L. Chin, "A novel CoMAC based cooperative spectrum sensing scheme in cognitive radio networks," in *Proceedings of the IEEE International Conference on Communication Workshop (ICCW)*, IEEE, London, UK, June 2015.
- [29] H. Hu, Y. Xu, Z. Liu, N. Li, and H. Zhang, "Optimal strategies for cooperative spectrum sensing in multiple cross over

- cognitive radio networks,” *KSII Transaction on Internet and Information System*, vol. 6, no. 12, pp. 3061–3080, 2012.
- [30] D. Lee, “Adaptive random access for cooperative spectrum sensing in cognitive radio network,” *IEEE Transaction on Wireless Communications*, vol. 14, no. 2, pp. 831–840, 2015.
- [31] R. Alhamad, H. Wang, and Y. Yao, “Cooperative spectrum sensing with random access reporting channels in cognitive radio networks,” *IEEE Transaction on Vehicular Technology*, vol. 66, no. 8, pp. 7249–7261, 2017.
- [32] J. So, “Cooperative spectrum sensing for cognitive radio networks with limited reporting,” *KSII Transaction on Internet and Information Systems*, vol. 9, no. 8, pp. 2755–2773, 2015.
- [33] R. Alhamad, H. Wang, and Y. Yao, “Reporting channel design and analysis in cooperative spectrum sensing for cognitive radio networks,” in *Proceedings of the IEEE 82nd Vehicular Technology Conference (VTC-2015-Fall)*, IEEE, Boston, MA, USA, September 2015.
- [34] Q. Peng, K. Zeng, W. Jun, and S. Li, “A distributed spectrum sensing scheme based on credibility and evidence theory in cognitive radio networks,” in *Proceedings of the 17th IEEE International Symposium on Personal, Indoor and Mobile Radio Communication*, pp. 1–5, IEEE, Helsinki, Finland, September 2006.
- [35] N. Nguyen-Thanh and I. Koo, “An enhanced cooperative spectrum sensing scheme based on evidence theory and reliability source evaluation in cognitive radio context,” *IEEE Communications Letters*, vol. 13, no. 7, pp. 492–494, 2009.
- [36] S. Yeelin and Y. T. Su, “A sequential test based cooperative spectrum sensing scheme for cognitive radios,” in *Proceedings of the IEEE 19th International Symposium on Personal, Indoor and Mobile Radio Communications*, pp. 1–5, IEEE, Cannes, France, September 2008.
- [37] Z. Qiyue, Z. Songfeng, and A. H. Sayed, “Cooperative spectrum sensing via sequential detection for cognitive radio networks,” in *Proceedings of the IEEE 10th Workshop on Signal Processing Advances in Wireless Communication*, pp. 121–125, IEEE, Perugia, Italy, June 2009.